EXPIRATORY TIME CONSTANT HETEROGENEITY IN EXPERIMENTAL ACUTE RESPIRATORY DISTRESS SYNDROME

by

WILLIAM ROY HENDERSON

M.D., The University of British Columbia, 1997

A THESIS SUBMITTED IN PARTIAL FULFILLMENT OF

THE REQUIREMENTS FOR THE DEGREE OF

DOCTOR OF PHILOSOPHY

i n

THE FACULTY OF GRADUATE AND POSTDOCTORAL STUDIES

(Kinesiology)

THE UNIVERSITY OF BRITISH COLUMBIA

(Vancouver)

June 2016

Abstract

Purpose

This thesis evaluated regional heterogeneity of pulmonary mechanical values within models of lung injury. To this end four separate studies were completed. I evaluated regional expiratory time constant (τ_E) heterogeneity and tissue strain (ε) in a lung model using functional respiratory imaging (FRI) (Study 1, Chapter 2), and developed an *in vivo* porcine model of lung injury (Study 2, Chapter 3). This model was used to assess changes in τ_E due to manipulations of respiratory gas density (Study 3, Chapter 4) and mechanical ventilation parameters (Study 4, Chapter 5).

Methods

Study 1: Using computerized tomography (CT) images we generated 3-dimensional lung models. These were used calculated global and regional values for resistance, elastance, ε and τ_E under three different airway pressure conditions.

Study 2: Experimental lung injury was induced in 11female Yorkshire X pigs. Necropsy, light and electron microscopy of lung was performed.

Study 3: I utilized a multi-compartment model to describe the effects of changes in tidal volume (V_T) and positive end-expiratory pressure (PEEP) on lung emptying during passive deflation before and after experimental lung injury in 6 adult female Yorkshire X pigs. Expiratory time constants (τ_E) were determined by partitioning the expiratory flow-volume ($\dot{V}V$) curve into multiple discrete segments.

Study 4: Tracheal pressure and flow were measured in 7 pigs before and after experimental lung injury. Gas density was altered by using helium-oxygen (He), sulfur hexafluoride-oxygen (SF_6) and nitrogen-oxygen (N_2) gas.

Conclusions

Functional respiratory imaging demonstrates regional variation in both ε and τ_E. These findings raise questions about the use of whole lung measures of ε and τ_E to guide clinical management of lung injury (Study 1). I developed a stable model of lung injury using SPA that replicates the light and electron microscopic findings seen in human ARDS (Study 2). A pragmatic strategy using changes in the pattern of expiration described by a multi-compartment model of τ_E reveals that alterations in and gas density (Study 3) as well as PEEP and V_T (Study 4) change expiratory pulmonary mechanics. These observations lay the groundwork for future clinical studies in lung injured patients.

Preface

This thesis describes work carried out at the UBC Centre for Comparative Medicine and the Jack Bell Research laboratory. All studies were approved by the UBC Animal Care Committee (specific certificate numbers are described below). I identified and designed the research program described in this document. The contributions of my collaborators are described below.

Chapter 1

A version of portions of Chapter 1 has previously been published as: Henderson WR, Sheel AW. Pulmonary mechanics during mechanical ventilation. Respir Physiol Neurobiol. 2012.180:162– 172.

Henderson WR was the primary author and played the principal role in identification and design of the review topic, performance of research and manuscript preparation. Sheel AW assisted in identification and design of the review topic and manuscript preparation.

A version of portions of Chapter 1 has previously been published as: Henderson WR, Pare PA, Ayas NT: Respiratory system mechanics and energetics. In Broaddus VC, Mason RJ, Murray JF, Nadel JA, King TE Jr, Ernst J, Lazarus SC, Slutsky AS (eds): Murray & Nadel's Textbook of Respiratory Medicine, 6/e. Philadelphia: Elsevier, 2014.

Henderson WR was the primary author and played the principal role in identification and design of the review topic, performance of research and manuscript preparation. Pare PA and Ayas NT assisted in identification and design of the review topic and manuscript preparation.

Chapter 2

A version of Chapter 2 is in preparation for submission as: Henderson WR, Molgat-Seon Y, Vos W, Lipson R, Ferreira F, Kirby M, Van Holsbeke C, Dominelli P, Griesdale DEG, Sekhon M, Coxson H, Mayo J, Sheel AW. Functional Respiratory Imaging, Regional Strain and Time Constants at three PEEP Levels in an ex-vivo Animal Model.

Henderson WR was the primary author and played the principal role in identification and design of the research program, performance of research, data analysis and manuscript preparation. Molgat-Seon Y, Lipson R, Dominelli PB, Griesdale DEG and Foster G assisted in data collection and analysis. Vos W, Ferreira F, Kirby M and Van Holsbeke C assisted in image registration and creating functional respiratory imaging models. Sekhon M, Coxson H, Mayo J and Sheel AW assisted in manuscript preparation

Chapter 2 is based on work conducted in the Jack Bell Research Centre, Vancouver, BC. The investigations were approved by the UBC Animal Care Committee and authorized as Certificate A11-0374.

Chapter 3

A version of Chapter 3 has previously been published as: Henderson WR, Barnbrook J, Dominelli PB, Griesdale DEG, Arndt T, Molgat-Seon Y, Foster G, Ackland GL, Xu J, Ayas NT, Sheel AW. Administration of intrapulmonary sodium polyacrylate to induce lung injury for the development of a porcine model of early acute respiratory distress syndrome. Intensive Care Medicine Experimental 2014 2:5.

Henderson WR was the primary author and played the principal role in identification and design of the research program, performance of research, data analysis and manuscript preparation. Barnbrook J, Dominelli PB, Griesdale DEG, Arndt T, Molgat-Seon Y and Foster G

assisted in data collection and analysis. Ackland GL, Ayas NT and Sheel AW assisted in manuscript preparation

Chapter 3 is based on work conducted in the UBC Centre for Comparative Medicine, Vancouver, BC. The investigations were approved by the UBC Animal Care Committee and authorized as certificate no. A11-0396.

Chapter 4

A version of Chapter 4 has previously been published as: Henderson WR, Molgat-Seon Y, Dominelli PB, Brasher PM, Griesdale DE, Foster GE, Yacyshyn A, Ayas NT, Sheel AW Gas density alters expiratory time constants before and after experimental lung injury. Exp Physiol. 2015 Oct 1; 100(10):1217-28.

Henderson WR was the primary author and played the principal role in identification and design of the research program, performance of research, data analysis and manuscript preparation.

Molgat-Seon Y, Dominelli PB, Griesdale DEG and Foster G assisted in data collection and analysis. Brasher PM assisted in data analysis. Yacyshyn A, Ayas NT and Sheel AW assisted in manuscript preparation.

Chapter 4 is based on work conducted in the UBC Centre for Comparative Medicine, Vancouver, BC. The investigations were approved by the UBC Animal Care Committee and authorized as certificate no. A12-028.

Chapter 5

A version of Chapter 5 has previously been published as: Henderson WR, Dominelli PB, Molgat-Seon Y, Lipson R, Griesdale DEG, Sekhon M, Ayas NT, Sheel AW. Effect of tidal

volume and positive end-expiratory pressure on expiratory time constants in experimental lung injury. Physiol Rep. 2016 Mar;4(5). pii: e12737.

Henderson WR was the primary author and played the principal role in identification and design of the research program, performance of research, data analysis and manuscript preparation. Dominelli PB, Molgat-Seon Y, Griesdale DEG and Sekhon M assisted in data collection and analysis. Lipson R assisted in data analysis. Ayas NT and Sheel AW assisted in manuscript preparation.

Chapter 5 is based on work conducted in the UBC Centre for Comparative Medicine, Vancouver, BC. The investigations were approved by the UBC Animal Care Committee and authorized as certificate no. A12-0272 and A11-0282.

Table of Contents

List of Tables

List of Figures

List of Symbols

A	Area
ARDS	Acute respiratory distress syndrome
BAL	Bronchoalveolar lavage
C	Compliance
CFD	Computational fluid dynamics
CON	Control
COPD	Chronic obstructive lung disease
EELV	End –expiratory lung volume
EFL	Expiratory flow limitation
EILV	End-inspiratory lung volume
E_{Lspec}	Specific elastance of lung
ETT	Endotracheal tube
ε	Strain
FRC	Functional residual capacity
FRI	Functional respiratory imaging
F	Force
G	Shear modulus
M	Young's Modulus
MRI	Magnetic resonance imaging
P	Pressure
$PaCO_2$	Partial pressure of carbon dioxide
PaO_2	Partial pressure of oxygen
PEEP	Positive end-expiratory pressure
P/F	PaO_2/FiO_2 ratio
PV	Pressure-volume
R	Resistance
SPA	Sodium polyacrylate
Ψ	Shear stress
γ	Shear strain
σ	Stress
τ	Time constant
τ_E	Expiratory time constant
τ_I	Enspiratory time constant
V	Volume
$\dot{V}$	Flow
VALI	Ventilator associated lung injury
V_T	Tidal volume
$\dot{V}V$	Flow-volume

Acknowledgements

This thesis describes the methods and results of my recent research, but more importantly, it reflects a process of collaboration and support between many exceptional people.

I am grateful for my doctoral supervisor, Dr Bill Sheel, for being willing to take a chance on a mid-career physician. His guidance and emphasis on scientific rigor has improved the quality of both my research and clinical work.

I thank Drs. Don McKenzie, Najib Ayas and Jeremy Road for serving on my thesis committee and providing encouragement when needed. Similarly, I would like to acknowledge all members of the Health and Integrative Physiology Lab (HIPL) for their enthusiasm for research in physiology, and I would be remiss if I did not specifically single out two of my doctoral studies colleagues for special thanks. Paolo Dominelli and Yannick Molgat-Seon were instrumental in bringing the work described in this document to fruition, and are proof that the future of science in this country is bright.

Finally, and most importantly, I am deeply indebted to Heather and all my family for their support and tolerance for the many hours that were devoted to this work.

Chapter 1: Introduction

Overview

The acute respiratory distress syndrome (ARDS) is a lethal lung injury caused by inflammation. Mechanical ventilation is a lifesaving intervention in patients with ARDS, but may itself lead to new injury. This may be, in part, due to regional differences in distending pressures and tissue strain within the injured lung itself. Bedside assessment of regional pulmonary mechanics has to date been elusive. In this thesis I outline a novel method of functional respiratory imaging (FRI) in the bedside assessment of regional strain in ARDS by linking regional strain to abnormalities in the flow-volume curve of passive expiration. I demonstrate this in an ex-vivo cadaveric pig lung model using high resolution 3D computerized tomography image registration (Chapter 2). Chapter 3 outlines the development of a novel porcine model of ARDS that we used to explore the effects of variations in respiratory gas density (Chapter 4) and mechanical ventilation parameters (Chapter 5) on the pattern of the expired flow-volume curve.

Definition and Epidemiology of ARDS

The acute respiratory distress syndrome (ARDS) is a lethal and morbid acute injury to the lungs characterized by severe hypoxic respiratory failure and alterations in pulmonary mechanics (154). First defined in 1967(10) and updated in 1994 (22) and 2012 (162), ARDS is currently defined as: severe hypoxia (PaO_2/FiO_2 ratio less than 300) within 1 week of a known clinical insult, new or worsening hypoxia not due to left heart failure, with bilateral opacifications on chest X-ray (Table 1.1 and Figure 1.1). The most frequently cited precipitating

events for ARDS are sepsis, pneumonia, aspiration, trauma, pancreatitis and blood transfusions (84, 96).

	Acute Respiratory Distress Syndrome		
Timing	Within 1 week of known clinical insult or new/ worsening respiratory symptoms		
Imaging	Bilateral opacities – not fully explained by effusions, lung collapse or nodules		
Edema	Not fully explained by cardiac failure of fluid overload		
	Mild	**Moderate**	**Severe**
Oxygenation	$200 < P_aO_2/ F_iO_2 \leq 300$ (with PEEP ≥ 5)	$200 < P_aO_2/F_iO_2 \leq 300$ (with PEEP ≥ 5)	$P_aO_2/ F_iO_2 \leq 100$ (with PEEP ≥ 5)

Table 1.1 The Berlin criteria for the diagnosis of ARDS
Source (162)

While there is significant geographic variation in ARDS incidence (26), a widely cited study placed the incidence of ARDS at 78.9 cases per 100 000 person/years (130). Some controversy exists with respect to rates of, and temporal changes in, ARDS related mortality. Retrospective observational studies and randomized controlled trials performed at single centres suggest that mortality had decreased to 22-25% by 2005 (53, 182). A recent trial of prone position ventilation reported mortality of 16% in the interventional group (79). However, many of these trials may have excluded patients with significant co-morbidities that might have increased mortality. Indeed, it appears that there is a difference in the mortality results found in observational versus interventional trials. The largest systematic review performed to date suggests that there has been little improvement in ARDS mortality in the last decade, with an overall pooled mortality rate of 44.3% (153).

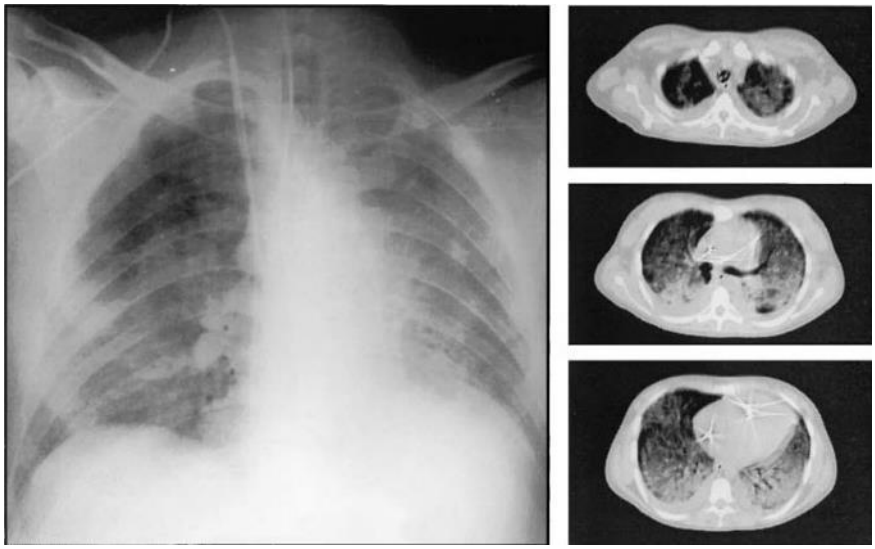

Figure 1.1 Anteroposterior chest x-ray (left panel) and CT scans—apex, hilum, and base—(right panels) in ARDS from sepsis
The chest x-ray shows diffuse ground glass opacification, sparing the right upper lung. The CT scans show inhomogeneous disease and both the craniocaudal and sternovertebral gradients. Reprinted with permission of the American Thoracic Society. Copyright © 2016 American Thoracic Society. From Gattinoni, *et al*. (60) The *American Journal of Respiratory and Critical Care Medicine* is an official journal of the American Thoracic Society.

The management of ARDS invariably involves aggressive supportive measures, including: i) a search for, and treatment of, the underlying cause, ii) supplemental oxygen, and iii) mechanical ventilatory support.

Pathophysiology of ARDS

Whether the inciting cause of ARDS is infectious or non-infectious, intra- or extra-pulmonary, the end results are: i) significantly increased permeability across the alveolar endothelial-epithelial barrier, ii) diffuse alveolar damage characterized by inflammatory infiltrates, thickened alveolar septae, and deposition of hyaline membranes, and iii) evidence of pulmonary physiological dysfunction such as impaired gas exchange and decreased lung compliance (103, 128). Both endothelial and epithelial injury appear necessary for the syndrome to develop (12, 125, 203).

Endothelial Injury

While the inciting trigger for ARDS varies among patients, a common pathogenic cascade occurs, involving both the lung endothelium/microvasculature and the alveolar epithelium. Abnormalities of inflammation, with disordered accumulation of activated neutrophils and platelets within alveoli, inappropriate activation of the coagulation cascade and impaired alveolar endothelial/epithelial barrier function are seen in all cases (126). Binding of products of cell injury or bacterial/viral products to toll-like receptors at the endothelial/epithelial barrier is a powerful driver of inflammation (142). Injury to lung endothelium by activated neutrophils appears to be a central mechanistic cause of alveolar barrier disruption and has been widely documented (44, 55, 56, 201, 214). After the inciting event in ARDS, activated neutrophils migrate and adhere to lung microvasculature, where they release a wide variety of procoagulant molecules and inflammatory mediators (including cytokines, free oxygen radicals and proteases) which increase endothelial permeability (126). Inflammatory mediators, whether from lung or distant sites of inflammation may act directly on lung microvascular endothelium, causing the release chemokines and cell surface molecules responsible for neutrophil chemotaxis, rolling and adhesion. This in turn causes further endothelial injury and neutrophil aggregation (23, 176, 204, 215).

Epithelial Injury

Despite advances in the understanding and treatment of ARDS, the mechanisms that cause alveolar epithelial injury are not well understood. During migration across the capillary-alveolar barrier into alveoli, neutrophils initially adhere to the basolateral epithelial surface, a process facilitated by β_2-adherins (211, 214). Normally, neutrophils will then migrate across the epithelial layer assisted by CD47 signalling and reseal their paracellular route through the

epithelial layer after migration (112, 185). This repair of the intercellular junctions after migration is essential to maintain the integrity of the epithelial layer and prevents alveolar fluid accumulation. In ARDS, due to the large numbers of activated neutrophils migrating across the epithelial layer, this does not occur. The release of cytotoxins during neutrophil migration across the epithelial layer causes apoptosis and necrosis of alveolar type I and II cells and disruption of epithelial tight junctions. Loss of epithelial integrity causes a progressive influx of protein-rich fluid into the alveoli, impairs physiologic transepithelial fluid transport, and inhibits the reabsorption of alveolar edema (122, 125, 200).

Surfactant Abnormalities

Pulmonary surfactant is a highly surface-active molecule found in the fluid layer that covers alveoli. In normal physiology, surfactant's principal functions are to prevent alveolar collapse at low lung volumes and to preserve bronchiolar patency. In addition to these mechanical roles, surfactant has a significant immunological role in preventing infection, as well as in the presentation of pathogens to host defense mechanisms (75). Biochemically, pulmonary surfactant is composed of approximately 90% lipid and 10% protein. Interaction between these constituents account for surfactant's primary biophysical role – that of lowering the surface tension at the air-water interface from the 73 $mN.m^{-1}$ expected at a pure plasma-air interface to approximately 0±1 $mN.m^{-1}$ with compression during expiration (7).

The role of surface tension (T), and therefore of surfactant, may be usefully understood by considering the law of Laplace, which expresses the relationship between transmural pressure (ΔP) across the wall of a sphere (such as an idealized alveolus) and it's radius (r):

$$\Delta P = 2T/r$$

While surfactant decreases alveolar surface tension through all phases on the inflation-deflation cycle, it possesses the unique ability to alter surface tension in inverse proportion to an alveolus' radius. That is, it has a greater effect on lowering surface tension when an alveolus is closer to end-expiration (smaller radius) than when it is near end-inspiration (larger radius). The surface tension of the alveolar air—fluid interface effects several key physiologic and biophysical features of ventilation. First, surface tension provides a force opposing lung inflation by increasing elastance (144). Therefore, high alveolar surface tensions will increase lung elastance, and therefore the work of breathing (and energy spent) required for lung inflation. By lowering ST, surfactant decreases the negative pleural pressures required to inflate alveoli. An implication of this phenomenon is that, without surfactant, recurrent alveolar collapse might occur at end-expiration, potentially causing ventilation-perfusion (V/Q) mismatching, shunt and hypoxia (7). Second, the law of Laplace implies that, in the absence of surfactant, gas would flow from smaller alveoli (with higher intra-alveolar pressures) to larger alveoli (with lower pressures) if they are connected. Thus, small alveoli will tend to collapse and large alveoli will tend to over-inflate (see Figure 1.2) – a situation that would lead to alveolar collapse and V/Q mismatch (193, 196). Surfactant prevents this instability by decreasing surface tension in small alveoli more than it does in large alveoli, thereby equalizing their intra-alveolar pressures. Finally, in addition to a critical role in alveoli, surfactant appears to stabilize bronchioli, and surfactant deficiency or dysfunction may promote closure of small airways (52, 111, 175). The presence of pathologic surface-active and water soluble agents in the alveoli due to loss of epithelial barrier integrity contributes to the inactivation of surfactant (80, 140, 170). Surfactant depletion and inactivation decrease alveolar stability, exacerbating or precipitating the alveolar collapse, lung atelectasis and hypoxia seen in ARDS.

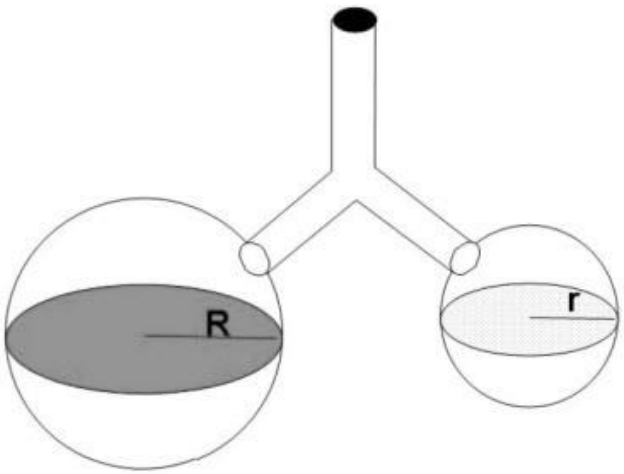

Figure 1.2 Stylized representation of the effects of the Law of Laplace on two connected alveoli of different sizes and *similar* surface tension
The pressure in a sphere (P_R or P_r) in a bubble is equal to 4 times the surface tension (T) divided by the radius (R or r). As applied to the grape-like alveolus, where only the inner wall has a liquid surface exposed to gas, the formula is P=2T/r. In this situation, P_r is greater than P_R as r is less than R, implying that gas will flow from the smaller to the larger alveolus. Used with permission from reference (157).

Measurement of Lung Volumes

In contrast to ambulatory patients, measurements of lung volumes such as forced expiratory volume in one second (FEV_1), forced vital capacity (FVC) and total lung capacity (TLC) are rarely measured in mechanically ventilated patients due to altered level of consciousness, acute illness, or significant hypoxia. One exception is the measurement of functional residual capacity (FRC). Potential methods for the measurement of FRC in mechanically ventilated patients now include plethysmography, computerized tomography, inert gas dilution and tracer gas wash-in/wash-out (90). We prefer a simplified method that provides clinically useful results and that has shown excellent reproducibility and agreement with CT scan based measurements (145).

In this technique, an impermeable syringe is prepared with a carefully measured volume of a calibrated oxygen–helium mixture. The syringe is attached to the endotracheal tube which

was tightly clamped at end expiration. The endotracheal tube is unclamped and several tidal breaths are inflated (allowing helium equilibration between the bag and the patient's respiratory system). Gas is then sampled and analyzed in a mass spectrometer for helium concentration. Calculation of the FRC can then occur thus:

$$C_1 \times V_1 = C_2 \times (V_1 + FRC)$$

where C_1 = initial (known) helium concentration in bag, C_2 = final (measured) helium concentration and V_1 = initial volume of gas in the bag. Therefore:

$$FRC = V_1 \times (C_1 - C_2)/C_2$$

While technically and conceptually straightforward, this technique has the theoretical disadvantage of allowing alveolar derecruitment during the clamping of the endotracheal tube, and care must be exercised to prevent depressurization of the respiratory system in patients on significant amounts of positive pressure ventilation.

Measurement of Static Pulmonary Mechanics

In the absence of gas flow, the static mechanical properties of the respiratory system may be measured. In mechanically ventilated patients unable to make respiratory efforts (whether due to disease, sedation or chemical paralysis) this can be achieved through the use of an inspiratory hold maneuvre, where the final inspiratory volume is held in the patient's lungs for a period of time. All current mechanical ventilators can automatically provide a brief end-inspiratory occlusion that allows the measurement of airway pressure with zero flow and a static tidal volume. The relationships between flow, pressure and volume may be displayed graphically (Fig. 1.3), and specific calculated values derived.

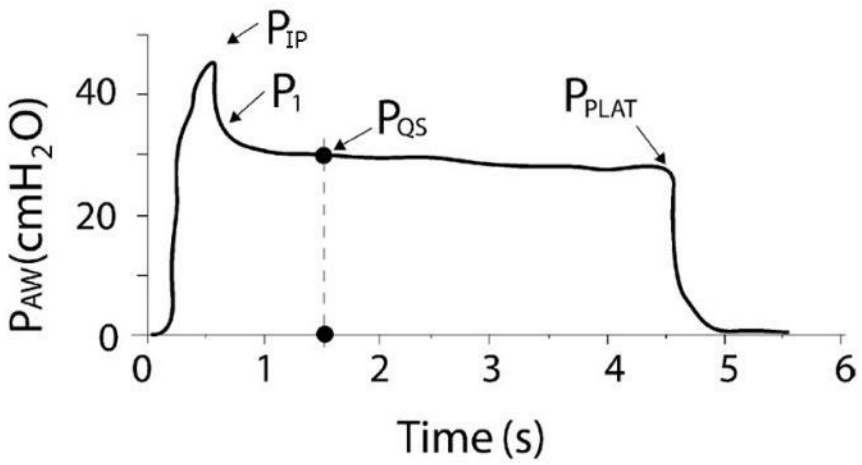

Figure 1.3 Representation of a ventilator screen image demonstrating changes in airway pressure (P_{AW}) versus time
Depicted are peak inspiratory pressure (P_{IP}), pressure after airflow equilibration (P_1), quasistatic pressure (P_{QS}) and plateau pressure (P_{PLAT}). With permission, from Henderson and Sheel.(90)

At the end of inspiration during mechanical ventilation, the pressure measured within the airway (P_{AW}) is at its highest value and is called the peak inspiratory pressure (P_{IP}). This is followed by a rapid drop in pressure (P_1 in Fig 1.3) and then a slow decay to a plateau (P_{PLAT} in Fig. 1.3). The drop in pressure from P_{IP} to P_1 represents the pressure or energy lost overcoming the resistance to gas flow within the airways, while the smaller drop from P_1 to P_{PLAT} is due to pendelluft and the redistribution of forces within tissue (viscoelastic forces). During the period from P_{IP} to P_{PLAT} there is redistribution of gas between alveoli with fast and slow time constants. P_{PLAT} represents the equilibrated plateau pressure which is assumed to be alveolar pressure (P_{ALV}).

Static Compliance

With tidal volume measured and the various components of the inspiratory pressure waveform defined, it is possible to calculate the mechanical properties of the static lung. The true static compliance ($C_{RS, STAT}$) of the respiratory system can be calculated as:

$$C_{RS, STAT} = V_T / P_{PLAT}$$

In this instance, there is no gas movement within the lung, and therefore there is no frictional component to the work done. Additionally, all viscoelastic forces have equilibrated. For these conditions to be true, a period of time in excess of 2–5 s must have passed between the occlusion maneuver and the measurement of pressure (18). For reasons of patient safety or comfort it is often unreasonable to maintain such a long inspiratory pause. If a shorter, but still significant pause is utilized between end-inspiration and pressure measurement (for example, 0.5–1.5 s) the pressure and thus compliance estimated will still be clinically useful, but not truly "static". This is called the quasistatic respiratory system pressure ($P_{RS,Q}$). The quasistatic compliance ($C_{RS,Q}$) may be calculated as:

$$C_{RS,Q} = V_{T/} P_{RS,Q}$$

In healthy individuals, there is little difference between $C_{RS,STAT}$ and $C_{RS,Q.}$ However, in patients with ARDS or severe chronic obstructive pulmonary disease (COPD), the difference may be significant (116, 117). The longer the pause prior to the measurement of the quasistatic pressure and compliance, the more accurately $_{CQS}$ will approximate C_{STAT}.

End Expiratory Pressure and Compliance

The assumption that P_{ALV} equals P_{ATM} at end expiration is generally true in healthy subjects. However, mechanically ventilated patients with expiratory flow limitation (such as in COPD or asthma), high ventilatory rates, or lung units with delayed emptying, may not fully exhale all inspired gases prior to the initiation of the subsequent breath. In this situation, the residual "trapped" gas causes a positive end expiratory pressure (PEEP). Because this PEEP is caused by patient characteristics, it is sometimes referred to as "intrinsic" PEEP ($PEEP_I$). In hypoxic respiratory failure, it is common for clinicians to program the ventilator to maintain a positive mouth pressure at the end of expiration in an attempt to enhance alveolar recruitment and thereby improve oxygenation. This

clinician determined pressure is often called "set" PEEP ($PEEP_{SET}$). In situations where $PEEP_I$ or $PEEP_{SET}$ (or both) are present, we must revise the equations for the calculations of compliance and resistance to account for these pressures: to account for this (32). Thus:

$$C_{STAT} = V_T / (P_{PLAT} - PEEP)$$

and

$$C_{QS} = V_T / (P_{QS} - PEEP)$$

Resistance: Much like static measures of compliance for the respiratory system, the static resistance of the respiratory system can be broken down into clinically useful segments. The total respiratory system resistance (R_{RS}) is determined by the net pressure drop ($P_{IP} - P_{PLAT}$) divided by the flow at end-inspiratory occlusion (V')(155). That is:

$$R_{RS} = (P_{IP} - P_{PLAT}) / V'$$

Partitioning Static Measurements

The placement of an esophageal balloon manometer allows the clinician or researcher to partition the pressures within the respiratory system into those experienced by the lung and those experienced by the chest wall (Fig. 1.4). This is only accurate if there is no pressure generated by the muscles of the respiratory system. Traditionally this has required neuromuscular paralysis, but deep sedation or careful monitoring with EMG, have been used to assure a passive respiratory measurement. While it is feasible to partition any of the measured pressures (i.e., P_{IP}, P_1 or P_{PLAT}) into lung and chest wall components, this is generally only done with P_{PLAT} and PEEP. The net pressure distending the respiratory system after the equilibration of gas flow, pendelluft and the redistribution of viscoelastic forces is the difference between P_{ALV} (synonymous with P_{PLAT} in this situation) and $P_{ATM.}$ The portion of this gradient that distends the lung is represented by $P_{ALV} - P_{PL}$,

while the portion that distends the chest wall is represented by $P_{PL} - P_{ATM}$. $P_{ALV} - P_{PL}$ is often referred to as the transpulmonary pressure (P_{TP}).

P_{PLAT} has been used to guide ventilating pressures during the management of ALI and ARDS with some success. However, P_{PLAT} is not the true pressure distending (and potentially injuring) an alveolus, P_{TP} is. For example, P_{PLAT} may be increased in ALI and ARDS due to chest wall edema or high intra-abdominal pressures due to an increased P_{PL}. If ventilating pressures in these situations were guided by P_{PLAT}, the inspiratory volumes used might be unnecessarily small. Similarly, high P_{PL} at end expiration may allow alveolar derecruitment if it exceeds the clinician $PEEP_{SET}$. It therefore seems reasonable to consider using P_{TP} as an indicator of the distending pressure seen by the alveolus rather than $P_{PLAT.}$ While no clinical trials have so far examined the outcome benefits of P_{TP} guided maximal inspiratory pressures or volumes, a recent trial demonstrated improvements in oxygenation and decreased duration of ventilator dependency in ARDS patients (187). Similarly, we have recently demonstrated that P_{PL} can vary dramatically in patients with ARDS and that P_L cannot be inferred from P_{AW} during high frequency oscillation ventilation (88).

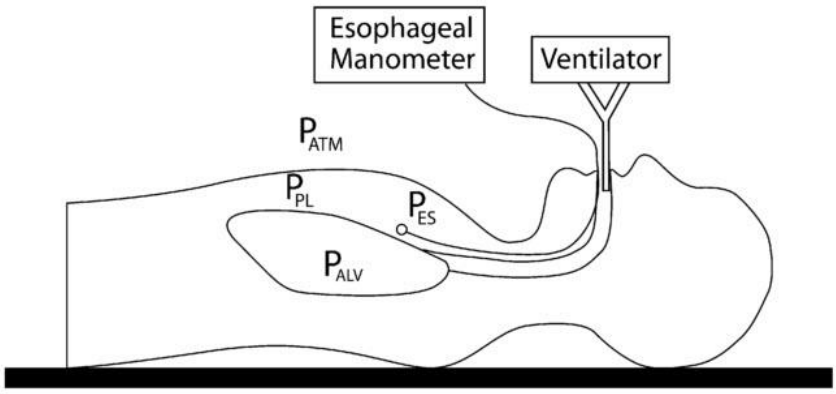

Figure 1.4 Diagram depicting the pressure measures useful in partitioning pulmonary mechanics
The clinician can directly measure atmospheric pressure (P_{ATM}) and airway pressure (P_{AW}). Esophageal pressure (P_{ES}) may also be directly measured and used as a surrogate for pleural pressure (P_{PL}). With these pressures measured, several additional pressures may be derived: respiratory system pressure (P_{RS}) = $P_{ALV} - P_{ATM}$, trans-pulmonary pressure (P_{TP}) = $P_{ALV} - P_{PL}$, and chest wall pressure (P_{CW}) = $P_{PL} - P_{ATM}$. With permission, from Henderson and Sheel.(90)

It is also useful to separate C_{STAT} into lung ($C_{STAT(L)}$) and chest wall ($C_{STAT(CW)}$) components. $C_{STAT(L)}$ can be calculated as:

$$C_{STAT(L)} = V_T / (P_{ALV} - P_{PL})$$

and the static compliance of the chest wall as:

$$C_{STAT(CW)} = V_T / (P_{PL} - P_{ATM})$$

The differentiation of the sources of compliance is relevant to clinicians, particularly in following the course of lung disease.

Creating Static Pressure–Volume Curves

The relationship between pressures and volumes within the respiratory system can be described graphically as a pressure–volume (PV) curve. Classically, a calibrated syringe(123) is used for PV curve determination. The syringe has calibrated 100 cm^3 markers on the piston shaft and a locking mechanism to ensure the accuracy of the amount of gas delivered. Stepwise inflation of the

respiratory system is effected from FRC to (potentially) TLC. Each stepwise injection of volume is followed by a 2–3 s pause to allow equilibration of forces. The pressure–volume coordinates are recorded at the end of each 100 cm^3 gas bolus and these points are then joined to form a static inflation PV curve. An analogous process using stepwise gas withdrawal can be used to create a deflation PV curve.

The PV loop for a patient with a healthy respiratory system is traced by the dashed line in Fig. 1.5. In this case there appears to be little change in C_{RS} (i.e., the slope of the PV loop) throughout the inflation or deflation limb of the loop throughout the range of normal tidal volumes. As such, the assumption of a linear relationship between pressure and volume through the range of normal tidal volumes appears to be respected.

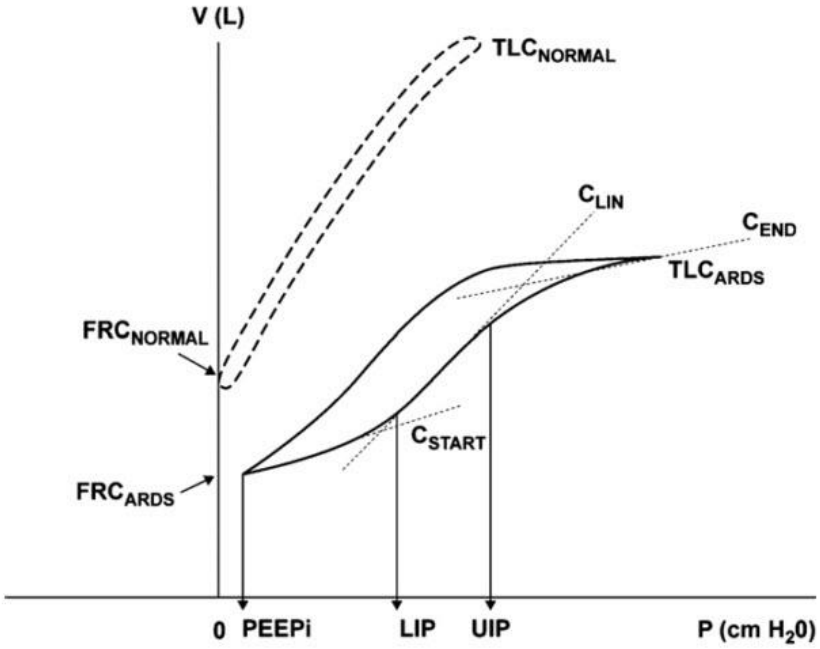

Figure 1.5 Pressure–volume (PV) loops for both normal subjects and those with acute respiratory distress syndrome (ARDS)
Both functional residual capacity (FRC) and total lung capacity (TLC) are decreased in ARDS. Additionally, the static PV loop for ARDS appears to demonstrate three distinct phases of compliance—starting compliance (C_{START}), a phase of linear compliance (C_{LIN}) and end compliance (C_{END}). The transitions between these three compliances are referred to as the lower inflection point (LIP) and the upper inflection point (UIP). With permission, from Henderson and Sheel.(90)

Pulmonary Mechanical Changes in ARDS

Alveolar consolidation (for example, due to pneumonia) and collapse leads to derecruitment of lung parenchyma in ARDS. This is reflected in decreased end expiratory lung volumes and increased respiratory system elastance. FRC may be decreased by as much as 45%, and is more variable, in mechanically ventilated ARDS patients than in healthy subjects due to derecruitment and atelectasis (86, 171). Much of our understanding of the pulmonary mechanical alterations in ARDS comes from evaluation of static pressure-volume curves generated from sedated or chemically paralysed patients with ARDS. In comparison to the PV loop created from a normal subject that from a patient with ARDS (Fig. 1.5, solid line) is clearly different. Significantly, the slope of the PV curve of the ARDS patient is significantly steeper, suggesting less compliant (or more elastant) lungs. Historically, the mechanical changes seen in ARDS were attributed solely to changes in lung parenchyma, and it was assumed that chest wall elastance was normal (155). It is now clear that in ARDS due to extrapulmonary causes (such as abdominal sepsis) changes in chest wall elastance contribute significantly to total respiratory elastance (65).

The large majority of research into pulmonary mechanics in ARDS has focused on abnormalities of compliance/elastance rather than changes in resistance (208). Interestingly, respiratory system resistance in ARDS increases three- to four-fold, primarily due to changes in the viscoelastic qualities of the lung (151, 189). However, it appears that there is a doubling of true airflow resistance, and that this is partly reversible with β-agonist bronchodilators (151, 189, 207).

Role of Ventilator Associated Lung Injury

Mechanical ventilation is a life-saving intervention in patients with ARDS, but it has been recognized for over fifty years that the high intrathoracic pressures used were associated

with lung parenchymal stress and injury ("barotrauma") (61, 107). Further research clarified that cyclic opening and closing of lung units ("atelectotrauma") and exposure of alveoli to supraphysiologic levels of mechanical stress ("biotrauma") were the mechanistic reasons for this observation. The development of new lung injury due to injurious ventilation is called ventilator associated lung injury (VALI). The histologic changes seen in VALI are extremely similar to those seen in ARDS; indeed, deliberate injurious ventilation (and thus VALI) is one method used to create experimental models of ARDS (129). ARDS appears to predispose lungs to the development of VALI (48, 91), and the two mechanisms of injury are often present in the same patient.

That ARDS and VALI appear similar and occur in the same patients is not a trivial consideration. A vast body of research has developed around therapeutic interventions for ARDS (179). The majority of this work has focussed on improved methods of mechanical ventilation. Some authors question whether these therapeutic interventions actually treat ARDS at all, but rather decrease the incidence of VALI. That is, all interventions to date simply reduce the rate of iatrogenic injury due to (necessary) mechanical ventilation, but do little to treat the initial injury (45, 197). To some degree this distinction may be academic, as the large majority of ARDS patients require mechanical ventilation to survive their illness, and advances in ventilation physiology that decrease the potential deleterious consequences of mechanical ventilation will benefit them.

Recognition of Anatomical Heterogeneity in ARDS and Impact on Clinical Management

Progress in the understanding of the physiology of ARDS has led to meaningful improvements in care over the last fifty years. Our conceptualization of ARDS has slowly evolved from one of regarding lungs during ARDS as being homogenously non-compliant to one

where there is recognition of substantial heterogeneity in the mechanical characteristics of lung tissue in different regions of the lung. This may be termed "anatomical heterogeneity." It is helpful to outline a general historical progression of recognition of the types of anatomical heterogeneity that are present in ARDS as:

i) Lack of recognition of heterogeneity
ii) Recognition that the lungs are "small" due to consolidation and atelectasis and require small tidal volumes
iii) Recognition that the decrease in lung size in ARDS is heterogenous and hard to predict
iv) Recognition of heterogeneity in the elastances of the lung and chest wall.

Lack of Recognition of Heterogeneity

Each new stage of recognition of anatomical heterogeneity has led to changes in management. For example, in the 1970s, ARDS was a well-recognized syndrome, but "the basis of the mechanical derangement of ARDS lungs is not clearly known" (152). ARDS was conceived of as a disorder where the lung was relatively homogenously non-compliant or "stiff". Tidal volumes of 12-14 ml/kg of body weight were prescribed with little recognition of the possibility that this level of lung distension might be injurious (62, 152). Indeed, as one leading clinician emphasized in 1972, "We ventilated thousands of patients in this way and the only side effect was hypocapnia" (156).

Recognition of Heterogeneity – Lungs are Smaller in ARDS than in Health

Over the next two decades it became increasingly clear that lungs during ARDS were "smaller" than in health due to atelectasis and consolidation (66). This led to the use of smaller tidal volumes during mechanical ventilation and more rigorous limitation of ventilating pressures (5, 31, 33, 184). The use of low tidal volumes during mechanical ventilation for lung injury has

led to improved clinical outcomes, presumably due to decreased alveolar distension and volutrauma (61). In a landmark study, tidal volumes were limited to 4 to 6 ml/kg of ideal body weight in an attempt to limit lung overdistension (8). However, others have argued that overdistension and cyclic recruitment-derecruitment of alveoli may still occur even with low tidal volumes in some patients (35, 191, 192), while ultra-low tidal volumes (4 ml/kg of ideal body weight or less) may decrease this phenomenon (164).

Recognition of Heterogeneity – Lungs are Unpredictably Smaller in ARDS

While limiting tidal volumes during mechanical ventilation has demonstrated benefit in decreasing ventilator associated lung injury, there is no clear limit below which further decreases will not improve outcomes (83). Previous trials have used a tidal volume prescription based on patients' ideal body weight. That is, lung volume was estimated from a calculation derived from patients' height. While estimates of lung volumes based on anthropometric data are moderately accurate in healthy populations, they are clearly not reliable in patients with ARDS. This has raised the possibility that many patients in these trials may have received tidal volumes that were still "large" in comparison to their actual lung sizes (127). Recent interest has developed in the use of measurements of FRC to predict safe tidal volumes in acute lung injury (ALI) and ARDS (39). FRC (which represents the amount of lung aerated at end-expiration) is theorized to better reflect the lung available to receive tidal breaths than is a standard, weight-based calculation (127).

Recognition of Heterogeneity – Elastance of the Components of Respiratory System Varies

The elastance of the respiratory system (E_{RS}) may be stated as:

$$E_{RS} = E_L + E_{CW}$$

During mechanical ventilation, P_{PLAT} represents the total pressure that distends the respiratory system at end-inspiration, such that:

$$P_{PLAT} = P_L + P_{PL}$$

Similarly(62), it may be seen that:

$$P_L = P_{PLAT} \times E_L/E_{RS}$$

or, restated, that:

$$P_L = P_{PLAT} \times E_L/(E_L+E_{CW})$$

In clinical practice, P_{PLAT} (pressure used to distend the respiratory system) is often used to estimate P_L (pressure used to distend the lung). This is a reasonable assumption when lung and chest wall compliance are normal, as pleural pressure will not be substantially greater than body surface pressure and E_L and E_{CW} each contribute half of E_{RS}. In this situation the E_L/E_{RS} ratio is 0.5.

Historically, the mechanical changes seen in ARDS were attributed solely to changes in lung parenchyma. It was assumed that E_{CW} did not vary substantially with ARDS (155) and that increases in E_{RS} during ARDS were due to changes in E_L. In this situation, P_L would continue to be predictable from P_{PLAT}. However, it has become clear that there is great variability of E_{CW} in ARDS, whether due to patient physique (obese and edematous patients have higher E_{CW} than other patients), intra-abdominal hypertension(147) or due to the inciting cause of ARDS (97, 102, 161, 186). In these situations, the E_L/E_{RS} ratio may vary widely, and P_L cannot be estimated from P_{PLAT} (64). Indeed, some investigators have suggested that measurement of pleural pressure

(with an esophageal balloon) to calculate P_L could be useful in titrating mechanical ventilation in ARDS (187).

Stress and Strain

Recent work has applied a bioengineering perspective to P_L and lung mechanics. To an engineer, *stress* is the net force acting on a surface divided by the surface area. That is:

$$\sigma = \sum_{n=1}^{\infty} F/A$$

where σ represents stress, F is a force acting on a surface, and A is the area of the surface. From the point of view of lung mechanics, stress reflects the difference between distending forces (for example, alveolar pressure) and collapsing forces (the pleural pressure in this case) and stress is therefore represented by P_L:

$$\sigma = P_L = P_{AW} - P_{PL}$$

The deformation of a structure by stress is called *strain* ("ε"), which is defined as the change in size or shape compared to the structure's initial shape or volume. Referring to Figure 1.6, ε is:

$$\varepsilon (x) = \Delta l/dl$$

With respect to lung mechanics:

$$\varepsilon = V_T / FRC$$

For example, if a lung is inflated with a 500ml tidal volume from an initial functional residual capacity (FRC) of 1000 ml, the strain associated with this is 0.5 (500ml/1000ml). The recommendation of a specific tidal volume for lung protective ventilation is predicated on the assumption that there is a uniform amount of lung able to receive the inspired volume. This volume is the amount of aerated lung at end expiration minus the FRC.

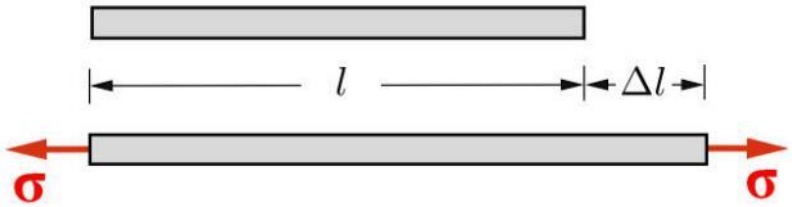

Figure 1.6 The dimensionless quantity ε is called strain
If, for example, a bar of the length l = 1 m undergoes an elongation of Δl =0.5 mm by the application of a stress (σ). In this example, $\varepsilon = 0.5 \times 10^{-3}$ (5mm/1000mm). With permission, from Gross, et al.(76)

Underlying this is the assumption that FRC can be predicted by ideal body weight – an assumption that is not correct in injured lungs (127). It is therefore understandable that, given the same ideal body weights and tidal volume prescriptions, two patients with ARDS might have significantly different calculations of lung strain if they have different FRCs. It therefore may be prudent to attempt to minimize strain during mechanical ventilation by measuring FRC and titrating tidal volume to this assessment rather than ideal body weight. From a practical point of view however, it is time consuming and laborious to measure FRC in a serial fashion. While there are commercially available FRC measurement systems available either as stand-alone systems or integrated into mechanical ventilators, the cost of these systems in not insignificant. Fortunately, it is possible to estimate strain from measurements of stress, as the two values are linked by a constant. Indeed, Hooke's Law states that:

$$\varepsilon = \sigma / M$$

where M is a constant (Young's Modulus in the case of engineering). In the specific case of lung mechanics, Young's Modulus is replaced by the specific elastance of lung (E_{Lspec}) such that:

$$\varepsilon = \sigma / E_{Lspec}$$

The value of E_{Lspec} is fairly constant throughout health and disease, with a value of approximately 13 cmH_20 (62, 167). Thus by measuring stress, strain may be inferred (i.e. approximately $1/13^{th}$ of stress).

Safe Stress and Strain Limits

There is some evidence that maintaining strain within specific limits may improve clinical and biochemical markers of lung parenchymal injury. For example, Protti et al. (2011) demonstrated that in pigs, mechanical ventilation with strains greater than 1.5-2 were associated with the development of VALI. Similarly, In an observational human study, patients with ARDS and high strain showed a fourfold increase of IL-6 and IL-8 concentrations in bronchalveolar lavage fluid, compared with patients with ARDS and normal strain (71).

Regional Temporal Heterogeneity (Time Constant Heterogeneity)

The awareness of anatomical heterogeneity in ARDS has led to meaningful improvements in patient care. The use of small tidal volumes, PEEP, assessment of FRC and the calculation of stress and strain have gained adoption in the clinical management of ARDS. Unfortunately, all of these measures are "whole lung" measurements, and none account for the local heterogeneity of mechanical characteristics found in injured lung. It is therefore possible that susceptible lung units are subject to critically injurious forces even when global measures of volume, pressure, stress and strain appear acceptable (133).

Imaging and autopsy research has demonstrated that the lung parenchymal injury in ARDS is patchy, or heterogeneous, in distribution. Some lung regions have severely abnormal values of resistance and/or compliance, while others may have values that are similar to those found in healthy lung. When gas flows into a lung unit, the time required to fill the unit depends

on the local compliance and resistance. Units with high resistance will take longer to fill because the flow will be reduced. Similarly, units with high compliance will take longer to fill because they will require more gas volume than less compliant units. The product of the resistance and compliance (R_{AW} x C_L) of a lung unit is the time constant (τ or *tau*) and represents the time required for the lung unit to fill to 63% of the final volume if a constant pressure is applied. Areas of the lung with short time constants (i.e., low resistance and/or low compliance) will fill more rapidly than areas with larger time constants. An analogous relationship between time constants and time to complete expiration exists – units with long time constants take longer to completely empty than do units with short time constants. Local variation in resistance and compliance between regions of lung tissue implies heterogeneity in inspiratory and expiratory time constants (τ_I and τ_E, respectively). If their τ differ, adjacent lung units may inflate and deflate at different rates. This may be termed "temporal" heterogeneity.

Regional and temporal heterogeneity in τ_E may have meaningful consequences in injured lung by: i) creating lung regions with higher or lower strain and normal stress than is evidenced by whole lung measures, or ii) creating zones of high shear stress between lung regions that fill or empty at different rates.

Consequences of Temporal Heterogeneity – Regional Amplification of Normal Stress and Normal Strain

It is an assumption of the strain and normal stress models described previously that lung tissue during mechanical ventilation is *isotropic* – that is, its mechanical properties are invariant with respect to the axis of measurement. In isotropic lung, the application of force causes strain and stress to be evenly distributed throughout the lung. The situation is different in injured lung where large deviations from isotropic conditions may occur.

Injured lung, with heterogenous mechanical properties, will have lung units with higher than average resistance and/or compliance that will require a longer than average inspiratory time to fill completely. If the inspiratory time during mechanical ventilation is shorter than the time required to fill these alveoli, their intra-alveolar volume at end-inspiration will be lower than the average for the lung. Similarly, if the expiratory time set during mechanical ventilation is shorter than that required for complete alveolar emptying, lung units with long τ_E will accumulate gas over time and develop a higher end expiratory pressure or volume than is average for the lung as a whole. In this situation, some lung regions will be overdistended, and some underdistended (or completely collapsed) throughout the respiratory cycle due to heterogeneity in their τ_I and τ_E. When this occurs, stress and strain are no longer homogenously distributed throughout tissue, but are rather concentrated around the areas of relative collapse or derecruitment (63). In a classic experiment, Meade and colleagues demonstrated that when one of two neighbouring lung units decreases elasticity (due to collapse or consolidation to 10% of its original volume) the stress of the open unit increases by a factor of 4.57 (133). Thus, in the example of two initially homogenous neighbouring units, each with a stress (P_L) of 30 cmH_2O, altering the volumetric ratio of the two units from 1:1 to 10:1 might concentrate stress in the normal unit to 140 cm H_2O, despite whole lung measurements of stress and strain that were well within acceptable limits. These theoretical calculations have largely been confirmed in a recent tomographic microscopy study using rat alveoli to determine true tissue strain during lung unit heterogeneity (163). Unfortunately, current bedside assessment of pulmonary mechanics typically provides only whole lung measurements of stress and strain and is silent with respect to their regional heterogeneity.

Consequences of Temporal Heterogeneity – Generation of Regional Stress and Strain

The discussions presented so far in this thesis have referred only to *normal* stress, where the vector of the force applied is perpendicular to the surface it acts upon. In this situation, net stress will create a volume change ("*normal* strain"). However it is possible for isovolumetric distortion of tissue to occur when forces are applied at an angle to the surface in question. To understand this, it is necessary to completely quantify the stress state at point P by three Cartesian stress vectors through P, each perpendicular to the others. The three sections can most easily be visualized if we imagine them to be the surfaces of a block of tissue with edge lengths dx, dy and dz at point P (Figure 1.7). Each stress vector acts on each of the tissue block's six surfaces and can be decomposed into those components perpendicular to the section (*normal* stress) and those tangential to the section (called *shear* stresses or Ψ)**. Shear stresses can be decomposed into sub-components, which are denoted by double subscripts: the first subscript indicates the orientation of the section by the direction of its normal vector whereas the second subscript indicates the direction of the stress component. For example, If we denote normal stress with the symbol σ, and shear stress with the symbol Ψ, then Ψ_{yx} is a shear stress acting in a section whose normal stress points in y-direction; the shear stress itself points in x-direction (Fig. 1.8).

** By convention, engineering uses the symbol "τ" to represent shear stress. However, in respiratory physiology, τ is widely understood to represent the concept of time constants. As this thesis deals primarily with respiratory physiology, I have retained the physiology rather than the engineering convention and have used τ to represent time constants and "Ψ" to represent shear stress.

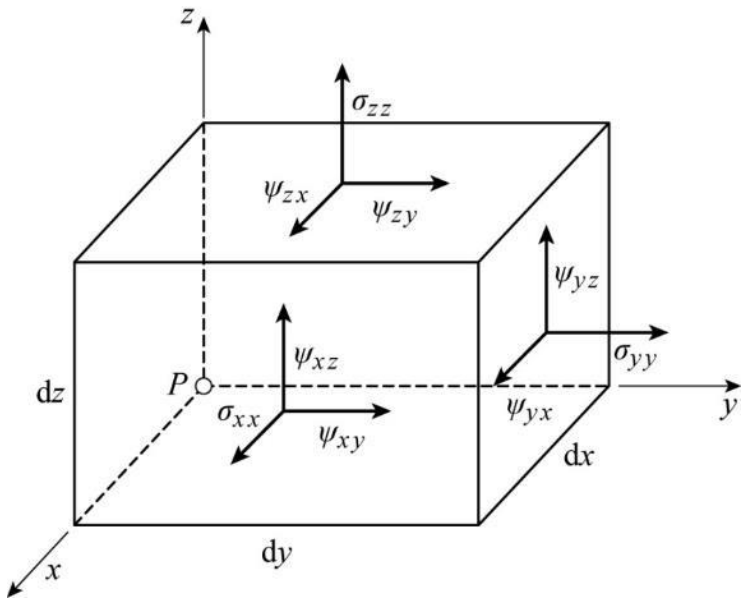

Figure 1.7 Idealized depiction of the normal stresses and shear stress acting on a block of material

By means of the decomposition of the three stress vectors into their components we have obtained three normal stresses (σ_{xx}, σ_{yy}, σ_{zz}) and six shear stresses (Ψ_{zy}, Ψ_{xz}, Ψ_{yx}, Ψ_{yz}, Ψ_{zx} and Ψ_{zy}). When there are net shear stresses acting on lung, tissue deformation will occur – *shear* strain (γ). For example, consider an isotropic lung tissue plane SPQR that is deformed to S'P'Q'R' – a plane with the same area, but a different shape (Figure 1.9). While no normal strain has occurred in this situation (that is, no change in area) it is obvious that the application of force (shear stresses) have changed the shape of the plane. The degree to which the plane has been deformed may be quantified by the *normal* strains in the x and y axes and the *shear* strains.

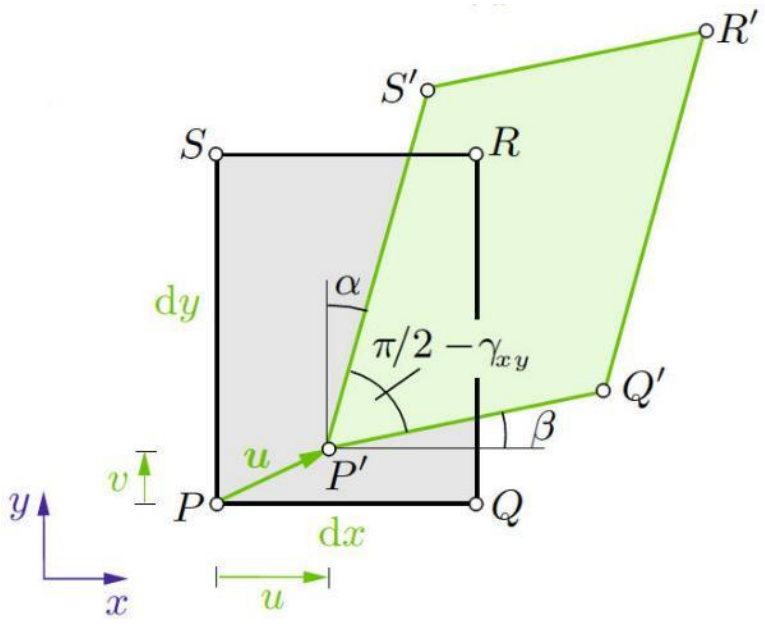

Figure 1.8 Depiction of the calculation of shear strain (γ) created in a plane of material due to the application of shear stresses.
With permission, from Gross, et al. (76)

The normal stains can be calculated by using partial differential equations of the change in length in the x and y axis (u and v, respectively) compared to the original length in the x and y axis:

$$\varepsilon_x = \partial u/\partial x \quad \text{and} \quad \varepsilon_y = \partial v/\partial y$$

The shear strain may be quantified by the sum of the changes in angles in the x and y axes:

$$\gamma_{xy} = \alpha + \beta = \partial u/\partial x + \partial v/\partial y$$

As previously described in this section, normal stress and normal strain are linked by Hooke's Law through the constant of Young's Modulus (M):

$$\varepsilon = \sigma/M$$

Similarly, shear stress and shear strain may be linked by Hooke's Law. However, rather than Young's Modulus, they are linked by the shear modulus (G):

$$\Psi = G\gamma$$

Effect of shear forces in lung tissue

The alterations in surfactant function and the presence of regional transpulmonary stress concentrations in ARDS lead to cyclic recruitment and derecruitment of alveoli during mechanical ventilation. The shear stresses associated with this regional heterogeneity of lung unit volume change has been demonstrated to lead to injury to alveolar epithelial and endothelial cells as well as ultrastructural changes (47, 57, 95). Similarly, the cyclic opening of collapsed/edematous distal airways during mechanical ventilation in ARDS models leads to severe cellular injury to airway epithelial cells (25).

Measurement of in vivo shear forces

The association of normal strain and stress with injury in in injured lung at the whole lung level has been explored. Indeed, the clinical use of bedside measures of whole lung stress and strain to manage mechanical ventilation in lung injury and ARDS is now common. However, relatively little attention has been paid clinically to regional heterogeneity in normal stresses/strains or to shear stresses/strains. In part, this may be due to technical limitations in our ability to assess shear forces in live subjects. For example, past investigations have determined values for E and G in *ex vivo* models (108, 141, 172, 183). More recently, innovative techniques have allowed the exploration of lung mechanical properties *in vivo*, including shear forces, through the use of image registration analysis using CT (6, 180, 209, 210) and magnetic resonance imaging (MRI) (37, 120) as well as subpleural microscopy (178) in animal models. Unfortunately, the literature is largely silent on the measurement of shear forces in human patients, particularly those with ARDS. This is partly due to the fragility of these patients – which may preclude invasive techniques such as subpleural microscopy and transportation for MRI or CT imaging, and also due to reticence in the use of ionizing radiation in human patients.

If regional stress, strain and shear are generated in part due to regional time constant heterogeneity, it follows that assessment of time constant heterogeneity may prove some insight into the degree of lung tissue expansion heterogeneity and thus shear force generation. For example, if changes in τ could be demonstrated to correlate with changes in ε, σ, Ψ and γ, and that manipulations that alter τ also alter ε, σ, Ψ and γ, then it is plausible that easily obtained bedside clinical information (to generate τ heterogeneity measurements) could guide interventions that decrease normal and shear stress and strain in injured lung.

Measuring time constant heterogeneity

Interventions that decrease τ heterogeneity may offer the possibility of decreasing the severity of these areas on asymmetrical tissue ε, σ, Ψ and γ and thus may confer a decreased risk of developing VALI. The slope of the flow-volume curve during passive expiration has been used to describe τ_E (1, 132, 216, 217). Other methods to assess τ_E include calculating the ratio of peak expiratory flow and volume exhaled (36) and multiplying respiratory system resistance and compliance as measured by the interrupter technique (73, 74). Common to all of these techniques is the assumption that a single compartment model can accurately describe the entirety of passive expiratory gas flow despite evidence that there is meaningful regional variation in ventilation in healthy lungs (202). The "single compartment assumption" may be invalid in healthy lung due to the non-linear nature of compliance and resistance (50, 59, 94) . Similarly, a linear single compartment model poorly describes pressures, volumes and flows within lungs during acute respiratory distress syndrome (ARDS), where significant mechanical and structural heterogeneity are present. Lungs units ARDS are characterized by greater heterogeneity of distension (135, 143, 177), as well as more variation in resistance and compliance (50, 98, 100) than are healthy lung units. Lung units with long time constants will be represented by a later portion of the

expiratory flow-volume curve than will those with short time constants. A single τ_E measure based on the single compartment model will not reflect the mechanical conditions of either. A method of differentiating the τ_E of faster emptying lung units from those of slower emptying units would allow the quantification of τ heterogeneity within the lung.

Numerous investigators have estimated τ_E using time-dependent or non-linear models in ARDS and chronic lung disease (81, 106, 118). To date, no link has been directly made between τ heterogeneity and heterogeneity of ε, σ, Ψ and γ within the lung. The purpose of this thesis was to begin to explore the links between τ_E and ε and to describe methods that may alter the variability of τ_E in healthy and injured lungs. It is my hope that this will lay some of the groundwork needed for future studies investigating the inter-relations between τ_E, ε, σ, Ψ and γ within the lung. In this thesis I evaluated regional expiratory time constant (τ_E) heterogeneity and regional ε in a lung model using a novel method of functional respiratory imaging (FRI) (Study 1, Chapter 2), and then developed an *in vivo* porcine model of acute respiratory distress syndrome (Study 2, Chapter 3) with which to assess changes in τ_E heterogeneity due to manipulations of respiratory gas density (Study 3, Chapter 4) and mechanical ventilation parameters (Study 4, Chapter 5). The value of this series of studies is to provide evidence that: 1) FRI can be used to provide meaningful data regarding regional ε and τ_E; 2) in injured and healthy lungs, τ_E may be inferred from a non-invasive, passive set of data that is obtainable at a patient's bedside; 3) τ_E and the pattern of τ_E in a multi-compartment model may be altered by the manipulation of resistance to gas flow and of mechanical ventilation parameters. These studies

have value as they will lay the groundwork for further work demonstrating the clinical utility of measuring τ_E in patients.

Summary

ARDS is characterized by variable degrees of alveolar epithelial and endothelial injury and surfactant dysfunction that lead to lung parenchymal atelectasis, diffuse alveolar damage and hypoxia. The recognition of the role of anatomical heterogeneity in ARDs has led to improvements in clinical care and outcomes. Similarly, applying an engineering perspective to the roles of transpulmonary stress and strain has provided valuable insights into the management of these patients. Unfortunately, none of these conceptualizations of ARDS have allowed the quantification of regional and temporal heterogeneity in lung mechanics. Specifically, the assessment of regional stress and strain forces within the lung is difficult with currently available imaging and measurement techniques in human subjects. The assessment of time constant heterogeneity may allow the bedside evaluation of strategies to mitigate the deleterious effects of regional strain heterogeneity and the subsequent shear forces in injured lung. The central goal of this thesis is to provide evidence that changes in time constant heterogeneity may be used as a proxy for changes in regional lung strain heterogeneity and to demonstrate how time constant heterogeneity is affected by interventions that may be applied in clinical management of ARDS.

Purpose

The purpose of this thesis was to evaluate regional heterogeneity of pulmonary mechanical values within models of lung injury. To this end four separate studies were completed. To this end, I developed a program of experiments with four main goals:

1. To demonstrate in a cadaveric animal model that changes in time constant heterogeneity and regional strain can be measured non-invasively using FRI, and that interventions that alter τ_E also alter regional ε.
2. To characterize a novel large animal model of ARDS due to epithelial injury.
3. To characterize the effects of changes in V_T and PEEP on lung emptying during passive deflation before and after experimental lung injury using a multi-compartment model to describe τ_E.
4. To characterize the effects of changes in respiratory gas density and air flow resistance on lung emptying during passive deflation before and after experimental lung injury using a multi-compartment model to describe τ_E.

Research Questions

1. Does altering PEEP alter regional ε and τ_E values (characterized by FRI) in a cadaveric lung model?
2. Does the administration of intratracheal sodium polyacrylate (SPA) create an experimental model of ARDS that demonstrates the physiologic and histologic features of early human ARDS due to alveolar epithelial injury and surfactant dysfunction?
3. Does altering tidal volume or PEEP in a large animal model of ARDS alter the pattern of τ_E before or after injury?
4. Does altering gas density in a large animal model of ARDS alter the pattern of τ_E before or after injury?

Hypotheses

1. Altering PEEP alters regional ε and τ_E values (characterized via FRI) in a cadaveric lung model.
2. The administration of intratracheal SPA creates an experimental model of ARDS that demonstrates the physiologic and histologic features of early human ARDS due to alveolar epithelial injury and surfactant dysfunction.
3. Alterations in tidal volume or PEEP alter the pattern of lung emptying and τ_E values before and after experimental lung injury.
4. Alterations in respiratory gas density and resistance to airflow alter the pattern of lung emptying and τ_E values before and after experimental lung injury.

Chapter 2: Functional Respiratory Imaging, Regional Strain and Time Constants at Three Peep Levels in an Ex-Vivo Animal Model

Introduction

Acute respiratory distress syndrome (ARDS) is a complex lung injury characterized by hypoxemia, impaired pulmonary mechanics and alveolar flooding (124). The mainstay of treatment is intubation and supportive mechanical ventilation. Current best practice assigns and assesses treatment based on indices of oxygenation or on aggregate measures of pulmonary function such as pressure volume curves or transpulmonary pressure (34, 70, 79). While pragmatic, these strategies do not account for regional variation in lung tissue mechanics (51, 92, 98, 100, 113, 135, 143, 177). Strain (ε) is the ratio of tidal volume (V_T) to functional residual capacity (FRC). High strain levels have been associated with new ventilator associated lung injury (VALI)(158). The heterogeneity in regional FRC due to atelectasis may lead to variations in regional ε that are not revealed by whole respiratory system measurements.

Similarly, the ratio of the resistance to elastance (R/E) of a lung unit during expiration is the expiratory time constant (τ_E or *tau*). Differential rates and inflation/deflation of adjacent lung units due to regional variation in τ_E may create localized regions of strain that are significantly greater than implied by whole lung measures of pressure or strain (98, 133, 149) Additionally, regional heterogeneity in τ_E may have clinical consequences in diseases such as asthma and chronic obstructive lung disease (COPD) by creating lung regions that are unable to completely fill or empty, thus predisposing patients to hypoxia, hypercapnia or the development of local gas trapping (121).

Currently, the measurement of regional variation in ε and τ_E is difficult to assess because it often relies on specialized technology (27, 169). Thin section computed tomography (CT) has proven useful in the assessment of airway and lung parenchymal structure (14, 30). In recent studies, the static images have been assessed using computational fluid dynamics (CFD) (14). To achieve this, numerical flow equations (Navier-Stokes equations) are solved using a computational grid and have historically required patient-specific models and boundary conditions (13, 110). The result of a CFD computation is a description of volume, pressure and flow characteristics throughout the entire respiratory system termed functional respiratory imaging (FRI). This validated approach (14) was proven to be more sensitive than classical lung function (15, 199) and has provided novel insights in the mode of action of hard to evaluate aerosolized compounds (16).

The purpose of this study was to describe the use of FRI with an *ex vivo* pig lung model to: i) demonstrate that CT based imaging studies can be used to assess global and regional values of ε and τ_E and, ii) demonstrate that the manipulation of positive end expiratory pressure (PEEP) will cause changes in total and regional ε and τ_E values.

Methods

Ex-vivo lung preparation

Five adult female Yorkshire X pigs were quarantined for one week prior to the experiments. All experiments were approved by the Animal Research Committee of the University of British Columbia, Vancouver, British Columbia and conformed to the policies and guidelines of the Canadian Council on Animal Care.

Anesthesia was induced by inhalation of isoflurane 3-5% in oxygen. Following tracheal intubation (9 mm internal diameter), total intravenous anesthesia was established with midazolam (0.1mg/kg IV bolus) and a propofol infusion (started at 200 mcg/kg/min and adjusted to between 150 and 300 mcg/kg/min) and inhalational anesthesia was discontinued. Subjects were mechanically ventilated (Puritan-Bennett 7200, Covidien, Ireland) with 0 cm H_20 of positive end expiratory pressure (PEEP) using a fraction of inspired oxygen (FiO_2) of 0.5, tidal volumes (V_T) of 12 cc/kg of body weight and an breathing frequency (fb) of 10-12 breaths/minute. Fb was adjusted to maintain an end tidal CO_2 ($ETCO_2$) measurement of 35-45 mmHg. Inspiratory flow rates were held constant at 45 L/minute. All subjects underwent minimally invasive intra-abdominal surgeries for training purposes. At the end of six hours of mechanical ventilation, subjects were euthanized using pentobarbital sodium (120 mg/kg intravenous). The lungs and trachea were removed *en block* through a sternal incision and an endotracheal tube (9.0 mm internal diameter) was placed into the trachea. The lungs and trachea were suspended from a non-metallic scaffold inside of a computerized tomography (CT) scanner (Aquilion One Volumetric CT scanner, Toshiba Medical Systems, Tustin, CA, USA).

The lungs were then initially ventilated (Puritan-Bennett 7200, Covidien, Ireland) with 0 cm H_20 of PEEP using a fraction of inspired oxygen (FiO_2) of 0.21, tidal volumes (V_T) of 6 cc/kg of body weight and a breathing frequency (fb) of 12 breaths/minute. Inspiratory and expiratory flows ($\dot{V}_I$ and $\dot{V}_E$) were measured using a heated pneumotachograph (Model 3813, Hans Rudolph, Kansas City, MO) placed between the ventilator tubing wye and the proximal end of the endotracheal tube. The pneumontachometer had previously been calibrated with a 2 L calibration syringe. Inspiratory flows were constant at 45 L/min with a square waveform. Inspiratory and expiratory volumes (V_I and V_E) were obtained by numerical integration of the

flow signals. Tracheal pressure (P_{TR}) was measured using a fenestrated polyethylene catheter placed 1 cm past the distal end of the endotracheal tube. The $P_{TR,}$ pressures were measured using a calibrated piezoelectric pressure transducer (Raytech Instruments, Vancouver, BC, Canada) and referenced to atmospheric pressure. An integrated 16-channel data acquisition and recording system (PowerLab/16SP model ML 795 and Chart v7, ADI, Colorado Springs, CO) was used to collect and record all data at a sampling frequency of 200 Hz.

Intervention

The lungs were ventilated as described above with PEEP of 0, 5 and 10 cm H_2O. The order of PEEP levels was randomly assigned, and 10 minutes of ventilation at each PEEP level occurred prior to recording imaging and physiological data.

Image acquisition and processing

All lungs underwent dynamic CT imaging during passive inspiration and deflation on the mechanical ventilator. CT imaging was performed with the lung suspended in the upright position. The CT settings were as follows: tube voltage, 120 kV; tube current, 200 mAs; rotation time, 0.35 sec; field of view, 400.4 mm; slice thickness, 0.50 mm; pixel spacing 0.782 mm; and convolution kernel, FC51. The images were acquired without moving the table (pitch: 0) and the acquisition began immediately prior to lung inflation and concluded after complete cessation of gas flow following passive deflation.

CT scan data was converted into 3D models of airways and lung lobes using Mimics (Materialise, Leuven, Belgium) a previously validated software package (Food and Drug Administration, K073468; Conformité Européenne certificate, BE 05/1191.CE.01). Airways were segmented using directional thresholding with automated leakage detection. Lungs were split into lobes by identification of the fissure lines from the CT scan. For both airway and lung

lobe segmentation manual updating of the automated algorithms was performed when needed. Lungs lobes and the respiratory tract could be extracted at several time points during inspiration and expiration (Figures 2.1 and 2.2). For data analysis used the end-expiratory scan for both lobar and airway analysis and the end-inspiratory scan for lobar analysis only.

We identified lobes as: right and left anterior lobes (RAL and LAL), right and left caudal lobes (RCL and LCL), right and left diaphragmatic lobes (LDL and LDL) and right internal lobe (RIL) (Figure 2.1). Airways were trimmed perpendicular to the local centerline in order to prepare the model for CFD airflow analysis. Airway models were split into a central part and airways leading to each previously defined lobe (Figure 2.2).

Calculation of strain and time constant values using computerized tomography data

Using the derived 3D lobar models, we calculated the volume of each lobe at end-inspiratory lung volume (EILV) and end-expiratory lung volume (EELV). Regional ε for each lobe was calculated as (EILV-EELV)/EELV using the appropriate lobar volumes. Thus, for example, the ε of the RDL (ε_{RDL}) was calculated as ($EILV_{RDL}$-$EELV_{RDL}$)/$EELV_{RDL.}$ Total respiratory system EELV ($EELV_{RS}$) and EILV ($EILV_{RS}$) were calculated by adding the lobar volumes. Total respiratory system ε, called $\varepsilon_{RS,}$ was calculated as ($EILV_{RS}$-$EELV_{RS}$)/$EELV_{RS}$.

Expiratory time constants were defined as R divided by E. Resistance was defined as the total pressure drop needed to drive flow through an airway section. Regional airflow can be obtained from the total airflow (($EILV_{RS}$-$EELV_{RS}$)/time of deflation) combined with the internal airflow distribution calculated on a lobar basis by: ($EILV_{RDL}$-$EELV_{RDL}$)/($EILV_{RS}$-$EELV_{RS}$). Expiratory laminar, steady CFD calculations were carried out using velocity inlets (inlet velocity = flow rate through region / total area of inlet in the region) at the terminal bronchi and a pressure outlet (total pressure = PEEP) at the trachea. From the CFD calculation the pressure

drop over each specific lobar region was obtained. Elastance was defined as the pressure change needed to obtain a known volume. The volume change was given by EILV-EELV and the pressure change was the pressure drop in the trachea throughout deflation.

Statistical measures

For lobe-specific models, lobe, PEEP and their interaction were included as main effects with a random effect for pig included to account for the possibility of intra-animal correlation. Testing for significance of fixed effects was done with F-Tests and type III sums of squares. Total lung measurements were not included in lobe-specific models and were modeled separately using a similar approach. All testing of differences in least squared means was adjusted for multiple comparisons using the Tukey-Kramer method.

Separate mixed effect models to assess the relationship between τ_E and ε were fit for each lobe and for the total lung so that separate R^2 values could be obtained. Each model included τ_E as the response, ε as the predictor, and a random effect for each animal. The pseudo-R^2 value $R^2_{LMM(m)}$, proposed by Nakagawa and Schielzeth for mixed effects models (137), was used for each lobe and for the entire lung, where $R^2_{LMM(m)}$ measures the proportion of the variance of τ_E explained by ε based on the fitted mixed effect model. $R^2_{LMM(m)}$ values of 1 indicate perfect correlation between τ_E and ε, while a value of 0 indicates no correlation between them. The measurement for Pig 2 at PEEP 5 in lobe RAL was excluded from analysis because expiratory volume exceeded inspiratory volume for this observation. Testing the significance of the relationship between τ_E and ε was performed with F-tests and type III sums of squares, and the Benjamini-Hochberg significance level was used to determine if the relationship between τ_E and ε was statistically significant while adjusting for multiple comparisons.

Results

Global resistance, elastance, strain and time constants

When considering the whole respiratory system using FRI, all variables were affected by PEEP ($p<.05$ for R, E, ε and τ_E). Estimated least squares mean values for these parameters can be found in Figure 2.3. After adjusting for multiple comparisons, R at PEEP 0 was significantly higher than at PEEP 10 ($p<.05$). Elastance was significantly higher at PEEP 10 compared to PEEP 0 and 5 ($p<.01$), strain was significantly higher at PEEP 0 than at PEEP 5 or 10 ($p<.05$) and τ_E at PEEP 0 and 5 was significantly higher than at PEEP 10 ($p<.05$).

Regional resistance, elastance, strain and time constants

In the model including lobe, R was affected by PEEP, lobe, and the interaction of PEEP and lobe ($p<.0001$); higher PEEP resulted in reduced resistance, but the effect of PEEP on R was significantly different from lobe to lobe. Detailed data regarding R values per lobe are in Table 2.3. Specifically, R in LAL was significantly different from all other lobes ($p<.0001$) and R at PEEP 0 was significantly higher than PEEP 5 and 10 ($p<0.01$).

Elastance was different for different levels of PEEP and lobe ($p<.01$, $p<.0001$), but the interaction was not significant ($p=0.18$); the relationship between PEEP and lobe was similar for all lobes. However, some specific differences did exist: E in RAL was significantly higher than in LAL, LCL, LDL, RCL and RDL ($p<0.01$) and was greater in RIL than in LDL and RDL ($p<0.01$). In addition, E was significantly higher at PEEP 10 than at PEEP 0 or 5 ($p<0.05$). Detailed data regarding E values per lobe are in Table 2.4

Strain was affected by PEEP and lobe specifically but not by the interaction of PEEP and lobe ($p<.0001$, $p<.05$, and $p=.57$, respectively). RAL was found to be significantly different from LAL and RDL with respect to ε ($p<.05$). Strain was highest at PEEP 0 compared to 5 and 10

(p<.0001) and was also higher at PEEP 5 than at PEEP 10 (p<0.05). Table 2.1 includes the model-adjusted means along with 95% confidence intervals of ε for each lung lobe and the entire lung at the different levels of PEEP.

Consistent with the relationship of τ_E to R, τ_E values were affected by PEEP, lobe, and the interaction between PEEP and lobe (p<.01, p<.01, interaction p<.05). The values of τ_E in LAL were also significantly higher than in all other lobes (p<.05) and τ_E was higher at PEEP 0 than at PEEP 5 or 10 (p<.05). Table 2.2 includes the model-adjusted means along with 95% confidence intervals of τ_E for each lung lobe and the entire lung at the different levels of PEEP.

Relationship between strain and time constants

After adjusting for multiple comparisons, there was evidence of a relationship between tau and strain in lobes LAL, LCL, RAL, RCL and RIL (p<0.01, Benjamini-Hochberg significance level 0.03). The pseudo-R^2 between tau and strain was high in lobes LCL and RAL ($R^2_{LMM(m)}$>0.9), moderate in lobes LAL, RCL and RIL (0.4<$R^2_{LMM(m)}$>0.9) and low in lobes LDL, RDL and in the total lung measurement ($R^2_{LMM(m)}$<0.2).

Discussion

There are three main findings in this study. First, FRI can be used to reveal differences between global and regional values of R, E, ε and τ_E. This technique may provide significant real time insight into lung mechanics. Of importance, image based measurements reveal regional variation that cannot be detected by traditional methods such as spirometry. Second, the manipulation of positive end expiratory pressure (PEEP) causes changes in regional and global ε and τ_E values. Finally, regional ε and τ_E were correlated in several lobes, suggesting the

possibility that regional τ_E could be used as a surrogate marker for regional ε in clinical decision making.

Global and regional strain with functional respiratory imaging

Recognition of the deleterious effects of large V_T during mechanical ventilation has increased over the last twenty years, with recommendations to both V_T in an attempt to minimize ε_{RS}. More recently, work by Chiumello (39) and Protti (158) have shown that ε_{RS} is a primary driver of VALI and that V_T is a poor surrogate for ε_{RS} (62, 71, 173). The estimation of functional residual capacity (FRC), when combined with the measurement of the inspired/expired volume has been used for the bedside calculation of $\varepsilon_{RS.}$ More recently, CT and MRI image registration studies have measured end-inspiratory and end-expiratory lung volumes and have used this data to calculate ε_{RS}. Indeed, the techniques described in this experiment allow the calculation of ε_{RS} in this fashion (Figure 2.3, Panel A). The ε_{RS} in the current experiment were relatively low. Previous work has suggested that ε_{RS} greater than 1-1.5 may cause new lung injury in a pig model and the low ε_{RS} seen in our data is consistent with the lung protective effects of low tidal volumes noted in previous studies of mechanical ventilation. ε_{RS} decreased with increasing PEEP (Figure 2.3, Panel A), an observation that has been previously documented and which was due to increased $EELV_{RS}$ in our experiment (28). More important than the fact that the techniques described in our study allow the measurement of ε_{RS}, is the ability to observe regional strain in real time. Inspection of Table 2.1 demonstrates that individual lobes had ε values that varied from approximately one third to twice the measured ε_{RS}. Statistical analysis of our data confirmed this impression, demonstrating that both PEEP and lobe

can independently change the strain measured in individual lobes. The clinical implications of this interlobe variability may be clinically relevant. For example, clinicians may use whole respiratory system measurements (such as ε_{RS}) in an attempt to minimize new lung injury during mechanical ventilation, but may unwittingly still subject some lung regions to high ε levels. This could occur, because some regional ε may be much higher than global values suggest. Heterogeneity in regional ε has previously been observed using methods such as CT scans, electrical impedance plethysmography and forced oscillation techniques supporting the regional variation documented in this experiment (42, 100, 159, 206).

Global and regional time constants with functional respiratory imaging

During passive expiration, τ_E conveys information about pulmonary mechanics that may guide therapy (4, 115). We calculated expiratory values τ_E using a novel method of FRI. When calculated as a single unit (τ_{ERS}) expiration was more rapid with increases in PEEP (Figure 2.3, Panel B). The decreases in τ_{ERS} seen were due to decreases in R, rather than increases in E (See Supplementary Tables 2.1 and 2.2). Significant interaction terms indicate that R and τ_E are differentially affected in specific lobes at different levels of PEEP. The findings of significant differences in the means in the total lung at different levels of PEEP agree with the results from the lobe model, with the directions of the effect of PEEP being the same in both models. It is useful to compare our results with those of other investigators. Kondili and colleagues observed that the addition of PEEP decreased R and $\tau_{ERS,}$ while Pesenti and colleagues found that PEEP increased R_{RS} (and by implication τ_{ERS}) (106, 150). One result of the application of PEEP is that small airways are "splinted" open, and are less likely to close prematurely. The increased

patency of small airways may allow more rapid exhalation, thereby resulting in smaller τ_E values with higher PEEP, particularly in late expiration.

Historically, methods of measuring τ_E were limited to whole lung measures and assumed that the lung is isotropic and are unable to address regional differences in lung mechanics. Kaczka and colleagues have demonstrated that regional values of R and E (and by implication, regional values of τ_E) may vary with both ventilation frequency and pressure (99). Similarly, our data demonstrate that there is substantial variation in τ_E between lobes and that this variation is not well represented by the global measure (τ_{ERS}). The significant interaction terms seen in our statistical model indicate that both PEEP and lobe affected τ_E in the per lobe analysis (Table 2.2). The clinical implication of this finding is that some lobes may require significantly longer to fill or empty than τ_{ERS} would suggest, potentially leading to areas of shunt or deadspace. This raises that possibility that a clearer understanding of the regional variation in τ_E could guide clinicians in modifying the parameters of mechanical ventilation used in patients with significant regional variation in τ_E.

Correlation between strain and time constants

The correlation between tau and strain was very strong in lobes RAL and LCL, but was weak for the total lung and reflects that heterogeneous nature of the relationship between tau and strain in the different lobes. This finding provides some support for the idea that regional τ_E variation could be a useful surrogate for regional ε variation. However, this possibility requires significant clarification in future studies before it has clinical utility.

Limitations

The current study demonstrates the potential utility of FRI to measure regional heterogeneity in both ε and τ_E, but some potential limitations should be acknowledged. First, the current study used cadaveric lungs that were not contained within a chest wall. In this situation both EELV and total system elastance will be lower than in intact subjects. These factors will increase strain measurements (particularly in the zero PEEP condition) and lengthen τ_E values as compared to live animals. Second, in the current experimental set up, the lungs were suspended vertically as opposed to horizontally. This may have altered the interlobar strain distribution as compared to intact subjects.

Conclusions

Functional respiratory imaging may be used to calculate real time values of ε and τ_E, pulmonary mechanical parameters that may be used to guide clinical care. Our data demonstrate that FRI can also demonstrate the significant differences between regional and global measures of ε and τ_E. We found limited evidence that ε and τ_E are correlated. While the clinical importance of this data may be important, further studies are required to clarify their use in clinical practice.

Tables

Table 2.1 Regional and Total Strain with varying PEEP conditions

Lung lobe	PEEP 0	PEEP 5	PEEP 10
LAL	0.40 (0.29, 0.51)	0.19 (0.08, 0.30)	0.07 (-0.04, 0.18)
LCL	0.31 (0.20, 0.42)	0.11 (0, 0.22)	0.10 (-0.01, 0.21)
LDL	0.30 (0.19, 0.41)	0.19 (0.08, 0.30)	0.09 (-0.02, 0.20)
RAL	0.09 (-0.02, 0.20)	0.08 (-0.04, 0.20)	0.04 (-0.07, 0.15)
RCL	0.37 (0.26, 0.48)	0.14 (0.03, 0.25)	0.07 (-0.04, 0.18)
RDL	0.35 (0.24, 0.46)	0.18 (0.07, 0.29)	0.09 (-0.02, 0.20)
RIL	0.28 (0.17, 0.39)	0.15 (0.04, 0.26)	0.06 (-0.05, 0.17)
Total	0.31 (0.22, 0.39)	0.16 (0.08, 0.25)	0.08 (0, 0.17)

PEEP 0/5/10, positive end expiratory pressure of 0/5/10 cm H_2O; LAL, left anterior lobe; LCL left caudal lobe; LDL, left diaphragmatic lobe; RAL, right anterior lobe; RCL, right caudal lobe; RDL' right diaphragmatic lobe; RIL, right internal lobe. Data is displayed as least squares means estimates with 95% confidence intervals. The model for specific lobes includes lobe, PEEP, and lobe x PEEP interaction and total lung values are fitted with PEEP alone.

Table 2.2 Regional and Total Time Constants with varying PEEP conditions

Lung lobe	PEEP 0	PEEP 5	PEEP 10
LAL	3.37 (2.62, 4.12)	1.23 (0.48, 1.98)	0.17 (-0.58, 0.92)
LCL	0.95 (0.20, 1.70)	0.24 (-0.51, 0.99)	0.14 (-0.61, 0.89)
LDL	0.73 (-0.02, 1.48)	0.79 (0.04, 1.54)	0.27 (-0.48, 1.02)
RAL	0.74 (-0.01, 1.49)	0.47 (-0.37, 1.30)	0.15 (-0.60, 0.90)
RCL	1.10 (0.35, 1.85)	0.56 (-0.19, 1.31)	0.18 (-0.57, 0.93)
RDL	0.78 (0.03, 1.53)	0.55 (-0.20, 1.30)	0.28 (-0.47, 1.03)
RIL	0.50 (-0.25, 1.25)	0.46 (-0.29, 1.21)	0.17 (-0.58, 0.92)
Total	0.59 (0.33, 0.84)	0.53 (0.27, 0.79)	0.21 (-0.05, 0.46)

PEEP 0/5/10, positive end expiratory pressure of 0/5/10 cm H_2O; LAL, left anterior lobe; LCL left caudal lobe; LDL, left diaphragmatic lobe; RAL, right anterior lobe; RCL, right caudal lobe; RDL' right diaphragmatic lobe; RIL, right internal lobe. Data is displayed in seconds and as least squares means estimates with 95% confidence intervals. The model for specific lobes includes lobe, PEEP, and lobe x PEEP interaction and total lung values are fitted with PEEP alone.

Table 2.3 Resistance estimates at varying PEEP conditions and 95% CIs

Lung lobe	PEEP 0	PEEP 5	PEEP 10
LAL	1.96 (1.66, 2.26)	0.77 (0.47, 1.06)	0.32 (0.02, 0.61)
LCL	0.65 (0.35, 0.95)	0.23 (-0.07, 0.53)	0.16 (-0.14, 0.46)
LDL	0.15 (-0.14, 0.45)	0.09 (-0.21, 0.39)	0.07 (-0.22, 0.37)
RAL	0.42 (0.12, 0.72)	0.36 (0.03, 0.69)	0.32 (0.02, 0.61)
RCL	0.44 (0.15, 0.74)	0.33 (0.03, 0.63)	0.22 (-0.07, 0.52)
RDL	0.11 (-0.19, 0.41)	0.07 (-0.23, 0.36)	0.07 (-0.22, 0.37)
RIL	0.52 (0.23, 0.82)	0.36 (0.06, 0.66)	0.35 (0.05, 0.65)
Total	0.03 (0.02, 0.04)	0.02 (0.02, 0.03)	0.02 (0.01, 0.03)

PEEP 0/5/10, positive end expiratory pressure of 0/5/10 cm H_2O; LAL, left anterior lobe; LCL left caudal lobe; LDL, left diaphragmatic lobe; RAL, right anterior lobe; RCL, right caudal lobe; RDL' right diaphragmatic lobe; RIL, right internal lobe. Data is displayed in $cmH_2O \cdot L^{-1} \cdot second^{-1}$ and as least squares means estimates with 95% confidence intervals. The model for specific lobes includes lobe, PEEP, and lobe x PEEP interaction and total lung values are fitted with PEEP alone.

Table 2.4 Elastance estimates at varying PEEP conditions

Lung lobe	PEEP 0	PEEP 5	PEEP 10
LAL	0.85 (-0.47, 2.16)	0.94 (-0.38, 2.25)	2.39 (1.07, 3.70)
LCL	1.35 (0.04, 2.67)	1.10 (-0.21, 2.42)	1.53 (0.21, 2.84)
LDL	0.20 (-1.11, 1.52)	0.16 (-1.15, 1.48)	0.31 (-1, 1.63)
RAL	3.53 (2.22, 4.85)	1.37 (-0.10, 2.84)	5.91 (4.60, 7.23)
RCL	0.57 (-0.74, 1.89)	0.74 (-0.58, 2.05)	1.35 (0.04, 2.67)
RDL	0.16 (-1.15, 1.48)	0.15 (-1.17, 1.46)	0.26 (-1.05, 1.58)
RIL	2.11 (0.80, 3.43)	1.44 (0.12, 2.75)	3.33 (2.02, 4.65)
Total	0.05 (0.04, 0.07)	0.05 (0.03, 0.07)	0.10 (0.08, 0.11)

PEEP 0/5/10, positive end expiratory pressure of 0/5/10 cm H_2O; LAL, left anterior lobe; LCL left caudal lobe; LDL, left diaphragmatic lobe; RAL, right anterior lobe; RCL, right caudal lobe; RDL' right diaphragmatic lobe; RIL, right internal lobe. Data is displayed in $cmH_2O \cdot L^{-1}$ and as least squares means estimates with 95% confidence intervals. The model for specific lobes includes lobe, PEEP, and lobe x PEEP interaction and total lung values are fitted with PEEP alone.

Figures

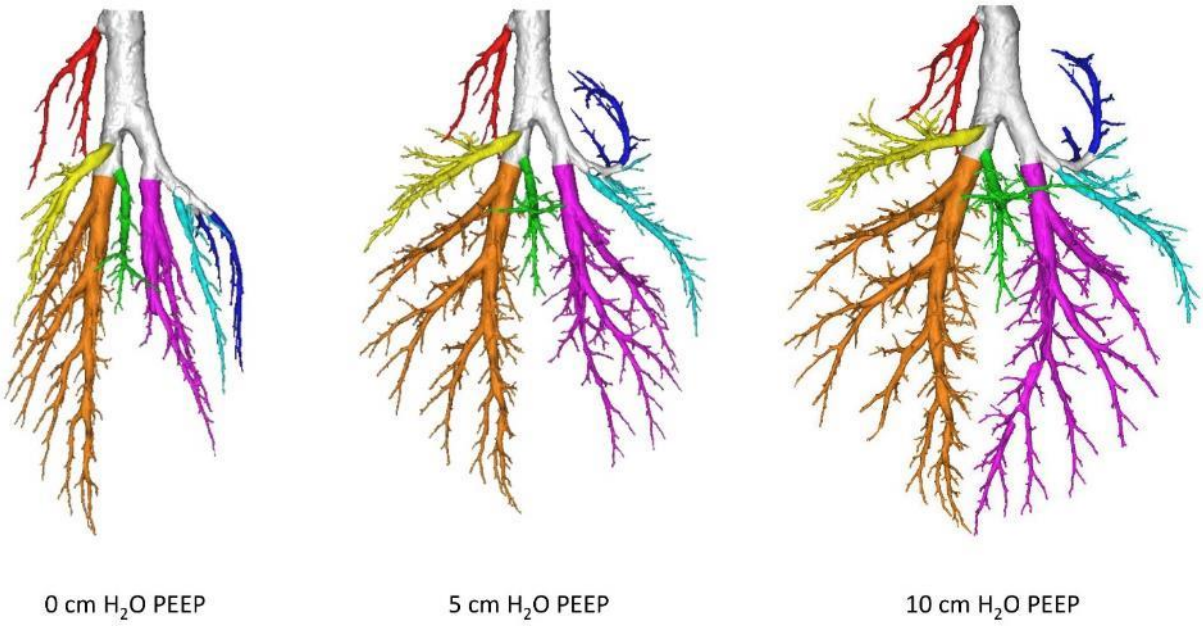

Figure 2.1 Pictorial representation of airway identification using composite 3D airway images at three positive end expiratory pressures

PEEP 0/5/10, positive end expiratory pressure of 0/5/10 cm H_2O. Red, right anterior lobe; Yellow, right caudal lobe; Orange, right diaphragmatic lobe; Green, right internal lobe; Purple, left diaphragmatic lobe; Light blue, left caudal lobe; Dark blue, left anterior lobe.

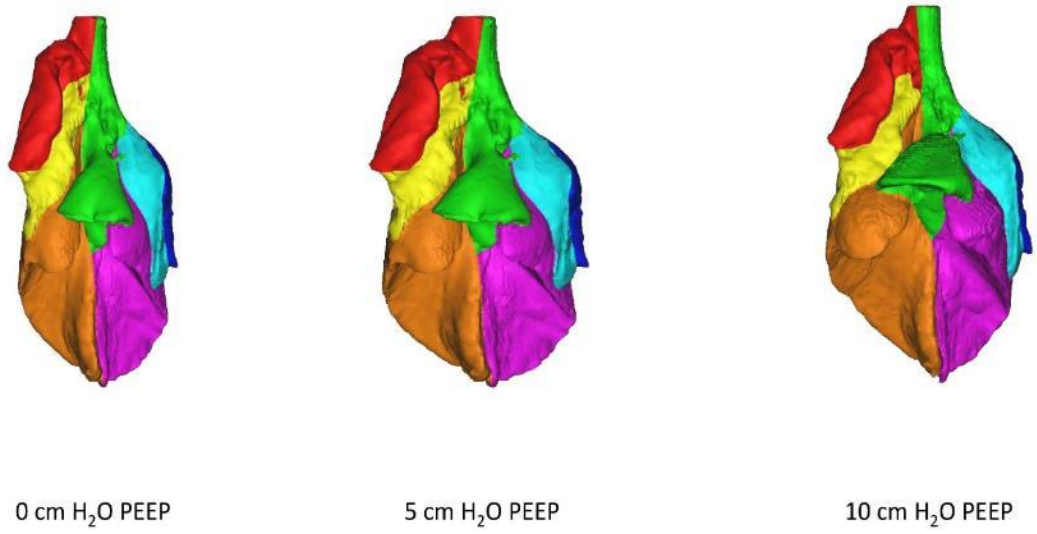

Figure 2.2 Pictorial representation of lung lobe identification using composite 3D lung images at three positive end expiratory pressures

PEEP 0/5/10, positive end expiratory pressure of 0/5/10 cm H_2O. Red, right anterior lobe; Yellow, right caudal lobe; Orange, right diaphragmatic lobe; Green, right internal lobe; Purple, left diaphragmatic lobe; Light blue, left caudal lobe; Dark blue, left anterior lobe.

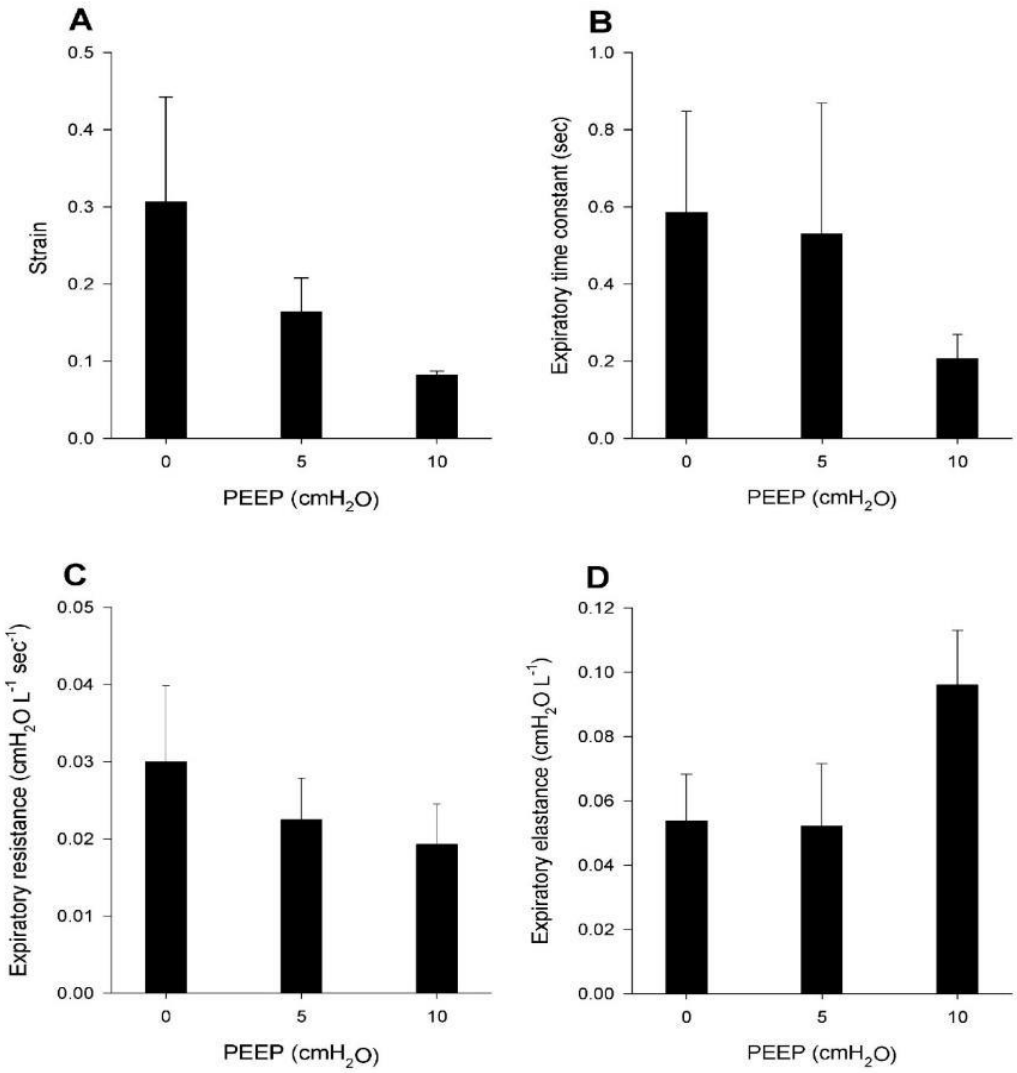

Figure 2.3 Total respiratory system strain (Panel A), expiratory time constant (Panel B), resistance (Panel C) and elastance (Panel D) at three levels of positive end expiratory pressure.

PEEP 0/5/10, positive end expiratory pressure of 0/5/10 cm H_2O; Data is displayed as least squares means estimates with 95% confidence intervals.

Chapter 3: Administration of Intrapulmonary Sodium Polyacrylate to Induce Lung Injury for the Development of a Porcine Model of Early Acute Respiratory Distress Syndrome

Introduction

Acute respiratory distress syndrome (ARDS) is characterized by severe hypoxic respiratory failure associated with high mortality and morbidity (154). Loss of alveolar epithelial and endothelial integrity cause a progressive influx of protein-rich fluid into the alveoli, impairs trans-epithelial fluid transport, and inhibits reabsorption of alveolar edema (122, 125, 200). The presence of surface-active and water soluble agents in the alveoli contributes to the inactivation of surfactant (80, 140, 170). Animal models are widely used to study the pathogenic mechanisms of ARDS and to assess the effects of interventions on clinical and biological outcomes (128, 129). It is recognized that different models emphasize different aspect of ARDS and that no model fully replicates the histologic findings of human ARDS (inflammatory infiltrates, thickened alveolar septae, intravascular microthrombosis and hyaline membrane deposition) and that a need exists to create animal models that more accurately mimic the histopathologic changes seen in in human ARDS (128). Despite advances in the understanding and treatment of ARDS, the mechanisms of alveolar epithelial injury are not well understood and additional models of lung injury that focus on the alveolar epithelium would be useful (126). A guideline committee of the American Thoracic Society concluded that a high quality model of experimental ARDS should include "very relevant" evidence of at least three out of four criteria:

i) tissue injury, ii) alteration of the alveolar capillary barrier, iii) presence of an inflammatory response, and iv) evidence of physiological dysfunction (128).

ARDS may be broadly characterized as being of pulmonary or extrapulmonary origin, with the primary pathologic lesion involving a direct insult to the alveoli (such as pneumonia) or an indirect insult to the lung parenchyma and pulmonary endothelial damage from an extrapulmonary disease such as sepsis (65). There is a substantial body of research suggesting that morphology and responses to clinical interventions differ between these two sub-groups of ARDS (3, 72, 109, 134, 138, 147, 166, 174). Similarly, experimental models of ARDS may be may be separated into those that target the alveolar epithelium (analogous to "pulmonary" ARDS) and those that target the vascular endothelium ("extrapulmonary" ARDS).

Sodium polyacrylate (SPA) is an anionic, osmotically active hydrophilic polymer known to absorb 250-times its weight in water (54). We hypothesized that intrapulmonary administration of SPA would lead to an experimental model of direct injury to alveolar epithelial cells that is meets the American Thoracic Society guidelines (128) by causing : i) accumulation of neutrophils and proteinaceous debris in the alveolar or the interstitial space; ii) evidence of interstitial and intra-alveolar edema; iii) an increase in the absolute number of neutrophils in bronchoalveolar lavage fluid; and iv) hypoxemia. Additionally, we intended to create a model with stable hemodynamics and that reflected the histologic and pulmonary mechanical alterations seen in ARDS of pulmonary rather than extra-pulmonary origin (65).

Materials and Methods

In vitro alveolar epithelial cell injury by SPA

After being warmed in a 70°C water bath for 15 min, 0.5 ml of sterile 1% SPA gel was placed in 4.5 mL of a cellular standard media (Complete Small Airway Epithelial Cell Growth

Media, PromoCell GmbH, Heidelberg, Germany) and was vortex mixed. This mixture was labeled "0.1% SPA". Using similar methods, mixtures with SPA concentrations of 0.03%, 0.01%, 0.003%, 0.001% and 0.0003% SPA were created. 1 ml of cryopreserved human lung epithelial cells (Lot 2102203, PromoCell, PromoCell GmbH, Heidelberg, Germany) were expanded in standard media. Cell viability was confirmed to be acceptable using 7-aminoactinomycin D dye exclusion evaluation (BD Via-Probe, BD Biosciences, San Jose, CA) and flow cytometry (Accuri C6, BD Biosciences, San Jose, CA). The cells/ml in the prepared suspension was evaluated using a cell counter (Coulter-Z, Beckman Coulter, Inc., Indianapolis, IN). The cell suspension was further diluted as required using standard media to prepare a stock cell suspension of 50,000 cells/mL. 100 µL aliquots of the diluted cell suspension were added to the appropriate wells of a 96-well plate to provide a final concentration of 5,000 cells/well. 100 µl aliquots of the appropriate SPA concentrations were dispensed to create 8 replicates of each dose concentration (and the background control). Plated cells were incubated for two days. For each plate, 100 µL of ATP-Enumeration Reagent (Hemogenix, Colorado Springs, CO) was then added to each well to lyse the cells, release ATP, and to produce bioluminescence. The bioluminescence emitted was detected and measured by plate luminometer (Spectramax L, Molecular Devices, Downingtown, PA) as relative luminescence units (RLU). Using an ATP standard curve, sample RLUs were converted to molar units of ATP and a dose response curve was generated.

In vivo experimental arrangement

Animals. Fourteen female adult Yorkshire X pigs were quarantined for 1 week prior to the experimental sessions. Eleven animals were subjected to experimental lung injury with SPA (SPA group). Three pigs served as controls and underwent all interventions and tests with the

exception of SPA administration (CON group). All experiments were approved by the Animal Research Committee of the University of British Columbia (certificate no. A11-0396) and conformed to the policies and guidelines of the Canadian Council on Animal Care.

The time of experimental arrangements in depicted schematically in Figure 3.1. After sedation (telazol, 4 to 6 mg/kg intramuscular), anesthesia was induced by inhalation (isoflurane, 3% to 5% in oxygen). The trachea was intubated with an endotracheal tube (8 or 9 mm diameter). Anesthesia was maintained with isoflurane inhalation (end-tidal concentration, 2% to 2.5% in oxygen) until intravenous anesthesia was established (midazolam, 0.1 mg/kg intravenous bolus, followed by propofol infusion [starting at 200 μg/kg/min, adjusted to 150 to 300 μg/kg/min according to depth of anesthesia]). Mechanical ventilation (Puritan-Bennett 7200, Covidien, Ireland) was maintained with the following parameters: positive end-expiratory pressure (PEEP), 0 cm H_2O; fraction of inspired oxygen (FIO_2), 0.5; and tidal volume (V_T), 12 mL/kg of body weight with constant inspiratory flows. These parameters were selected to mimic V_T and PEEP noted in similar investigations of experimental ARDS in pigs(77, 158, 195). The respiratory rate was 15 breaths/minute initially and was adjusted to maintain end-tidal carbon dioxide partial pressure ($PetCO_2$) within 35 to 45 mm Hg.

A catheter was placed in the right femoral artery to allow continuous blood pressure measurement (calibrated at the level of the heart) and collection of arterial blood samples. A pulmonary artery catheter was placed percutaneously in the right jugular vein to allow measurement of cardiac output and pulmonary vascular hemodynamic parameters. A urinary catheter and rectal temperature probe were placed. Core temperature was maintained between 35.5°C and 36.5°C with a heated operating table. Mean arterial blood pressure was maintained > 65 mm Hg by infusion of phenylephrine (0.1 to 0.3 μg/kg/min) when required.

Before all measurements of pulmonary mechanical parameters, a bolus of midazolam (0.1 mg/kg intravenous) was given and neuromuscular blockade was induced with pancuronium (0.05 to 0.1 mg/kg intravenous) or rocuronium (1 mg/kg intravenous) and monitored by assessment of response to train-of-four stimulation with a peripheral nerve stimulator.

Lung injury in the SPA group was caused by injecting sequential aliquots (5 mL, each) of 1% SPA gel in aqueous solution into the distal airway with a rubber catheter through the endotracheal tube. The SPA was dispersed throughout the lungs by manual bag ventilation (approximately 200cc/breath). Aliquots of SPA were given approximately every 5 minutes until hypoxemia was observed, defined by arterial partial pressure of oxygen (Pa_{O_2}) < 150 mm Hg. Control animals had a red rubber catheter placed through the endotracheal tube and received manual bagging (approximately 200cc/breath) but no intratracheal SPA.

Pulmonary mechanics, oxygenation, and hemodynamics

Inspiratory and expiratory flows were measured with a pneumotachograph (Model 3813, Hans Rudolph, Kansas City, MO) that was calibrated with a 2 L calibration syringe. Volumes were obtained by numerical integration of the flow signals. Mouth pressure was measured at a port placed between the ventilator wye and the endotracheal tube. Esophageal pressure was measured using a balloon-tipped catheter (No. 47-9005, Ackrad Laboratory, Cranford, NJ) placed in the lower third of the esophagus. Catheter position was deemed satisfactory when the change in esophageal pressure was equal to the change in airway pressure during passive inspiration (188). Both esophageal and airway pressures were measured with calibrated piezoelectric pressure transducers (Raytech Instruments, Vancouver, BC, Canada). Dynamic and static pulmonary mechanical variables were calculated as previously described (19, 90). Functional residual capacity (FRC) was measured using a previously described helium dilution

method to assess lung recruitment before and after injury (119). Arterial blood gases were measured immediately before and 1 hour after lung injury. Arterial blood pressure, pulmonary artery pressure, and heart rate from a surface electrocardiogram were monitored continuously. All data was collected and recorded with an integrated 16-channel data acquisition and recording system (PowerLab/16SP model ML 795 and LabChart v7, ADI, Colorado Springs, CO). Cardiac output was measured using thermodilution curves generated from injection of 5 mL boluses of cold 0.9% saline solution that were analysed with the same software. Three bolus injections were performed, sequentially once pulmonary artery temperature returned to baseline, with the average reported.

All animals were euthanized at the end of the experiment with an intravenous bolus of pentobarbital sodium (120 mg/kg). Death was confirmed by the absence of cardiac electrical activity on continuous surface electrocardiography.

Gross and microscopic pathology

All animals underwent bronchoalveolar lavage (BAL) immediately before SPA lung injury or sham and again before death using previously described procedures (58, 139). Direct cellular counts were performed on aliquots of BAL fluid by an automated cell counter. Direct and cytocentrifuge smears were prepared for cytologic examination using modified Wright-Giemsa stain. The white blood cell and differential counts were performed with 100 to 300 cells and percentages were determined.

Samples of lung tissue from SPA treated animals were excised from areas with visible injury and fixed in 10% buffered formalin for 48 hours before trimming. Similar samples were retrieved from control animals. Fixed tissues were processed (Tissue-Tek VIP 5 Vacuum Infiltration Tissue Processor, Sakura Finetek USA, Torrance, CA), embedded in paraffin,

sectioned (thickness, 4 μm), and stained with hematoxylin-eosin. For each animal, 10 randomly selected fields were assessed (original magnification x400) for: (i) alveolar fibrin deposition; (ii) alveolar inflammatory cell infiltration; and (iii) interstitial and intra-alveolar edema (101).

Electron microscopy was performed on post-mortem lung tissue. To achieve this, after death, lungs were flushed with glucose-containing Krebs buffer. After perfusion with 2.5% glutaraldehyde that was buffered in 0.1 M sodium cacodylate, the lungs were excised and sampled for damage. Excised tissue was cut into smaller pieces (1 mm^3) and further fixed in 2.5% glutaraldehyde in 0.1 M sodium cacodylate buffer for 24 hours. The tissue was washed with 0.1 M sodium cacodylate buffer, postfixed in a mixture of 2% potassium ferrocyanate and 2% osmium tetroxide in 0.1 M sodium cacodylate, dehydrated in a graded series of acetone solutions, infiltrated, and embedded. Sections (thickness, 500 nm) were cut (Leica EM UC6 microtome, Leica Microsystems, Wetzlar, Germany) and viewed with light microscopy. Sections (thickness, 60 nm) were stained with saturated uranyl acetate and lead citrate and examined with a transmission electron microscope (Tecnai 12 Transmission Electron Microscope, FEI, Hillsboro, OR) at original magnification x1850 to x9700.

Data analysis

Data were reported as mean ± SD, unless otherwise stated. Continuous variables were analyzed using paired t-tests (for within subject) or independent t-tests (for between subject) where appropriate. All tests were 2-sided, and statistical significance was defined by $P < 0.05$. Statistical analyses were performed using STATA 10.0 Statistical Software (StataCorp, College Station, TX).

Results

In vitro alveolar epithelial cell injury by SPA

Data was obtained on all wells of human alveolar cells cultured with and without SPA. The mean ATP content found after incubation with 0.1% SPA (0.92±0.27 µM/well) was approximately 15% of that found for the background control (6.30±0.37µM/well, $p<0.001$). The effect of lower doses of SPA on alveolar cell culture viability are presented in Figure 3.2. The addition of progressively higher doses of SPA decreased the viability of human alveolar epithelial cells as evidenced by absolute µM/well of ATP. SPA's effect on cell culture survival displayed a dose-response curve best described by a reverse sigmoidal function, with an R^2 value of 0.96. The SPA concentration that inhibited 50% of cells in the preparation used (IC_{50}) was estimated to be 0.008%.

In vivo experiments

The 14 pigs had an average body weight 29.5 ± 4.5 kg. The SPA group received 15.5 ± 4.2 mL SPA (0.54 ± 0.18 mL/kg intratracheal) while the CON group received none. SPA pigs were ventilated with a V_T of 12.53±1.34 cc/kg and CON pigs with a V_T of 13.68 ±1.91 cc/kg ($p=0.25$).

Pulmonary mechanics, oxygenation, and hemodynamics

All pulmonary mechanical data is presented in Table 3.1. Elastances of the respiratory system (E_{RS}) and of the lung (E_L) were significantly higher after injury as compared to before injury in SPA. E_{RS} was greater in SPA than in CON after injury and increases in E_{RS} in the SPA group were driven exclusively by changes in E_L as E_{CW} did not increase after injury. No differences were seen in E_{RS}, E_L or E_{CW} in CON when pre-injury and post-injury values were compared. E_{RS} was greater in SPA than in CON after injury. While there were no differences in measures of resistance between SPA and CON prior to injury, respiratory system resistance

(R_{RS}) more than doubled after injury in the SPA group and appeared to be driven by increases in lung resistance (R_L). Chest wall resistance (R_{CW}) did not change from before to after injury in SPA, and measures of resistance did not change significantly in CON when before and after injury data were compared.

FRC declined from 16.4±3.2 ml/kg prior to injury to 10.7±3.3 ml/kg after injury in SPA ($p<0.001$) and was unchanged in CON with values before and after sham injury of 13.8±2.2 ml/kg and 12.77±1.52 ml/kg ($p=0.54$). PaO_2 decreased in SPA with injury from 224.6±48.4 mmHg to 72.27±12.51 mmHg ($p<0.001$) and was unchanged in CON with values before and after sham injury of 250.67±108.61 mmHg and 244.67±27.14 mmHg ($p=0.93$). PaO_2 values were no different between SPA and CON prior to injury ($p=0.53$), but were different after injury ($p<0.001$).

As expected by design, cardiac output and mean arterial pressure did not change when values from before and after injury were compared in SPA and CON (All hemodynamic data is presented in Table 3.2). Pulmonary artery pressures increased in SPA with injury but not in CON leading to a difference between the two groups after injury. No animals required vasopressor support prior to injury. Following injury, 2 of 11 SPA animals and none of the CON animals required vasopressors.

Gross and microscopic pathology

Bronchoalveolar lavage fluid retrieved before injury showed white blood cell differential counts that were similar between SPA and CON and that were within acceptable reference intervals (58, 67). BAL fluid retrieved from SPA after injury demonstrated an increase in white blood cells and neutrophilia while BAL fluid from CON after injury demonstrated no changes from pre-injury values. Detailed results from BAL samples are described in Table 3.3.

At necropsy, lungs from CON were normal to visual inspection. Light microscopy examination of lungs from CON animals revealed normal appearing lungs with regions of atelectasis. There was no significant active inflammation in the lungs (Figure 3.3, panels A and B). At necropsy, lungs from SPA treated pigs demonstrated marked consolidation and congestion of the dorsal lung lobes (approximately 45% of total lung tissue), with sparing of the cranial lobes. The cut surfaces of the affected tissues were congested, hemorrhagic, and edematous. Light microscopy of lung specimens showed bronchiolar and alveolar spaces filled with neutrophilic infiltrate, proteinaceous debris, and fibrin deposition (Figure 3.3, panels C and D). Although minimal epithelial damage was noted in large airways, peribronchiolar and interstitial edema and intravascular congestion were evident. Early epithelial hyperplasia with transmigration or exudation of neutrophils across the bronchiolar wall into the airspace was widespread. Similarly, electron microscopy of lung tissue from SPA animals showed injury to the alveolar epithelium and basement membranes, including intra-alveolar neutrophils, fibrin on the alveolar surface and intravascular fibrin (microthrombosis) (Figures 3.4 and 3.5).

Discussion

In our study, intrapulmonary administration of SPA resulted in rapid development of the physiologic and histologic changes seen in ARDS, including diffuse alveolar damage, necrosis of alveolar epithelial cells, inflammatory cell infiltration and proteinaceous alveolar and interstitial edema. With respect to the published ATS criteria (128) for a high quality model, the present model of SPA induced ARDS satisfies these requirements with: i) accumulation of neutrophils and proteinaceous debris in the alveolar or the interstitial space; ii) evidence of interstitial and intra-alveolar edema; iii) an increase in the absolute number of neutrophils in BAL fluid; and iv) hypoxemia.

Both our *in vitro* and *in vivo* data suggest that SPA creates a model of ARDS that represents a "pulmonary" origin due to epithelial injury. Our data shows that SPA decreases the viability of cultured human alveolar cells in a dose dependent fashion. SPA is an intensely hydrophilic anionic polymer that has significant osmotic activity (54, 212). Previous investigations have demonstrated local and systemic toxicity of variable severity with parenteral, enteral and intratracheal SPA administration in animals (93, 131). Given the evidence of alveolar epithelial cytotoxicity and the histological evidence of alveolar inflammation presented here, we cautiously speculate that SPA caused ARDS through a direct injury to the alveolar epithelium.

Similarly, our *in vivo* data reflect an injury to the lungs, rather than a systemic injury, and is therefore consistent with a model of ARDS of pulmonary origin. In contrast to the CON animals, SPA injured animals rapidly developed hypoxemia and decreases in FRC. Current clinical definitions for ARDS use the PaO_2/FiO_2 ratio (P/F) to categorize ARDS severity as mild (P/F<300), moderate (P/F<200) or severe (P/F<100). (162). The average P/F ratio after SPA administration was 144.5±25, and all SPA animals had a P/F ratio that qualified as moderate ARDS. The mean FRC decreased by 36% in the SPA group, a decrease that is consistent with alterations in FRC seen in patients who have ARDS (24). The alterations in elastance and resistance seen in the SPA group were attributable to changes in E_L and R_L rather than E_{CW} and R_{CW}, suggesting that the injury was intrinsic to the lung (Table 3.1). In this context, pulmonary artery pressures increased more in SPA injured animals than in controls but there were few systemic hemodynamic changes in either group as quantified by cardiac output, mean arterial pressure, or need for vasoactive medications.

We have demonstrated that intrapulmonary administration of SPA causes an experimental model of ARDS of pulmonary origin, plausibly due to direct alveolar epithelial

injury. As such, SPA causes interstitial edema, intraalveolar fibrin deposition and a neutrophilic alveolitis, rather than the microvascular congestion and less severe alveolar damage typically seen in extrapulmonary causes of ARDS. It is therefore reasonable to compare experimental ARDS due to SPA with other models that cause a primarily alveolar injury – such as saline lavage, injurious mechanical ventilation, hyperoxia, and acid aspiration. There currently exists variability in the characteristics and quality of these experimental models of ARDS, and injury with SPA may provide advantages when attempting to study the role of epithelial injury in ARDS. For example, saline lavage precipitates acute hypoxia due to alveolar collapse, but is not associated with a significant change in alveolar-capillary permeability or inflammation, and thus does not reflect the histology generally associated with human ARDS (68, 129, 168). Injurious mechanical ventilation produces a model of ARDS characterized by hypoxemia and inflammation, but the presumed mechanism is that of mechanotransduction of injurious forces rather than direct epithelial injury. As such it represents a useful model of ventilator associated lung injury in already susceptible lungs, but does not represent a likely mode of injury to previously healthy lung (165). Similarly, while hyperoxia causes inflammation and injury in some animal models (41), it is questionable if it initiates ARDS at all in humans (17, 129). Acid aspiration (classically HCL with a pH of 1.5) causes a model of ARDS similar to that of SPA, with inflammation and direct injury to alveolar epithelial cells (56, 104, 160). However, humans do not usually aspirate strong acids. Rather, gastric contents are a combination of particulate matter, bacteria and fluids with a pH considerably greater than 1.5. SPA, which is neutral in terms of pH, may allow insights into direct epithelial injury at normal pH. Finally, the excellent hemodynamic stability seen in the SPA injured animals allows the potential to separate the

effects of epithelial injury from those of hypotension and hypoperfusion, two potential confounders seen in other models.

Our model also has several limitations that merit consideration. First, the short duration of our study precludes the ability to describe the evolution of the injury produced beyond the first few hours. While our model appears to accurately mimic the physiologic and histologic changes seen in early ARDS, we did not demonstrate that the injury precipitates the delayed histological findings of ARDS. Second, human trials have suggested that V_T greater than 6 ml/kg may be harmful to injured lung (154). The animals in our study were ventilated with larger V_T (12.53±1.34 cc/kg in the SPA group) and without PEEP, raising the possibility that the changes may have been due to injurious ventilation rather than due to SPA. However, pigs have significantly lower specific lung elastance than humans and tolerate V_T of up to 22 ml/kg without evidence of lung injury (39). The ventilator settings used in our trial were recently used in a similar trial in pigs that did not demonstrate the anatomic or histologic changes of ARDS (158). Our control animals did not demonstrate physiological or histological evidence of alveolar injury after several hours of this ventilation strategy. We therefore believe that the injury seen in our model is due to SPA rather than due to an intrinsically injurious ventilation strategy *per se*. Third, we have presented cytotoxicity data from *in vitro* experiments. While it seems probable that these data clarify the potential mechanisms of SPA induced lung injury, these experimental models do not fully replicate the biochemical or physiological milieu found in porcine or human lungs. Importantly, the concentrations of SPA used in the in vitro experiments are at best an estimate of the concentrations that might have been found locally in alveoli in the in vivo experiment. Finally, interspecies differences may mean that the findings in this porcine model should only be cautiously applied to human patients.

Conclusions

We have demonstrated that intrapulmonary administration of SPA results in a rapid exudative lung injury. Our study reports an animal model of ARDS that is of pulmonary origin. Moreover, the model will be useful in clarifying the role of direct alveolar injury in the pathogenesis of ARDS. Further studies are needed to better characterize the mechanisms underlying this model of lung injury and its potential contribution in patients with ARDS.

Tables

	SPA group before Injury	CON group before injury	P-value SPA versus CON before injury	SPA group after injury	CON group after injury	P-value SPA vs. CON after injury	P-value SPA before versus after injury	P-value CON before versus after injury
E_{RS}	33.56±	31.88±	0.77	65.08±	32.88±	0.04	<0.01	0.99
(cm H_2O/L)	10.03	2.53		29.78	13.72			
E_L	21.06±	19.13±	0.76	56.87±	23.68±	0.11	<0.01	0.70
(cm H_2O/L)	8.34	2.15		25.07	13.82			
E_{CW}	15.98±	13.15±	0.66	18.24±	11.52±	0.64	0.73	0.79
(cm H_2O/L)	8.32	5.51		19.01	4.72			
R_{RS}	10.66±	15.26±	0.31	21.55±	12.99±	0.22	0.01	0.60
(cmH_2O/L/sec)	6.83	6.43		10.99	2.15			
R_L	9.59±	16.17±	0.22	21.00±	13.18±	0.29	<0.01	0.67
(cmH_2O/L/sec)	6.55	8.05		9.61	2.07			
R_{CW}	1.58±	1.21±	0.68	2.48±	0.93±	0.57	0.43	0.73
(cmH_2O/L/sec)	1.15	0.66		3.55	0.75			

Table 3.1 Pulmonary mechanics of animals before and after real injury with sodium polyacrylate (SPA) or sham injury (CON)

E_{RS}, E_L, E_{CW} = elastance of the respiratory system, lung and chest wall respectively. R_{RS}, R_L, R_{CW} = resistance of the respiratory system, lung and chest wall respectively. All values reported as mean ± standard deviation.

	SPA group before Injury	CON group before injury	P-value SPA vs. CON before injury	SPA group after injury	CON group after injury	P-value SPA vs. CON after injury
MAP (mm Hg)	82.96± 8.88	86.4± 4.36	0.54	79.84± 15.58	88.8± 8.64	0.37
CO (ml/kg)	50.31± 8.29	43± 13.74	0.35	49.72± 7.25	35.55± 4.59	0.26
MPAP (mm Hg)	20.96± 4.06	18± 4.25	0.29	34.83± 5.95	26.27± 4.2	0.04
Subjects requiring vasopressors (n)	0	0	1.0	2	0	1.0

Table 3.2 Selected hemodynamic parameters of animals before and after real injury with sodium polyacrylate (SPA) or sham injury (CON)

MAP = mean arterial pressure, CO = cardiac output, MPAP = mean pulmonary arterial pressure. All values reported as mean ± standard deviation.

	SPA group before Injury	CON group before injury	P-value SPA vs. CON before injury	SPA group after injury	CON group after injury	P-value SPA vs. CON after injury
RBC x 10^{12}/L	0.01± 0.01	0.10± 0.00	<0.01	0.05± 0.10	0.02± 0.01	0.53
WBC x 10^{9}/L	0.40± 0.22	0.61± 0.39	0.25	3.20± 1.63	0.36± 0.21	0.02
Macrophages (% of WBC)	65.89± 22.21	54.00± 16.37	0.42	5.56± 5.73	48.33± 14.43	<0.01
Small lymphocytes (% of WBC)	23.78± 18.85	23.33± 5.77	0.97	2.33± 0.71	31.67± 12.58	<0.01
Neutrophils (% of WBC)	10.33± 14.00	22.67± 16.17	0.23	91.44± 5.48	26.67± 20.21	<0.01

Table 3.3 Bronchoalveolar lavage results of animals before and after injury with sodium polyacrylate (SPA) or sham injury (CON)
RBC = red blood cells, WBC = white blood cells, All values reported as mean ± standard deviation.

Figures

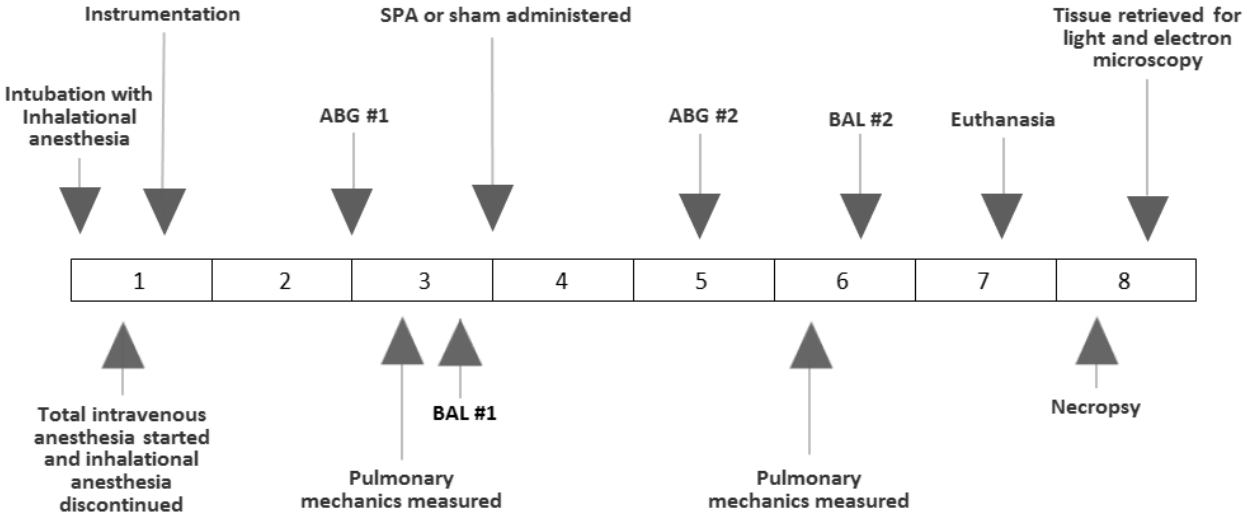

Figure 3.1 Schematic timeline of procedures and data collection during the study
Horizontal numbers in the centre of the figure represent time from initial anesthetic.
ABG Arterial blood gas; BAL Brochoalveolar lavage; SPA Sodium polyacrylate.

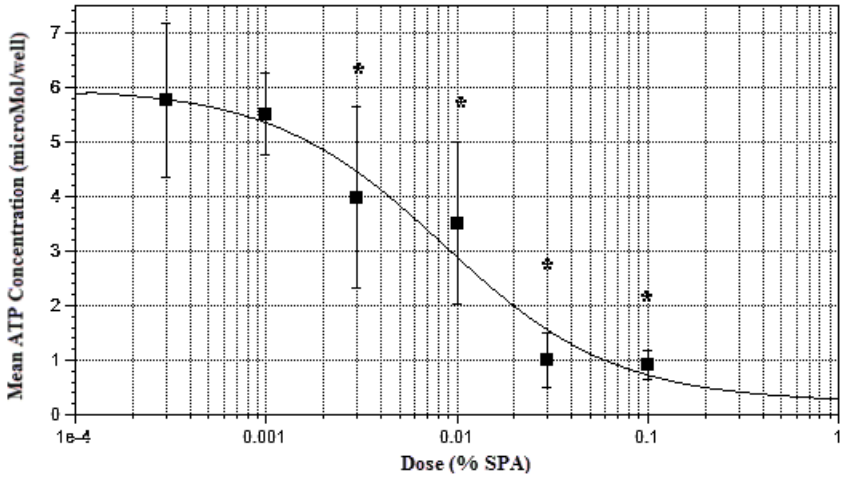

Figure 3.2 Mean concentration of ATP found in wells of human alveolar cells after incubation with sodium polyacrylate (SPA)

*Represents $p<0.05$ for values compared with baseline.

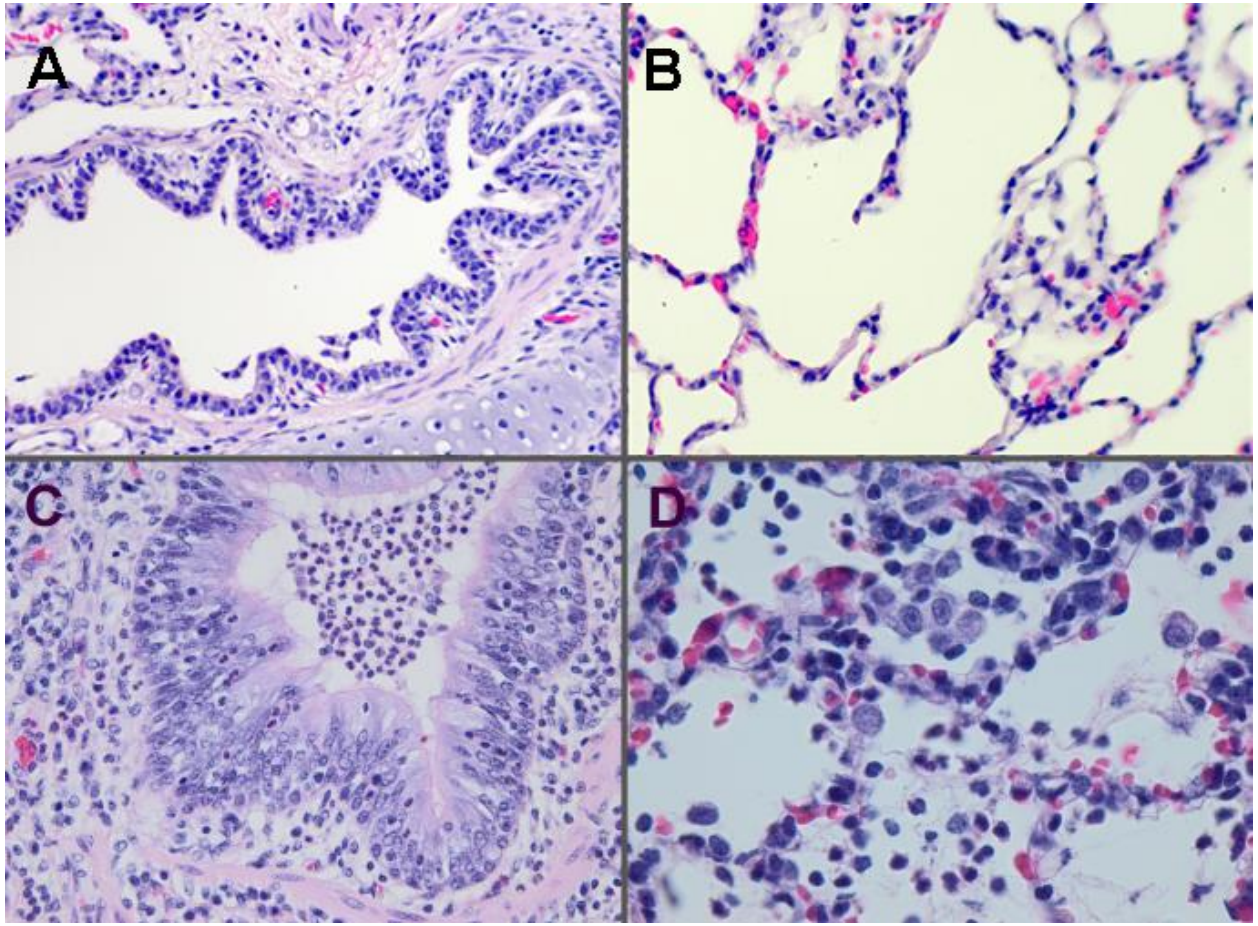

Figure 3.3 Histology of lung tissue from control (CON) (panels A and B) and sodium polyacrylate (SPA)-treated (panels C and D) animals 6 h after administration of SPA or sham

(A) Bronchiole from CON animal demonstrating normal epithelial structure (hematoxylin-eosin stain, original magnification x20). (B) Normal alveolar structure in CON animal (hematoxylin-eosin, original magnification x40). (C) Bronchiole from SPA-treated animal filled with degenerated and viable neutrophils, with transmigration of neutrophils across the respiratory epithelium. Cilia are intact and mild epithelial hyperplasia is present. The subjacent alveoli contain inflammatory cells and fibrin (hematoxylin-eosin stain, original magnification x20). (D) Macrophages, neutrophils and fibrin strands in an area of alveolar inflammation and consolidation in tissue from an SPA-treated animal (hematoxylin-eosin stain, original magnification x40).

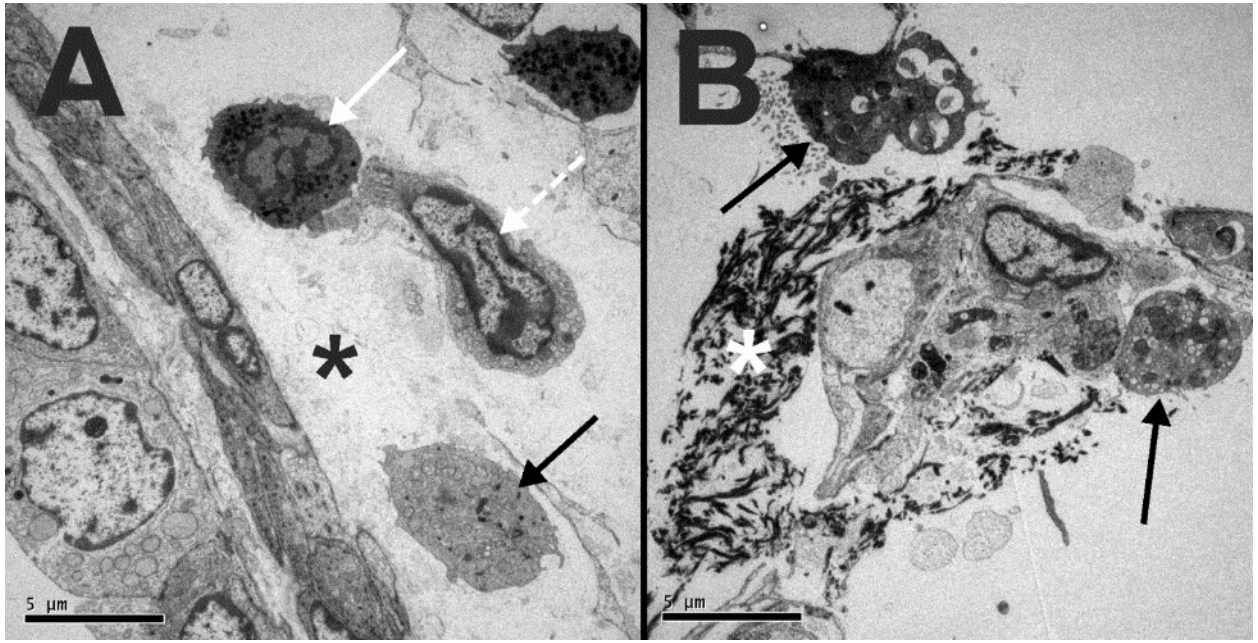

Figure 3.4 Transmission electron microscopy of lung tissue from a pig subjected to experimental injury with intratracheal sodium polyacrylate

(a) Interstitium and adventitia of a terminal bronchus with migrating polymorphonuclear leukocyte (solid white arrow), macrophage (dashed white arrow) and monocyte/macrophage (solid black arrow). Edematous exudate (asterisk) is noted (original magnification x3900). (b) Alveoli with type 2 pneumocytes (black arrows) and dense fibrin deposition (white asterisk) (original magnification x3900)

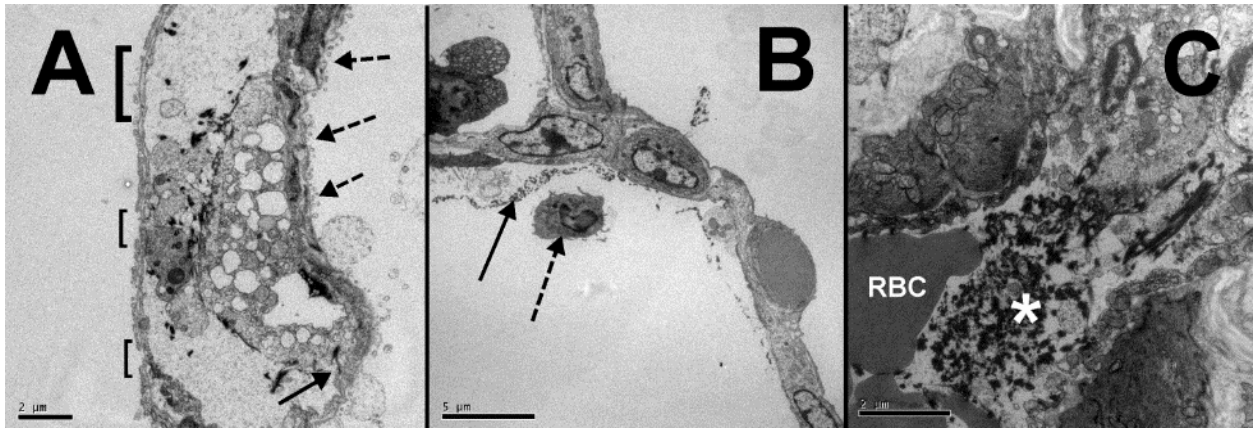

Figure 3.5 Transmission electron microscopy of lung tissue from a pig subjected experimental injury with intratracheal sodium polyacrylate

(a) Alveolar-capillary interface with gaps in the capillary epithelium (open brackets denoting size of gap), necrosis of alveolar epithelium (dashed arrows), and gap in endothelium (solid arrow) (original magnification x5800). (b) Alveolus with fibrin deposition (solid arrow) and a neutrophil in the air space (dashed arrow) (original magnification x3900). (c) Perialveolar blood vessel containing fibrin (white asterisk) and a red blood cell (RBC) (original magnification x9700)

Chapter 4: Gas Density Alters Expiratory Time Constants Before and After Experimental Lung Injury

Introduction

Acute lung injury in humans is heterogeneous in distribution (43). Some lung units have severely abnormal values of resistance (R), elastance (E) or both, while other lung units have values that are similar to healthy lungs (143). For a given lung unit, the product of R and the reciprocal of E is the time constant (τ). Areas of the lungs with short τ (i.e., low R and/or high E) will fill or empty earlier than areas with longer time constants. Regional variation of lung resistance (R_L) and elastance (E_L) implies regional heterogeneity in expiratory time constants (τ_E). If τ_E differs in adjacent lung units, then volume change during expiration in these units may occur at different rates. After injury, lung tissue is characterized by a greater heterogeneity of distension (135, 143, 177) as well as a greater variation in R_L and E_L than is healthy lung (50, 98, 100), and therefore have greater heterogeneity in τ_E than uninjured lungs.

Widely-used methods of calculating τ_E assume that all lung units inflate and deflate homogenously, acting as a single compartment and are unable to differentiate between fast and slow filling and emptying units (1, 36, 132). Instead, a model that allows the quantification of τ_E at multiple points throughout expiration would more accurately describe the heterogeneity of τ_E. To achieve this, previous investigations have described the pattern of lung emptying during passive deflation by partitioning the expiratory flow-volume ($\dot{V}V$) curve into several discrete segments and individually calculate τ_E for each of these segments (81, 105, 106, 115). While the

effect of altering elastance using positive end expiratory pressure (PEEP) on τ_E values has been documented (106), the effect of manipulating gas flow resistance on τ_E is unknown. We reasoned that altering airflow resistance could change the pattern of lung emptying during passive expiration by changing the rate at which short and long τ_E lung units empty.

We hypothesized that, as values of R_L and E_L and their heterogeneity are greater in injured than in uninjured lungs, τ_E would be more heterogeneous in injured lungs compared with uninjured lungs in the same animal. We further hypothesized that the heterogeneity of expiration within a single animal (as characterized by greater variability between the τ_E of early versus late segments of an expiration) would be greater after injury than before. To this end, we sought to characterize the effects of variations in gas density on τ_E before and after the induction of an experimental model of lung injury.

Methods

Animals and instrumentation

The experimental protocol was approved by the Animal Research Committee of the University of British Columbia and conformed to the ethical guidelines for animal experimentation as outlined by the Physiological Society (Grundy, 2015). In seven adult female Yorkshire X pigs (average weight 28.9 kg±3.5 kg), anaesthesia was induced (isoflurane 3-5% in oxygen) after sedation (telazol 4-6 mg kg^{-1} intramuscular injection). After endotracheal tube placement (9mm internal diameter), total intravenous anaesthesia was established with midazolam (0.1 mg kg^{-1} intravenous), propofol (150 to 300 µg kg^{-1} min^{-1} intravenous) and fentanyl (1-2 µg kg^{-1} intravenous, repeated as needed). Inhalational anaesthesia was then

discontinued. Under deep anesthesia, a brief period of neuromuscular blockade was induced prior to all measurements of pulmonary mechanical parameters using midazolam bolus (0.1 mg kg^{-1} intravenous) and pancuronium (0.05 mg kg^{-1} to 0.1 mg kg^{-1} intravenous) or rocuronium (1 mg kg^{-1} intravenous). Paralysis was monitored by assessment of response to train-of-four stimulation using a peripheral nerve stimulator. The adequacy of anesthesia was confirmed by the absence of cardiovascular response to minor noxious stimulus and was assessed every fifteen minutes using physical examination, assessment of vital signs and electrocardiography. Mechanical ventilation (Puritan-Bennett 7200, Covidien, Ireland) provided a fraction of inspired oxygen (FiO_2) of 0.5, tidal volumes (VT) of 12 ml kg^{-1} of body weight and 0 cmH_2O of positive end expiratory pressure (PEEP). Breathing frequency was initially 15 breaths/minute and was adjusted to maintain an end tidal partial pressure of carbon dioxide of 35-45 mmHg. Inspiratory flow rate was 45 $l\,min^{-1}$ with an inspiratory to expiratory ratio of 1:1. These parameters were selected to reflect similar investigations of experimental lung injury in pigs (3, 134, 174). Right femoral artery cannulation allowed continuous blood pressure measurement and collection of arterial blood samples. A pulmonary arterial catheter was placed through the right or left jugular vein to allow the measurement of cardiac output by a bolus thermodilution method and other cardiorespiratory variables using previously described methods (85). At the end of the experiment, euthanasia was achieved with pentobarbital sodium (120 mg kg^{-1} intravenous). Death was confirmed by the absence of a pulse and cardiac electrical activity on continuous surface electrocardiography.

Induction of lung injury

We used a previously described method (87) of lung injury that produces profound neutrophilic alveolitis, diffuse alveolar damage and an experimental model of lung injury that

satisfies current American Thoracic Society guidelines for a high quality model (128). One percent sodium polyacrylate (SPA) gel in an aqueous solution was injected into the distal airways through the endotracheal tube using a rubber catheter and was manually dispersed throughout the lungs by bagging. One 5 ml aliquot was given approximately every five minutes until a partial pressure of oxygen (PaO_2) of less than 150 mmHg while receiving an FiO_2 of 0.5 was observed.

Interventions

Prior to experimental lung injury, the animals were ventilated with 50% oxygen (O_2) and either 50% nitrogen (N_2), 50% helium (He) or 50% sulphur hexafluoride (SF_6), in a computer generated random order. The animals were ventilated for twenty minutes with each gas mixture to allow complete equilibration of gas composition prior to obtaining measurements. As described below, pulmonary mechanical data was collected during ventilation with each gas mixture. After lung injury the same procedures were repeated.

Measurement of pulmonary mechanics

Inspiratory and expiratory flows ($\dot{V}_I$ and $\dot{V}_E$) were measured using a heated pneumotachograph (Model 3813, Hans Rudolph, Kansas City, MO). Expiratory volume (V) was obtained by numerical integration of the flow signals. Airway pressure (P_{AW}) was measured at a port distal to the ventilator wye. Tracheal pressure (P_{TR}) was measured using a fenestrated polyethylene catheter placed 2 cm past the distal end of the endotracheal tube. Oesophageal pressure (P_{OES}) was measured using a balloon-tipped catheter (no. 47-9005, Ackrad Laboratory, Cranford, NJ) placed in the lower third of the oesophagus and was assumed to approximate pleural pressure (P_{PL}). Functional residual capacity (FRC) was measured before and after injury using a previously described helium dilution method (145).

Descriptive measures of whole breath pulmonary mechanics were calculated using previously described methods and end-inspiratory plateau pressures (20, 90). Further details of our methods can be found in Appendix 1.

Characterization of the pattern of expiratory time constants

While descriptive whole breath measures of pulmonary mechanics (above) were measured and calculated using differences between end-expiratory and end-inspiratory measurements, characterization of the expiratory flow pattern occurred using methods similar to those of Guttmann (81) and Kondili (106) wherein the expiratory breath is subdivided into segments. Specifically, we combined ten individual breaths to create ensemble $\dot{V}V$ and PV curves for each animal for all combinations of injury state and gas mixture. To account for the effect of the flow dependent resistance of the endotracheal tube and ventilator apparatus, one set of $\dot{V}V$ and PV traces were created using P_{AW} and a second set with P_{TR} (Figure 4.1A). To allow the assessment of the pattern of expiratory flow, the V from the point of maximum $\dot{V}_E$ to the end of expiration for each ensemble was divided into five segments of equal size as defined by expired volume. This method allowed the calculation of time constants that included the contributions of the respiratory system, the ventilator and endotracheal tube for each of the five volume segments ($\tau_{E,TOT1}$ through $\tau_{E,TOT5}$) and for the respiratory system alone ($\tau_{E,RS1}$ through $\tau_{E,RS5}$) from peak expiratory flow to end exhalation (Figure 4.1C). The central concept in calculating τ_E with and without the resistance of the ETT and ventilator is that $\tau_{E,TOT}$ does not equal $\tau_{E,RS}$ (because of the ETT tube). A detailed description of our methods may be found in Supplementary Material 1 - Methods.

Statistical analyses and model

Descriptive data are reported as mean ± standard deviation (SD), unless otherwise indicated. Continuous variables for gas cardiorespiratory variables (cardiac output, PaO_2, $PaCO_2$, physiologic and anatomic dead space and shunt fraction) were analyzed using repeated measures ANOVA with the between-subject effects being *gas* (N_2, He, SF_6) and the within subject effect being *injury*. We also included a *gas* by *injury* interaction along with the main effects. Continuous variables for pulmonary mechanics (elastance and resistance of the chest wall, lung and respiratory system) were analyzed by paired Students t-test. All tests were two-sided and the statistical significance was defined at $P<0.05$. Statistical analyses were performed using STATA 10.0 Statistical Software (StataCorp, College Station, TX).

We summarized the profile of $\log(\tau_E)$ over volume segment with a polynomial function that included a linear and a squared term. To assess the effect of injury and respiratory gas composition on both $\tau_{E,TOT}$ and $\tau_{E,RS}$, linear mixed-effects regression models were used to assess group differences in the average profile and variability of the change of $\log(\tau_E)$ over volume segment. Details of the statistical methods used in this process may be found in Supplementary Materials 2 - Statistics.

Results

Before induction of experimental lung injury, the animals demonstrated a PaO_2 of 185±37mmHg while receiving an FiO_2 of 0.5. After injury, PaO_2 decreased to 68±16 mmHg ($P<0.001$ compared with pre-injury values) while receiving an FiO_2 of 0.5 as an N_2/O_2 mixture. Relative to pre-injury, cardiac output and oxygenation were reduced post-injury ($P=0.042$ and $P<0.001$, Table 4.1). Physiologic dead space, alveolar dead space and shunt were significantly

increased after injury when compared with before injury (P=0.002, P<0.001 and P=0.002, Table 4.1). Changes in inhaled gas density did not alter any of these variables.

Pulmonary mechanics

The FRC prior to the induction of experimental lung injury was 519±91 ml and decreased to 314±96 ml following experimental injury (P=0.002). E_{RS} and R_{RS} both increased with experimental injury for all gas conditions. These changes were driven by significant increases in E_L and R_L. E_{CW} and R_{CW} did not change significantly following injury for any gas condition. All descriptive pulmonary mechanical data are presented in Table 4.2.

Time constants of the total system

Prior to injury, $\tau_{E,TOT}$ was greater for SF_6 than for He or N_2 (P = 0.0004 and < 0.0001, respectively, Figure 4.2 and 4.3) and not different between He and N_2 (P = 0.57, Figure 4.2 and 4.3); there were no statistically significant differences in the progression of $\tau_{E,TOT}$ over volume segments between any of the gases before injury. After injury, $\tau_{E,TOT}$ was greater for SF_6 than for He or N_2 (P = 0.002 and 0.008, Figure 4.2 and 4.3) and not different between He and N_2 (P = 0.42); there were no statistically significant differences in the progression of $\tau_{E,TOT}$ over volume segments between He and N_2 (P = 0.25) or between He and SF_6 (P =0.35). The progression of $\tau_{E,TOT}$ over volume segments was less steep for SF_6 than for N_2 (P=0.036). Raw data for $\tau_{E,TOT1}$ to $\tau_{E,TOT5}$ as well as the component R and E values are displayed in Supplementary Material 3 - Data.

Time constants of the respiratory system

For all three gas conditions the variability between the curves increased after injury (P < 0.001, Figures 4.4 and 4.5). Prior to injury, $\tau_{E,RS}$ was greater for SF_6 than for He (P<0.0001) or

N_2 ($P < 0.0001$) and greater for N_2 than for He ($P = 0.0016$, Figure 4.4). After injury, $\tau_{E,RS}$ for SF_6 was greater than for He ($P < 0.001$, Figure 4.4) or N_2 ($P < 0.001$, Figure 4.4) and greater for N_2 than for He ($P = 0.002$, Figure 4.4). The progressive increases in τ_E over volume segments τ_{ERS1} to τ_{ERS5} were not different between He and N_2 ($P=0.66$) prior to injury. The increase in $\tau_{E,RS}$ over volume segments prior to injury was less steep for SF_6 compared with He ($P=0.0027$) and N_2 ($P=0.052$). After injury, the progressive increases in $\tau_{E,RS}$ over volume segments $\tau_{E,RS1}$ to$\tau_{E,RS5}$ were not statistically different between He and N_2 ($P=0.14$) or between He and SF_6 ($P=0.078$) after injury. The progression of $\tau_{E,RS}$ over the volume segments for SF_6 was less steep than for N_2 ($P=0.0003$). Raw data for $\tau_{E,RS1}$ to $\tau_{E,RS5}$ as well as the component R and E values are displayed in Supplementary Material 3 - Data.

Discussion

The main findings in the current study are threefold: i) when a multiple segment model was used, τ_E values decreased from before to after injury and the absolute value was affected by the gas density, ii) sequential values of τ_E increased throughout expiration both before and after injury, and the rate of increase in τ_E was decreased by SF_6 but not affected by other gas mixtures. The interposition of an endotracheal tube largely obscured the changes in τ_E during expiration before and after injury, and this effect was not altered by the gas density, and iii) altering inhaled gas density did not alter indices of oxygenation or shunt. Collectively, these findings demonstrate that gas density alters the pattern of passive expiration before and after injury and that SF_6 decreases the difference in τ_E values between early and late expiratory volume segments.

Therefore, SF_6 produces a series of τ_E segments with more similar values than those produced by He or N_2, meaning that gas volume will differ less between lung units with SF_6 than with other gases as lung units will fill and empty more homogenously with SF_6 than with He or N_2. With respect to our hypotheses, we demonstrated that values of R_L and E_L and their heterogeneity are greater in injured compared with uninjured lungs. Moreover, τ_E was more heterogeneous in injured lungs compared with uninjured lungs (as characterized by greater differences between the τ_E of early versus late segments of an expiration). We further demonstrated that interventions that alter regional R_L, such as alterations in gas density, alter τ_E values but do not alter indices of oxygenation, shunt and dead space.

Injury and gas density alter expiratory time constants

In the current experiment, changes in R_{RS} and E_{RS} were driven entirely by changes in R_L and E_L, and not by changes in R_{CW} or $E_{CW,}$ indicating that the injury used in our experimental model was confined to the lungs (Table 4.2). As the increases in E_L were greater than the increases in R_L, $\tau_{E,RS}$ decreased after injury. Lung compliance (the reciprocal of E_L) has been demonstrated to increase throughout passive expiration, which will cause τ_E to increase throughout expiration (38). However, although lung injury is conceptualized as a process that increases elastance, three to four-fold increases in resistance have been observed (50, 87, 98, 100). While this is primarily due to changes in the viscoelastic qualities of the lung, a doubling of airflow resistance may occur (151, 189, 207). Due to its high density, SF_6 will increase airflow resistance thereby increasing the time required for passive expiration, and He, with its relatively low density, will have the opposite effect. The slope of the $\dot{V}V$ curve during passive expiration and derived values of resistance and elastance have been used to describe τ_E (1, 132, 216, 217). Other

methods to assess τ_E include calculating the ratio of peak expiratory flow and volume exhaled (36) and multiplying respiratory system resistance and elastance as measured by the interrupter technique (73, 74). Common to all of these techniques is the assumption that a single compartment model can accurately describe the entirety of passive expiratory gas flow despite evidence that there is meaningful regional variation in ventilation in healthy lungs (202). Similarly, when expiration in our animals was considered using a single compartment model, $\tau_{E,TOT}$ and $\tau_{E,RS}$ increased with increasing gas density, demonstrating the importance of airflow resistance and gas density. However, single compartment models of τ_E will disproportionately reflect lung units with small time constants (121). Lung units with large τ_E will be represented by a later portion of the expiratory $\dot{V}V$ curve than those with small τ_E. A single τ_E measure based on the single compartment model will not reflect the mechanical conditions of either large or small τ_E. It follows that a method of differentiating the τ_E of faster emptying lung units (those with small τ_E) from those of slower emptying units (larger τ_E) would allow the quantification of τ_E heterogeneity within the lung. Unfortunately, previous studies have not assessed the differences in τ_E in the same subjects before and after injury, nor have they assessed the possibility that altering R_L might alter τ_E heterogeneity.

Gas density alters expiratory time constants and their heterogeneity

In our animals, both before and after injury, the increase in $\tau_{E,RS}$ from segment $\tau_{E,RS1}$ through $\tau_{E,RS5}$ was less steep for SF_6 than for N_2. Before injury, the increase in $\tau_{E,RS}$ from segment $\tau_{E,RS1}$ through $\tau_{E,RS5}$ was less steep for SF_6 than for He, but this finding was not significant after injury (Figures 4.4 and 4.5, and Figure 4.6 in Supplementary Materials 2).

Collectively, our experimental observations demonstrate that the $\tau_{E,RS}$ for early and late emptying lung units were more similar with SF_6 than for He or N_2. It is interesting to note that SF_6, the gas with the longest average $\tau_{E,}$ is also the gas that demonstrated the least difference in the lengths of $\tau_{E,RS1}$ through $\tau_{E,RS5}$ before and after injury. This may be due to the non-linear relationship between gas density and expiratory flow resistance. Thus, SF_6 will slow the early, faster emptying units to a greater extent than the later, slower emptying units when compared with N_2 or He. Accordingly, gas volume will differ less between lung units with SF_6 than with other gases.

In their initial analysis of the relationship between expiratory volume and τ_E in mechanically ventilated lung injury patients, Guttmann and colleagues observed that the τ_E for sequential volume segments (equivalent to $\tau_{E,TOT1}$ through $\tau_{E,TOT5}$ in the current study) were almost identical throughout expiration, a finding contrary to their expectations (81). As in our data, this was due to the significant flow resistance of the endotracheal tube and ventilator (R_{ETT}) (82, 208). As R_{ETT} and thus R_{TOT} increases with flow, $\tau_{E,TOT}$ must also increase with flow. In our data, the presence of an endotracheal tube and ventilator did not completely obscure the effect of injury in decreasing $\tau_{E,TOT}$ or the ability of increasing gas densities to increase $\tau_{E,TOT}$ (Figures 4.2 and 4.3). Given that flow is greatest at the beginning of passive expiration, the contribution of R_{TOT} has a large effect on $\tau_{E,TOT}$ in early expiration and less in late expiration, creating similar values for each segment of expired volume in both Guttmann's data and our animals. For example, when comparing Figures 4.3 and 4.5, it may be seen that the steady upward progression in τ_E segments in $\tau_{E,RS}$ data is lost in the $\tau_{E,TOT}$ data. With respect to the effect of gas density when

the endotracheal tube and ventilator apparatus were included, SF_6 increased $\tau_{E,TOT}$ compared with He and N_2 both before and after injury. However, SF_6's effect on the heterogeneity between values of $\tau_{E,TOT1}$ through $\tau_{E,TOT5}$ was less evident. As with $\tau_{E,RS}$, SF_6 produced more similar $\tau_{E,TOT}$ segments after injury than the other two gases, but this effect was not found prior to injury.

In injured lung parenchyma, strain is no longer homogenously distributed throughout tissue, but are rather concentrated around areas of relative over- or under-distension (63, 163), which may lead to injury. Altering the pattern of expiration to decrease the variability between early and late expiring lung units, as done in the current experiment with SF_6, could mitigate this heterogeneity of distension and thereby mitigate injury. For example, in a recent experiment altering the pattern of passive expiration by controlling expiratory flow in pigs led to decreased physiologic and biochemical markers of lung injury (69). Cyclic recruitment and derecruitment of alveoli in injured lung has been postulated to lead to new lung injury (46, 181). Animal models provide evidence that this may be mitigated by increasing extrinsic PEEP, presumably by decreasing the fraction of alveoli that collapse with each expiration. Similar experiments have shown that increasing intrinsic PEEP (by increasing respiratory rate, thereby preventing full expiration) or altering the I:E ratio alter the shunt fraction and may improve oxygenation in lung injury models (29). Prolonging τ_E could be anticipated to decrease cyclic derecruitment and thus improve shunt, deadspace and oxygenation. Contrary to our expectations this was not seen in our subjects before or after injury, suggesting that altering the pattern of τ_E may not significantly affect end-expiratory alveolar recruitment and shunt. Similarly, expiratory flow limitation (EFL) may occur in humans with lung injury, at least under conditions of no PEEP. However, it is unclear that similar limitations occur in other species. For example, Guérin and colleagues found

no EFL at zero PEEP in a porcine model of lung injury (77). This difference between humans and pigs may be due in part to differences in the mechanical properties of the chest wall and lungs. In Guérin's study (77) , the ratio of E_{CW} to E_L was 0.25 after injury, a value that may help maintain end-expiratory small airway patency (2). In humans with lung injury, this ratio has been reported to be as high as 0.57 (65). In the current study this value was 0.38, suggesting that species' specific respiratory mechanics may have prevented the development of EFL. Consistent with this possibility, examination of $\dot{V}V$ curves did not reveal sudden changes in the expiratory slope, a finding that would indicate flow limitation. Second, we did not observe gas flow at the end of expiration in the ensemble $\dot{V}V$ curves, a finding, that if present, might suggest the accumulation of gas within the injured lungs and the presence of intrinsic PEEP.

Study limitations

Four potential limitations of the current study must be recognized. First, the early portion of passive expiration may reflect viscoelastic and inertial effects and some authors (81, 106) have therefore removed this portion of $\dot{V}V$ curves from their analyses. To ensure that this effect did not confound our data, we performed our analysis on all five volume segments (as described) and on only the last four volume segments for all conditions of respiratory gas and injury state (data not shown). There was no substantive difference between the results of these two analyses. Second, our experiments were short term in nature and did not use a specifically lung-protective ventilation strategy. Moreover, a model with more severe injury and hypoxia might demonstrate greater alterations in mechanics and physiologic variables than were seen in the present experiment. Our data need elaboration in a more long-term study that focusses on the effects of gas density on inflammatory response and injury under the conditions of lung protective ventilation modes. Third, if manipulations of gas density alter ventilation heterogeneity, this

finding could potentially have been clarified by the addition of imaging modalities such as computerized tomography or electrical impedance tomography. Finally, while animal models and experimental methods of injury are widely used to investigate lung injury, neither provides an ideal replacement for human lung injury, and data generated from experimental animal models must be applied cautiously to human patients.

Conclusions

The use of SF_6 in ventilating gas mixtures lengthens total expiratory time constants before and after lung injury compared with both N_2 and He mixtures. Importantly, SF_6 mixtures also decrease the difference and variability of τ_E between fast and slow emptying compartments before and after injury when compared when nitrogen and helium mixtures. These effects, as well as the true shape of the τ_E curve, are obscured when measurements are made distal to an endotracheal tube. Both indices of gas exchange (oxygenation, shunt fraction and dead space) and the shape of the τ_E curve changed from before to after injury. However, alterations in gas density did not appear to affect indices of gas exchange either before or after injury. We have demonstrated that manipulations of gas density may alter the expiratory $\dot{V}V$ curve. Further investigation of these effects in future studies will help clarify whether gas density manipulation to improve pulmonary mechanics in lung injury alters clinical outcomes.

Tables

Table 4.1 Selected cardiorespiratory variables before and after injury with each gas mixture

	Gas	Pre	Post	P-value for interaction between injury and gas
Cardiac output ($L \cdot min^{-1}$)	He	1.40±0.16	1.12±0.41	0.55
	N_2	1.35±0.21	1.15±0.15	
	SF_6	1.33±0.19	1.26±0.15	
	P-value before vs. after injury = 0.042			
Mean Arterial Pressure (mmHg)	He	80 ± 4.0	80 ± 6.0	0.67
	N2	84 ± 2.6	83 ± 6.8	
	SF6	77 ± 3.2	84±10.3	
	P-value before vs. after injury = 0.62			
Mean Pulmonary Arterial Pressure (mmHg)	He	20 ± 1.0	35 ± 2.2	0.18
	N2	21 ± 1.8	34 ± 2.5	
	SF6	21 ± 1.46	31 ± 1.5	
	P-value before vs. after injury < 0.001			
PaO_2 (mmHg)	He	189±35	72±18	0.63
	N_2	185±37	68±16	
	SF_6	189±46	78±21	
	P-value before vs. after injury < 0.001			
Physiologic dead space (L)	He	0.18±0.04	0.37±0.15	0.38
	N_2	0.29±0.19	0.40±0.09	
	SF_6	0.17±0.09	0.25±0.08	
	P-value before vs. after injury = 0.002			
Alveolar dead space (L)	He	0.11±0.03	0.27±0.10	0.3
	N_2	0.10±0.05	0.25±0.06	
	SF_6	0.08±0.06	0.16±0.04	
	P-value before vs. after injury < 0.001			
Shunt fraction (%)	He	0.09±0.05	0.11±0.02	0.48
	N_2	0.09±0.03	0.12±0.04	
	SF_6	0.07±0.04	0.11±0.03	
	P-value before vs. after injury = 0.002			

He, helium-oxygen; N_2, nitrogen-oxygen; SF_6, sulphur hexafluoride-oxygen; Pre, before injury; Post, after injury. All data presented as mean ± standard deviation.

Table 4.2 Pulmonary mechanical data before and after experimental lung injury with different inspired gas mixtures

	E_{RS} ($cmH_20 \cdot L^{-1}$)	R_{RS} ($cmH_20 \cdot L^{-1} \cdot sec^{-1}$)	E_L ($cmH_20 \cdot L^{-1}$)	R_L ($cmH_20 \cdot L^{-1} \cdot sec^{-1}$)	E_{CW} ($cmH_20 \cdot L^{-1}$)	R_{CW} ($cmH_20 \cdot L^{-1} \cdot sec^{-1}$)
He, Pre	35±7	4±1	20±9	2±3	15±4	1±0
He, Post	83±27*	12±6*	64±24*	12±5*	18±12	2±4
N_2, Pre	39±8	4±1	24±11	3±1	15±6	1±0
N_2, Post	80±26*	14±6*	66±31*	13±6*	14±7	1±1
SF_6, Pre	36±10	5±1	26±8	4±1	14±4	1±1
SF_6, Post	85±48*	16±9*	71±33*	15±8*	21±14	1±1

E_{RS}, elastance of the respiratory system; E_L, elastance of the lung; E_{CW}, elastance of the chest wall; R_{RS}, resistance of the respiratory system; R_L, resistance of the lung; R_{CW}, resistance of the chest wall; He, helium-oxygen; N_2, nitrogen-oxygen; SF_6, sulphur hexafluoride-oxygen; Pre, before injury; Post, after injury; All values were calculated using tracheal pressures. * $P<0.05$ for difference between before and after induction of experimental acute respiratory distress syndrome. All data presented as mean ± standard deviation.

Figures

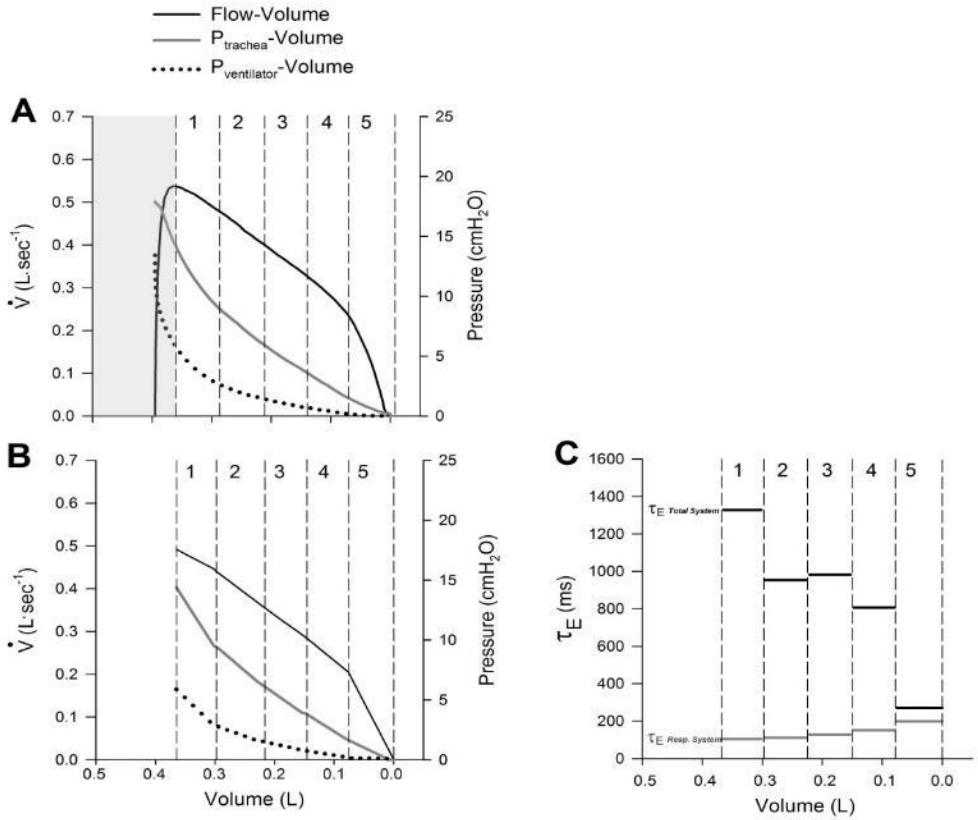

Figure 4.1 Graphical representation of determination of segment values for expiratory time constants (τ_E)
A: flow-volume ($\dot{V}V$) curve (black line), a pressure-volume (PV) curve using pressures measured at the ventilator wye and included the effects of the endotracheal tube and ventilator apparatus (dotted line), and a PV curve using tracheal pressures that excluded the effects of the endotracheal tube and ventilator apparatus (gray line) were created for each animal. Each ensemble from maximum expiratory flow to end expiration was divided into 5 equivolumetric segments. B: For each segment the $\dot{V}V$ curve was replaced by a least-squares fitted straight line. C: The slope of each straight line gives the τ_E of the corresponding volume segment ($\tau_{E,\,TOT1}$ through $\tau_{E,TOT5}$ and $\tau_{E,\,RS1}$ through $\tau_{E,RS5}$ for the total system and respiratory system, respectively).

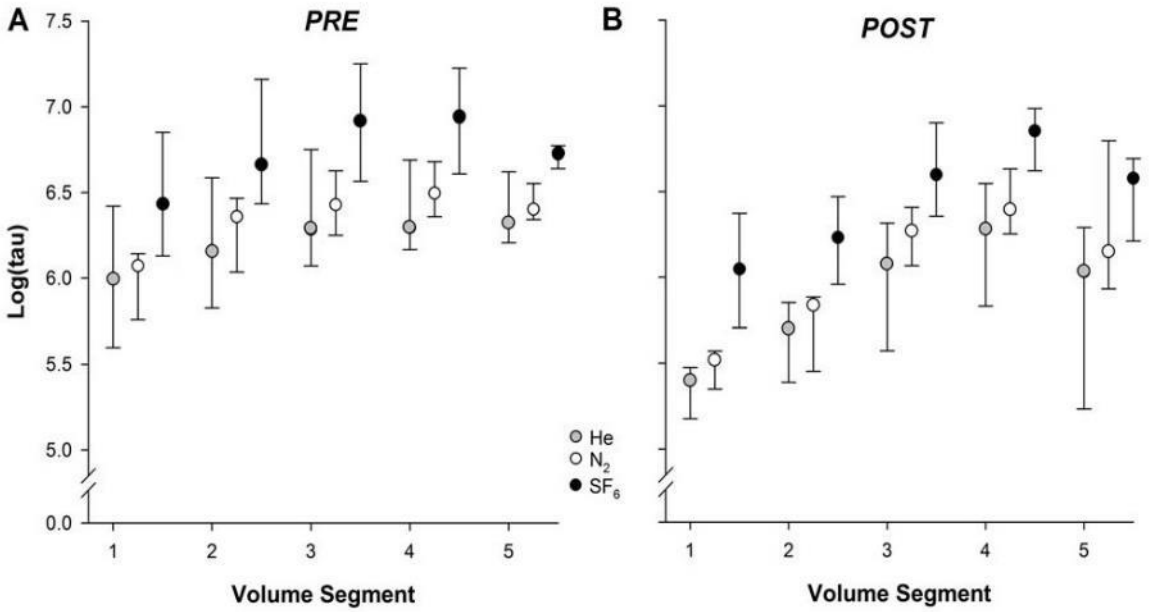

Figure 4.2 Values for $\tau_{E,TOT1}$ to $\tau_{E,TOT5}$ before and after injury are displayed as median values with interquartile ranges

He, helium-oxygen; N_2, nitrogen-oxygen; SF_6, sulphur hexafluoride-oxygen; Pre, before injury; Post, after injury.

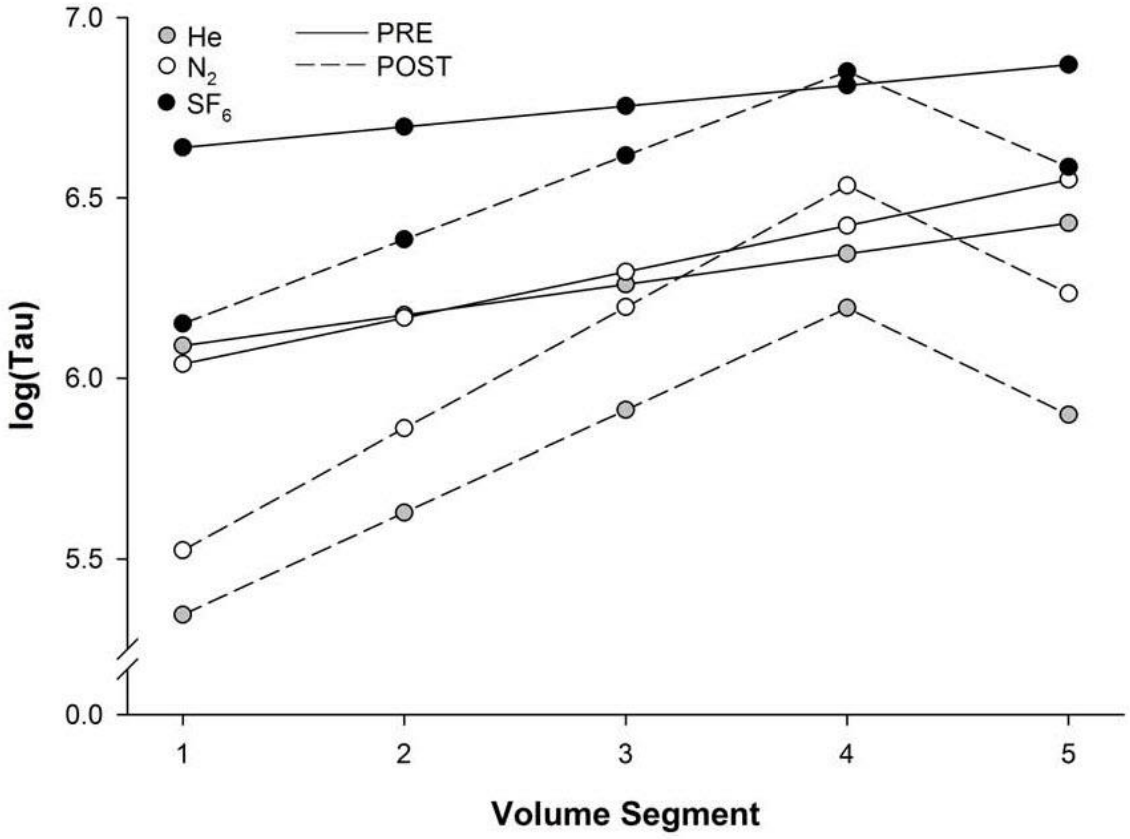

Figure 4.3 Values for $\tau_{E,TOT1}$ to $\tau_{E,TOT5}$ using the fitted model before and after injury
He, helium-oxygen; N_2, nitrogen-oxygen; SF_6, sulphur hexafluoride-oxygen; Pre, before injury; Post, after injury.

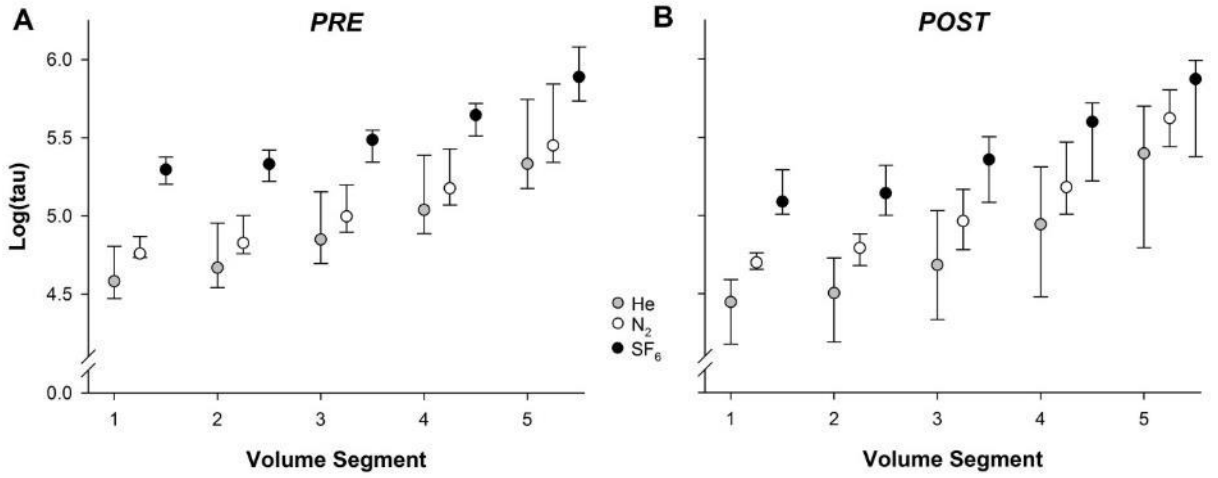

Figure 4.4 Values for $\tau_{E,RS1}$ to $\tau_{E,RS5}$ before and after injury are displayed as median values with interquartile ranges

He, helium-oxygen; N_2, nitrogen-oxygen; SF_6, sulphur hexafluoride-oxygen; Pre, before injury; Post, after injury.

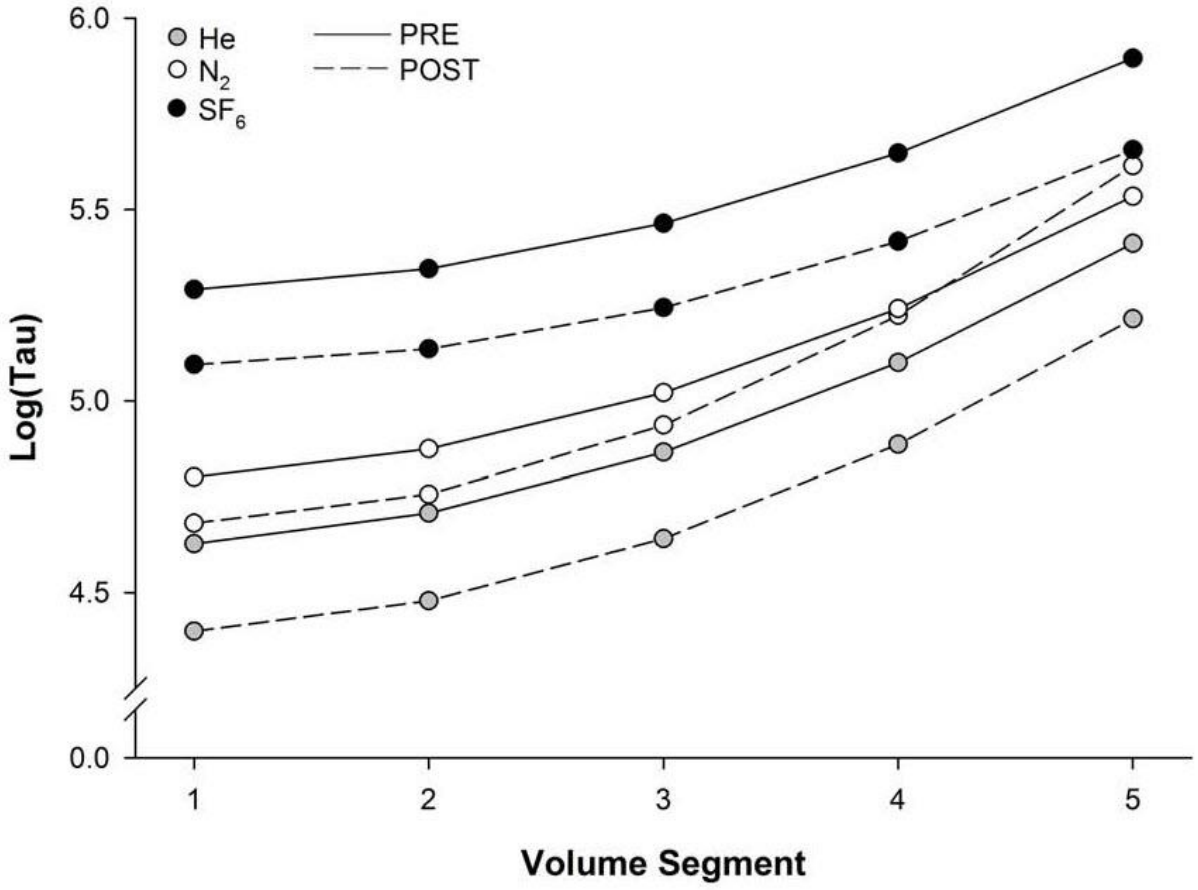

Figure 4.5 Values for $\tau_{E,RS1}$ to $\tau_{E,RS5}$ using the fitted model before and after injury
He, helium-oxygen; N_2, nitrogen-oxygen; SF_6, sulphur hexafluoride-oxygen; Pre, before injury; Post, after injury.

Supplementary Materials 1 –Methods

Measurement of pulmonary mechanics

Inspiratory and expiratory flows ($\dot{V}_I$ and $\dot{V}_E$) measured using a heated pneumotachograph (Model 3813, Hans Rudolph, Kansas City, MO). Expiratory volume (V) was obtained by numerical integration of the flow signals. Airway pressure (P_{AW}) was measured at a port distal to the ventilator wye. Tracheal pressure (P_{TR}) was measured using a fenestrated polyethylene catheter placed 2 cm past the distal end of the endotracheal tube. Oesophageal pressure (P_{OES})

was measured using a balloon-tipped catheter (no. 47-9005, Ackrad Laboratory, Cranford, NJ) placed in the lower third of the oesophagus and was assumed to approximate pleural pressure (P_{PL}). To calibrate the flow signals for different gas mixtures, the pneumotachograph was removed from the ventilator circuit and attached to an isolated closed circuit with an evacuated balloon. For each gas mixture, the entire apparatus was flushed with the experimental gas. A calibrated syringe filled with the appropriate gas mixture was then attached and used to inject 1 L of gas through the pneumotachograph.

Airway pressure (P_{AW}) was measured at a port distal to the ventilator wye. Tracheal pressure (P_{TR}) was measured using a fenestrated polyethylene catheter placed 2 cm past the distal end of the endotracheal tube. Oesophageal pressure (P_{OES}) was measured using a balloon-tipped catheter (no. 47-9005, Ackrad Laboratory, Cranford, NJ) placed in the lower third of the oesophagus and was assumed to approximate pleural pressure (P_{PL}). A modification of the Baydur test (21) was used to assess balloon position, which was further verified by the presence of cardiac pulsation in the trace and by the adequacy of waveform shape during mechanical ventilation (188). The P_{AW}, $P_{TR,}$ and P_{OES} pressures were measured using calibrated piezoelectric pressure transducers (Raytech Instruments, Vancouver, BC, Canada) and referenced to atmospheric pressure. An integrated 16-channel data acquisition and recording system (PowerLab/16SP model ML 795 and Chart v7, ADI, Colorado Springs, CO) was used to collect and record all data at a sampling frequency of 200 Hz.

Descriptive measures of whole breath pulmonary mechanics were calculated using previously described methods and end-inspiratory plateau pressures (20, 90). Total system elastance (including the endotracheal tube and ventilator apparatus) for the whole expiration was called E_{TOT} and was calculated as $\mathbf{\Delta}P_{AW}/\mathbf{\Delta}V$. Elastance of the respiratory system (that is, without

the interposition of the endotracheal tube or ventilator apparatus) for the entire expiration was called E_{RS} and was calculated as $\mathbf{\Delta}P_{TR}/\mathbf{\Delta}V$, Whole expiration lung elastance (E_L) was calculated as $\mathbf{\Delta}P_{TP}/\mathbf{\Delta}V$ where P_{TP} is $P_{TR} - P_{OES}$. Whole expiration chest wall elastance (E_{CW}) was calculated as $\mathbf{\Delta}P_{OES}/\mathbf{\Delta}V$. The whole expiration resistance of the total system including the endotracheal tube and ventilator apparatus (R_{TOT}) was calculated as $\mathbf{\Delta}P_{AW}/\mathbf{\Delta}\dot{V}$. The flow dependent resistance of the endotracheal tube and ventilator apparatus alters values of R measured distal to the endotracheal tube. We therefore calculated the whole expiration resistance of the respiratory system without the effect of the endotracheal tube and ventilator (R_{RS}) as $\mathbf{\Delta}P_{TR}/\mathbf{\Delta}\dot{V}$. Similarly, whole expiration lung resistance (R_L) was calculated as $\mathbf{\Delta}P_{TP}/\mathbf{\Delta}\dot{V}$ where P_{TP} is $P_{TR} - P_{OES}$. Whole expiration chest wall resistance (R_{CW}) was calculated as $\mathbf{\Delta}P_{OES}/\mathbf{\Delta}\dot{V}$. Functional residual capacity (FRC) was measured before and after injury using a previously described helium dilution method (145).

Characterization of the pattern of expiratory time constants

While descriptive whole breath measures of pulmonary mechanics (above) were measured and calculated using differences between end-expiratory and end-inspiratory measurements, characterization of the expiratory flow pattern occurred using methods similar to those of Guttmann (81) and Kondili (106) wherein the expiratory breath is subdivided into segments. Specifically, we combined ten individual breaths to create ensemble $\dot{V}V$ and PV curves for each animal for all combinations of injury state and gas mixture (Figure 4.1A). Using the $\dot{V}$, V and P values for each segment, we calculated E_{TOT} and R_{TOT} using the equation:

$$V(t)\times E_{TOT} + \dot{V}(t)\times(R_{ETT}(\dot{V}) + R_{EX}) = \mathbf{\Delta}P_{AW}$$

To account for the effect of the flow dependent resistance of the endotracheal tube and ventilator apparatus, one set of $\dot{V}V$ and PV traces were created using P_{AW} and a second set with

P_{TR}. If P_{AW} was used, then the values derived were E_{TOT} and R_{TOT}, while if P_{TR} was used to generate values, the values created were E_{RS} and R_{RS}.

To allow the assessment of τ_E heterogeneity, the V from the point of maximum expiratory flow to the end of expiration for each ensemble was divided into five segments of equal size as defined by expired volume (Figure 4.1B). We chose to use five segments in keeping with methods published in previous similar studies (81, 106).

Each segment was assumed to have E_{TOT}, R_{TOT} as well as flow-dependent resistance caused by the endotracheal tube and ventilator apparatus (R_{ETT}) values that did not vary throughout the duration of the segment. For each V segment, the τ_E was calculated as the resistance of the total system (R_{TOT}) during the relevant volume portion divided by elastance of the total system (E_{TOT}) during the same volume segment:

$$\tau_E = (R_{TOT})/E_{TOT}$$

This method allowed the calculation of unique respiratory system time constants for each of the five volume segments ($\tau_{E,TOT1}$ through $\tau_{E,TOT5}$) from peak expiratory flow to end exhalation (Figure 4.1C). Using the airway pressure measured at the outer end of the endotracheal tube the analysis gives the volume-dependent resistance including R_{ETT}; using the directly measured tracheal pressure gives the volume-dependent resistance of the respiratory system alone. We therefore repeated the same series of calculations to create values of $\tau_{E,}$ for the respiratory system, excluding the endotracheal tube and ventilator apparatus ($\tau_{E,RS}$). The five segments generated by this method were $\tau_{E,RS1}$ through $\tau_{E,RS5}$.

Supplementary Materials 2 – Statistics

We summarized the profile of log(τ_E) over volume segment with a polynomial function that included a linear and a squared term. To assess the effect of injury and respiratory gas composition on both $\tau_{E,TOT}$ and $\tau_{E,RS}$, linear mixed-effects regression models were used to assess group differences in the average profile and variability of the change of log(τ_E) over volume segment. All equations were fitted using restricted maximum likelihood methods and with the assumption of normality for the error term, and log transformation was used to reduce. Experimental condition (type of gas), volume segment (1 to 5, treated as continuous) and volume segment squared were included as fixed effects and group-specific intercepts and slopes were employed. Random effects included condition-specific intercepts and slopes for volume segment. A random effect of volume segment squared was not needed. The model used can be specified as:

$$log\ (\ tau_{jk(i)}) = \ \beta_{0i} + \beta_{1i}VS_j + \beta_{2i}VS_j^2 + b_{0k(i)} + b_{1k(i)}VS_j + \varepsilon_{jk(i)}$$

where $\log(tau_{jk(i)})$ represents the natural log of tau for the k^{th} pig in the i^{th} group at volume segment j. The model is presented graphically in Figure 4.6 for He pre injury. There is an average curve (thick grey line) for the *group* of animals, which is represented by the fixed effects:

$$log\ (\ tau_{jk(i)}) = \ \beta_{0i} + \beta_{1i}VS_j + \beta_{2i}VS_j^2$$

about which the *individual* animals are allowed to vary (thin grey lines). For example, the curve for the first pig would be:

$$log\ (\ tau_{j1(i)}) = \ (\beta_{0i} + b_{01(i)}) + (\beta_{1i}\ + b_{11(i)})VS_j + \beta_{2i}VS_j^2 + \varepsilon_{j1(i)}$$

The animal-specific regression parameters (i.e. the random effects) b_{0k} and b_{1k} reflect the natural heterogeneity in the animals.

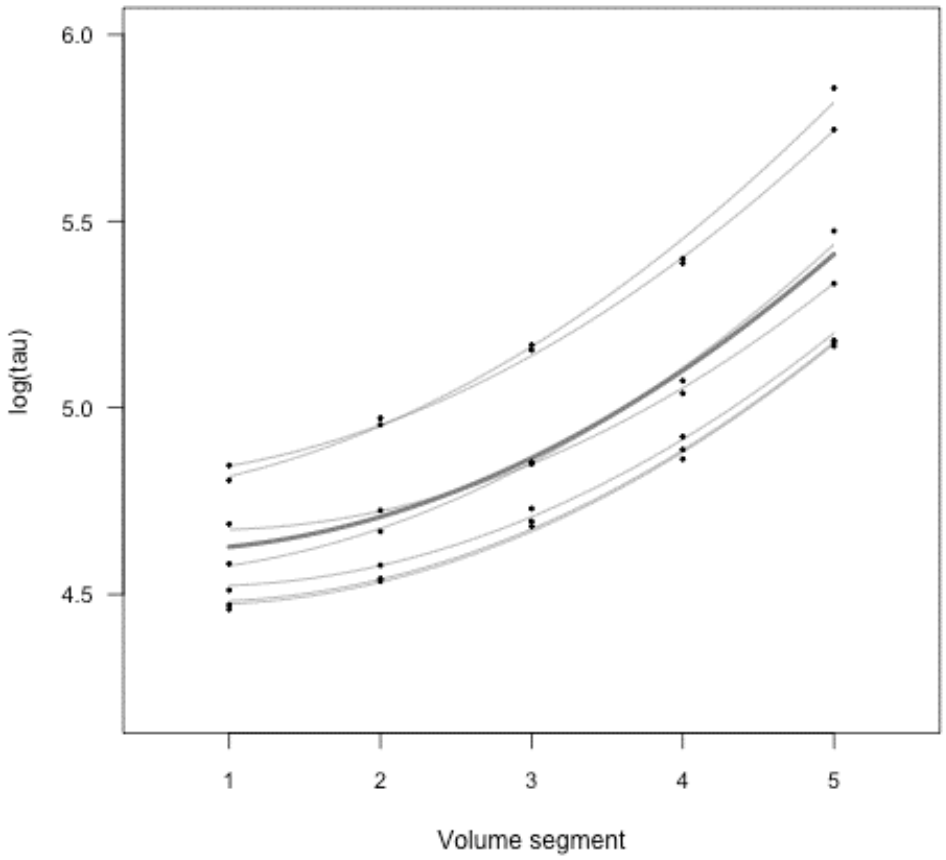

Figure 4.6 Demonstrating the relationship between individual animals (thin grey lines) and the group (thick grey line) in the model

Comparison of the fixed effects between groups was achieved by comparing the average curves. Comparison of the random effects was achieved by comparing the variability estimates. For example, comparing the intercepts $\beta_{0.HE}$ and $\beta_{0.N2}$, compared the average starting level of the two groups He and N_2. Comparing the coefficient "sets" ($\beta_{1.HE}$, $\beta_{2.HE}$) and ($\beta_{1.N2}$, $\beta_{2.N2}$) compares the evolution over volume segment of the groups (i.e., the combined linear and quadratic trends).

Differences in the average response profiles of the three groups can be assessed by pair-wise comparisons of $\beta_{0H}, \beta_{0N}, \beta_{0s}$ and $(\beta_{1H}, \beta_{2H}), (\beta_{1N}, \beta_{2N}), (\beta_{1s}, \beta_{2s})$; the latter assessing the rate of change in log(tau). Differences in the variability of the response about their respective average curves can be assessed from the random effects.

The profile of log(τ_E) over volume segment was summarized with a polynomial function that included a linear and a squared term. We used the logarithmic transformation to reduce the heteroscedasticity (increasing variance with increasing mean). Comparing the average profiles between gases or between injury states allows for a more parsimonious comparison than comparing groups at each volume segment value.

Supplementary Material 3 – Data

Gas	Segment	PRE			POST		
		R_{RS} ($cmH_20 \cdot L^{-1} \cdot sec^{-1}$)	E_{RS} ($cmH_20 \cdot L^{-1}$)	$\tau_{E,RS}$ (msec)	R_{RS} ($cmH_20 \cdot L^{-1} \cdot sec^{-1}$)	E_{RS} ($cmH_20 \cdot L^{-1}$)	$\tau_{E,RS}$ (msec)
He	1	2.21±0.42	25.86±3.92	86.33±5.29	5.62±0.82	76.58±9.09	73.63±6.05
	2	2.13±0.39	22.25±2.95	94.37±6.25	3.97±0.44	51.52±7.08	80.16±7.73
	3	2.74±0.35	24.18±1.90	111.66±8.20	3.58±0.30	39.43±5.24	98.05±11.72
	4	2.69±0.42	19.07±1.52	137.55±11.12	4.74±0.61	47.79±13.63	123.35±16.57
	5	3.06±0.71	14.83±2.55	194.71±19.48	3.61±0.77	21.99±4.67	180.96±28.04
N_2	1	3.53±0.47	33.27±2.77	104.07±5.86	7.29±1.24	77.27±11.68	93.54±4.12
	2	3.21±0.38	28.17±2.01	112.19±6.90	4.31±0.52	42.62±4.44	101.10±5.02
	3	3.41±0.49	25.18±2.18	131.95±8.93	4.11±0.48	32.89±2.72	124.50±9.28
	4	3.89±0.48	23.84±1.58	160.49±12.07	5.15±0.43	34.15±4.98	162.38±16.81
	5	2.93±0.75	12.61±2.50	221.55±20.22	6.09±1.69	31.29±11.76	262.56±49.79
SF_6	1	5.48±0.60	31.06±2.82	174.97±7.68	11.05±1.77	76.39±13.66	149.96±13.69
	2	4.51±0.48	24.35±1.77	183.04±9.33	7.62±1.14	52.72±10.18	153.53±14.24
	3	5.17±0.52	24.23±1.34	210.04±11.93	6.54±0.91	39.40±6.81	176.40±19.21
	4	5.53±0.65	21.79±1.72	249.88±16.20	7.21±1.31	39.71±12.53	212.35±25.89
	5	5.93±1.01	17.54±1.86	324.20±27.10	7.18±1.67	31.50±11.50	272.66±37.81

Gas	Segment	PRE			POST		
		R_{TOT} ($cmH_20 \cdot L^{-1} \cdot sec^{-1}$)	E_{RS} ($cmH_20 \cdot L^{-1}$)	$\tau_{E,TOT}$ (msec)	R_{TOT} ($cmH_20 \cdot L^{-1} \cdot sec^{-1}$)	E_{RS} ($cmH_20 \cdot L^{-1}$)	$\tau_{E,TOT}$ (msec)
	1	13.34±2.09	25.86±3.92	742.35±278.83	19.69±2.15	76.58±9.09	272.33±32.97
	2	13.44±2.20	22.25±2.95	700.71±176.52	18.86±2.19	51.52±7.08	387.95±46.98
He	3	13.61±2.25	24.18±1.90	557.57±79.51	18.07±2.21	39.43±5.24	496.62±73.08
	4	12.48±2.20	19.07±1.52	676.33±126.80	18.50±2.41	47.79±13.63	547.64±117.83
	5	10.32±1.30	14.83±2.55	832.43±188.42	9.43±1.10	21.99±4.67	513.60±80.78
	1	17.94±2.90	33.27±2.77	529.62±57.46	23.99±2.40	77.27±11.68	338.53±39.37
	2	17.49±2.96	28.17±2.01	604.76±71.66	21.68±2.29	42.62±4.44	530.45±64.48
N_2	3	16.50±2.98	25.18±2.18	636.28±77.56	20.86±2.59	32.89±2.72	625.56±45.95
	4	15.97±2.55	23.84±1.58	654.13±75.08	20.82±3.10	34.15±4.98	628.89±65.91
	5	9.40±1.02	12.61±2.50	701.76±50.06	12.97±1.89	31.29±11.76	759.26±197.42
	1	27.55±4.06	31.06±2.82	912.23±129.90	39.88±3.92	76.39±13.66	694.22±206.73
	2	26.35±4.05	24.35±1.77	1086.50±146.90	36.90±3.81	52.72±10.18	894.62±223.56
SF_6	3	25.42±3.84	24.23±1.34	1031.30±125.25	35.58±3.73	39.40±6.81	1106.00±271.12
	4	23.69±3.70	21.79±1.72	1089.90±158.27	31.67±3.25	39.71±12.53	1390.50±520.63
	5	16.73±1.52	17.54±1.86	1010.40±132.27	19.17±2.17	31.50±11.50	894.01±199.56

Table 4.3 Supplementary unlogrithmatized pulmonary mechanical data for the respiratory system and total system before and after experimental lung injury with different inspired gas mixtures

E_{RS}, elastance of the respiratory system; E_L, elastance of the lung; E_{CW}, elastance of the chest wall; R_{RS}, resistance of the respiratory system; R_L, resistance of the lung; R_{CW}, resistance of the chest wall; $\tau_{E,TOT}$, expiratory time constant of the total system; $\tau_{E,RS}$, expiratory time constant of the respiratory system; He, helium-oxygen; N_2, nitrogen-oxygen; SF_6, sulphur hexafluoride-oxygen; Pre, before injury; Post, after injury; All data presented as mean ± standard deviation.

Chapter 5: Effect of Tidal Volume and Positive End Expiratory Pressure on Expiratory Time Constants in Experimental Lung Injury

Introduction

Acute respiratory distress syndrome (ARDS) is a lung injury characterized by hypoxia and impaired pulmonary mechanics. The associated histologic changes, such as alveolar flooding and collapse, airway edema, and altered surfactant function, are heterogeneous in distribution within the lungs (43). Because of this heterogeneity, some lung units have abnormal values of resistance (R) and/or elastance (E), while others have values that are similar to those found in healthy lung (50, 98, 100, 135, 143, 177). The R and E of a lung unit determine it's time constant (*tau* [τ]), which is defined as the time required to inflate or deflate 63% of the volume of a given lung unit. The regional variation of R and E of lung tissue implies that there is regional heterogeneity in expiratory time constants (τ_E).

Currently, there is scant information regarding the extent to which the pattern of τ_E is altered by the development of lung injury in a given subject. We have recently demonstrated that the τ_E pattern of lung passive expiration in the same subject differs with injury status and that these patterns can be altered by manipulating the density of the ventilating gas (89). Kondili and colleagues have examined changes in τ_E due to manipulation of positive end-expiratory pressure (PEEP) following lung injury (106). They found that in patients with ARDS at zero PEEP, τ_E increased throughout expiration due to progressive increases in respiratory system resistance (R_{RS}). The application of PEEP decreased R_{RS} (primarily in late expiration), resulting in τ_E values that were smaller and less varied throughout lung emptying. Similarly, Kondili and colleagues

found that the addition of PEEP increased respiratory system elastance (E_{RS}) and τ_E during the early portion of expiration.

No studies have documented the role of altering PEEP or tidal volume (V_T) on the pattern of τ_E in the same subject before and after injury. This is relevant, as a more complete understanding of how PEEP and V_T interact with injury status may allow clinicians to more accurately choose strategies for mechanical ventilation. For example, the optimal combination of PEEP and V_T may differ in the same patient as lung injury evolves and resolves. Recognition of these changes may allow clinicians to optimize the pattern of lung emptying and minimize the risk of new ventilator induced lung injury.

We reasoned that interventions that alter regional E and R, such as alterations in V_T or PEEP, should alter τ_E values and the pattern or passive expiration. We hypothesized that the effects of both PEEP and V_T on τ_E would differ between the uninjured and injured states. To this end, we undertook to characterize the effects of changes in PEEP and V_T on τ_E, R_{RS} and E_{RS} before and after the induction of an experimental model of lung injury.

Methods

Animals and instrumentation

The Animal Research Committee of the University of British Columbia (certificate #: A12-0272) reviewed and approved the experimental procedures. Anesthesia was induced with inhaled isoflurane (3-5% in oxygen) after sedation with telazol (4-6 mg/kg intramuscular injection) in 6 adult female Yorkshire X pigs (weight, 31.42 ± 5.42 kg). After tracheal intubation, inhalational anesthesia was discontinued once total intravenous anesthesia was established with midazolam (0.1 mg/kg intravenous) and a propofol infusion (200 mcg/kg/min and adjusted to

between 150 and 300 mcg/kg/min). The adequacy of anesthesia was assessed every fifteen minutes using assessment of vital signs, physical examination and electrocardiography. The animals were mechanically ventilated (Puritan-Bennett 7200, Covidien, Ireland) with 0 cm H_2O of PEEP using an inspired oxygen fraction (FiO_2) of 0.5 and V_T of 10 cc/kg. Breathing frequency was initially set at 15 breaths/minute and was adjusted to maintain end-tidal CO_2 between 35-45 mmHg with an inspiratory flow of 45 L/minute. A right femoral artery catheter was used to collect arterial blood samples into pre-heparinized syringes, which were immediately analyzed by calibrated blood gas analyzer (ABL 80 CO-OX Flex). Neuromuscular blockade was induced when needed prior to all measurements of pulmonary mechanical parameters using pancuronium (0.05 to 0.1 mg/kg intravenous) after a bolus of intravenous midazolam (0.1 mg/kg). Paralysis was monitored by assessment of response to train-of-four stimulation using a peripheral nerve stimulator. At the end of the experiment, euthanasia was achieved with pentobarbital sodium (120 mg/kg intravenous). Death was confirmed by the absence of a pulse and cardiac electrical activity on continuous surface electrocardiography.

Induction of lung injury

We used a previously published method (87) of lung injury that that satisfies the current American Thoracic Society's guidelines for a high quality model of ARDS and that demonstrates a profound neutrophilic alveolitis with diffuse alveolar damage (128). 1% sodium polyacrylate gel in aqueous solution was injected through the endotracheal tube and was manually dispersed throughout the lungs by bagging. One 5 ml aliquot was given every five minutes until an arterial oxygen tension (PaO_2) of less than 150 mm Hg, while receiving a fraction of inspired oxygen (FiO_2) of 0.5 was observed. The ratio of PaO_2/FiO_2 less than 300 was chosen to be consistent with current definitions of ARDS (162).

Interventions

Prior to and subsequent to experimental lung injury, animals were ventilated in a computer generated random order with six different combinations of V_T and PEEP: V_T of 5, 10, 12 and 15 cc/kg all at 0 cmH_2O PEEP along with 5 and 10 cmH_2O PEEP at 12 cc/kg. PEEP and V_T levels were chosen to allow the assessment of a range of clinically relevant PEEP and V_T values and reflect those used in recent similar studies (106, 148). Prior to each set of measurements, the animals were ventilated for twenty minutes at each combination of V_T and PEEP to eliminate the effect of volume history.

Measurement of pulmonary mechanics

All data was collected and recorded digitally (PowerLab/16SP model ML 795 and Chart v7, ADI, Colorado Springs, CO). Using heated pneumotachographs (Model 3813, Hans Rudolph, Kansas City, MO), inspiratory and expiratory flows ($\dot{V}_I$ and $\dot{V}_E$) were measured and subsequently integrated to determine inspiratory and expiratory volumes (V_I and V_E). Airway pressure (P_{AW}) was measured at a port distal to the ventilator wye and pleural pressure was assumed to be approximated by the measurement of esophageal pressure (P_{ES}) with a balloon-tipped catheter (Ackrad Laboratory, Cranford, NJ). The catheter was positioned in the lower third of the esophagus and balloon position was verified by the presence of cardiac pulsation in the trace and the adequacy of waveform shape during mechanical ventilation (21, 188). P_{AW} and P_{ES} were referenced to atmospheric pressure and measured using calibrated pressure transducers (Raytech Instruments, Vancouver, BC, Canada).

Tracheal pressure (P_{TR}) is often assumed to be estimated by P_{AW}. This assumption may not be valid under dynamic conditions such as when flow dependent resistance across the endotracheal tube creates a time-dependent pressure drop across the endotracheal tube ($P_{ETTV(t)}$).

The drop in pressure causes P_{TR} to differ significantly from P_{AW} (194). To overcome this, P_{TR} at a specific time ($P_{TRV(t)}$) may be measured directly or calculated at any time point given that $(P_{TRV(t)}) = P_{AW(t)} - (P_{ETTV(t)})$ (82). To calculate $P_{TRV(t)}$ we used a previously validated multifactor formula that estimates the pressure drop across the endotracheal tube from three known values: the endotracheal tube length and diameter, $\dot{V}V$ and P_{AW} (81, 82). The model is defined as: $P_{TRV(t)} = P_{AW}(t) - K_1 \cdot \dot{V}^{K2}$ where K_1 and K_2 are empirically derived values from previous work (82).

Elastance of the respiratory system (E_{RS}), that is, without the interposition of the endotracheal tube or ventilator apparatus for the entire expiration, was calculated as $\mathbf{\Delta}P_{TR}/\mathbf{\Delta}V$. Lung elastance ($E_L$) was calculated as $\mathbf{\Delta}$ ($P_{TR} - P_{ES}$) /$\mathbf{\Delta}V$. Chest wall elastance (E_{CW}) was calculated as $\mathbf{\Delta}P_{ES}/\mathbf{\Delta}V$. Descriptive E_{RS}, E_L and E_{CW} data (as opposed to that used to calculate τ_E) were collected during end-inspiratory plateau conditions. As the flow dependent resistance of the endotracheal tube and ventilator apparatus alters values of R measured distal to the endotracheal tube (82, 208), we calculated the resistance of the respiratory system without the effect of the endotracheal tube and ventilator (R_{RS}) as $\mathbf{\Delta}P_{TR}/\mathbf{\Delta}\dot{V}_E$. Transpulmonary pressure (P_{TP}) was defined as $P_{TR} - P_{ES}$ and lung resistance (R_L) was calculated as $\mathbf{\Delta}P_{TP}/\mathbf{\Delta}\dot{V}_E$. Chest wall resistance (R_{CW}) was calculated as $\mathbf{\Delta}P_{ES}/\mathbf{\Delta}\dot{V}_E$. Functional residual capacity (FRC) was measured before and after injury using a previously described helium dilution method (145). Arterial blood gas analysis was performed prior to injury, after injury and at the end of the experimental session.

Calculation of expiratory time constants

Calculating a single value for τ_E assumes that all lung units inflate and deflate as a single compartment and does not allow differentiation between fast and slow filling/emptying units (1, 36, 132). The assumption that a single all lung units have identical τ_E may have important consequences; heterogeneous rates of alveolar filling/emptying can create localized areas of high

tissue strain, which may cause new lung injury and/or exacerbate existing injury (158). To address this issue, we and others have utilized a multi-compartment model to describe lung emptying during passive deflation by partitioning the expiratory flow-volume ($\dot{V}V$) curve into multiple discrete segments and individually calculating τ_E for each these segments (81, 89, 105, 106, 114). The multisegment method allows a more nuanced description of the changes in τ_E throughout expiration, and therefore facilitates better understanding of the physiology of passive expiration than does a single compartment model.

We combined ten individual $\dot{V}V$ and pressure-volume (PV) traces taken at the end of 20 minutes of ventilation at each PEEP and V_T combination using methods described by Guttmann (81) and Kondili (106). From this data, we created ensemble $\dot{V}V$ and PV curves for each animal for all combinations of injury state, each combination of V_T and PEEP. From this data, we calculated values for τ_E of the respiratory system *excluding* the endotracheal tube and ventilator apparatus using P_{TR}. To allow the assessment of τ_E heterogeneity, the V_E from the point of maximum $\dot{V}_E$ to the end of expiration (defined as $\dot{V}_E$ less than 0.05 L/s) for each ensemble was divided into five equal volume segments (V_{E1}-V_{E5}). We chose to use five segments in keeping with methods from similar studies (81, 106). Each of the five V_E segments was assumed to have E and R values that did not vary throughout the duration of the segment. Therefore for each V_E segment, the τ_E was calculated as the quotient of R_{RS} and E_{RS}. R_{RS} was calculated as $(P_{TR} - P_{ATM})/\dot{V}_E$ and E_{RS} as $\Delta P_{TR} / \Delta V_E$ for the V_E segment in question. This method allowed the calculation of unique respiratory system time constants for each of the five V_E segments (named τ_{E1} through τ_{E5}) from the point of maximum $\dot{V}_E$ to end expiration (Figure 5.1).

Statistical analyses and model

Values are displayed as mean and 95% confidence intervals (CI). Continuous variables were analyzed using paired t-tests (within animal) or two-sample t-tests (between animals) where appropriate. All tests were two-sided and the statistical significance was defined at $P<0.05$. Statistical analyses were performed using STATA 10.0 Statistical Software (StataCorp, College Station, TX) and SAS (SAS Institute, Inc., NC).

Expired time constants values were analyzed by linear mixed-effect model, including a random effect for each animal and fixed effects for segment, PEEP, V_T, and pre-post injury.

Significance of model coefficient estimates, least squares means, and differences in least squares means were determined by T-test. Main effects and interactions were confirmed by use of F-tests with Type III sums of squares. All tests were performed at the 0.05 significance level. Differences in least squares means were adjusted for multiple testing using the Tukey-Kramer adjustment.

Results

Before lung injury, the animals demonstrated a PaO_2 of 197±51mmHg while ventilated with a V_T of 10cc/kg, 0 cm H_2O PEEP and an FiO_2 of 0.5. Thirty minutes after injury, PaO_2 decreased to 68±10mmHg and was 69±19mmHg prior to euthanasia ($p<0.01$ for both time points compared to pre-injury values). During the same pre-injury ventilation conditions, FRC was 14.3±2.5 ml/kg and decreased to 9±2.9 ml/kg after injury ($p<0.01$). E_{RS} and R_{RS} both increased with experimental injury due to significant increases in both E_L and R_L ($p<0.01$ for both) and no changes in E_{CW} or R_{CW} ($p>0.05$). Descriptive pulmonary mechanical data are presented in Table 5.1.

Effect of injury status, PEEP and tidal volume on expiratory time constants

Under all conditions of PEEP and V_T, τ_E increased throughout expiration both before and after injury (Table 5.2 and Figure 5.2). Segmented τ_E values increased throughout expiration with a slope that was different than zero ($p<0.01$). The expired time constant increased by an average of 45.08 msec per segment when τ_E segment was treated as a continuous variable (36.07, 54.08; 95% CI). The model used for this analysis included an interaction between segment and injury. The main effect of segment as a continuous covariate was significant with and without interaction terms. Congruent with these findings, τ_{E1} and τ_{E2} were significantly smaller than τ_{E4} and τ_{E5}, τ_{E3} showed significant difference from τ_{E4} and τ_{E5}, and there was a difference between τ_{E4} and τ_{E5} ($p<0.01$ for all comparisons). When an interaction between injury status and τ_E segment was included in the model, it was found to be significant ($p<0.05$), indicating that later segments had higher τ_E values post injury. Examining the difference between segments within injury status yielded nearly identical results to those cited over all injury states; only pre injury τ_{E3} was no longer significantly different from pre injury τ_{E4}.

Higher PEEP and V_T values were associated with higher τ_E values (Figures 5.3 and 5.4). The increase in τ_E per 1ml/kg increase in V_T and 1 cmH_2O increase in PEEP and were 5.97 msec (3.23, 8.70; 95% CI) and 4.53 msec (2.34, 6.72; 95% CI), respectively. No evidence was found for an interaction between injury status and V_T, or between injury status and PEEP.

Effect of injury status, PEEP and tidal volume on resistance and elastance

To further clarify the causative factors behind changes in τ_E segments throughout expiration, we analysed R_{RS} and E_{RS} on a per segment basis using the same methods applied to τ_E segments τ_{E1} to τ_{E5}. Both R_{RS} and E_{RS} were significantly increased after injury compared to before injury in early V_E segments (Tables 5.3 and 5.4). Segment values for R_{RS} and E_{RS} after

injury were statistically similar to values before injury ($p>0.05$). The raw segment values for R_{RS}, E_{RS} and τ_E are shown in Table 5.5.

The differing values for R_{RS} and E_{RS} between pre and post injury status was confirmed by the presence of a significant interaction effect between injury status and segment ($p<0.01$). The effect of segment on R_{RS} as a continuous variable was not significant. However, segment as a categorical covariate was significant ($p <0.01$) in determining the value of R_{RS}. The estimated slope of E_{RS} by segment was -6.76 (-10.14, -3.38; 95% CI) and was significant ($p <0.01$). Segment remained a significant continuous covariate when included in the model for E_{RS} without an interaction term. No evidence of other interactions was found.

Relative values (comparing post-injury to pre-injury state) for R_{RS} and E_{RS} for each volume segment are shown in Figure 5.5, while raw values are shown in Table 5.5. Over both states of injury, R_{RS1} is significantly different from all subsequent segments except for R_{RS5} ($p<0.01$), as is the difference between R_{RS5} and R_{RS1}- R_{RS4} ($p <0.01$). However, the differences in R_{RS} by segment may have been driven by post injury values, as no significant differences were found between R_{RS} segments pre-injury. Post injury, R_{RS1} differs from all other segments post injury ($p<0.01$). For E_{RS}, E_{RS1} and E_{RS2} were significantly different from E_{RS3}, E_{RS4}, and E_{RS5} ($p<0.01$), as is the E_{RS3} from E_{RS4} and E_{RS5} ($p<0.01$). Within injury state, post injury differences again outnumbered the pre injury segment differences; Post injury, E_{RS1} is different from all others ($p<0.01$), E_{RS2} is significantly different from E_{RS3}, E_{RS4}, and E_{RS5} ($p <0.01$), and E_{RS3} and E_{RS5} are different ($p<0.01$). Pre injury, only E_{RS1} is significantly different from E_{RS4} and E_{RS5} ($p <0.05$).

Finally, we found that changes in PEEP or V_T altered R_{RS} and E_{RS}. A one cmH_2O increase in PEEP increased R_{RS} by 0.21 cmH_2O/L/sec (0.09, 0.33; 95% CI), and increased E_{RS} by 1.21 cmH_2O/L (0.34, 2.08; 95% CI). A one ml/kg increase in V_T increased R_{RS} by 0.24 cmH_2O/L/sec (0.09, 0.38; 95% CI) but did not have any significant effect on E_{RS}.

Discussion

The current study has three main findings. First, consistent with our previous work (89), τ_E increased throughout expiration, and injury increased the difference between late and early τ_E segments compared to before injury. These changes were due to increases in both R_{RS} and E_{RS}. Second, we found that manipulating PEEP or V_T did not have a differential effect on τ_E between injured and uninjured states in a segmented model of expiration. Third, increases in both PEEP and VT increased R_{RS}, a finding that is somewhat counterintuitive and that has potential clinical implications for the choice of mechanical ventilation strategy in patients with ARDS or lung injury.

Injury and time constants

Using a single compartment model rather than a segmented model, we observed that injury decreased average segmental τ_E values compared with before injury (Table 5.2). The decreased τ_E observed in the post-injury state is related to increases in both R_{RS} and E_{RS}. Following lung injury, we found that increases in R_{RS} and E_{RS} were driven by increases in R_L and E_L with no significant changes in R_{CW} and E_{CW}. Accordingly, the absence of mechanical alterations to the chest wall suggests that the injury used in this model was confined to the lungs (Table 5.1). When assessed from the perspective of a single compartment (that is, not segmented), increases in E_L were greater than those in R_L and therefore τ_E decreased after injury.

Many methods of calculating τ_E assume that all lung units inflate and deflate as a single compartment and are thus unable to distinguish between units that fill/empty quickly and units that require greater time. We therefore employed a segmental method can be used to more accurately describe the pattern of lung emptying during passive expiration, potentially providing more insight into the degree of pulmonary mechanical heterogeneity than is afforded by a single compartment model (81, 89, 105, 106, 115). When a segmented model was used to analyse our data, we were able to observe the mechanical properties of passive expiration with a higher degree of resolution than is afforded by the single compartment model. In a segmented model, injury increased the difference between later versus earlier segment τ_E values - that is, injury decreased the average τ_E in early segments, and increased the average τ_E for later segments compared to the uninjured state (Table 5.2 and Figure 5.2).

When compared with uninjured values, both R_{RS} and E_{RS} after injury are roughly three-fold higher at the beginning of expiration (Panel A, Figure 5.5) before returning to values similar to those in uninjured lungs by the end of expiration. While both R_{RS} and E_{RS} increased post-injury, the increase in E_{RS} in absolute terms was greater, causing early τ_E values (for example τ_{E1} in Table 5.2) to be smaller after injury compared to before injury. Throughout expiration, values of E_{RS} decreased more rapidly than $R_{RS,}$ causing late τ_E segment values to be higher (for example τ_{E5} in Table 5.2).

PEEP and tidal volume

We found that increasing both PEEP and V_T increased τ_E, but that these effects did not differ between the uninjured and injured states (Figures 5.3 and 5.4). We demonstrated that increases in PEEP increased R_{RS} and increased E_{RS} while increases in V_T increased R_{RS} alone.

The independent effects of PEEP and V_T on τ_E segments appeared consistent throughout expiration, that is they were not confined to early or late τ_E segments.

It is instructive to compare our results with those of other investigators. Kondili and colleagues reported effects of PEEP that differed from ours (106). They found that in subjects with ARDS who were ventilated without PEEP, τ_E and R_{RS} increased significantly in late expiration and that the addition of PEEP eliminated these findings. One result of the application of PEEP is that small airways are "splinted" open, and are less likely to close prematurely. The increased patency of small airways may allow more rapid exhalation, thereby resulting in smaller τ_E values with higher PEEP, particularly in late expiration. This widely accepted concept supplies a satisfying explanation for the effect of PEEP in Kondili's results. However, other authors have found patterns of expiration and effects of applied PEEP that are more similar to our results. Pesenti and colleagues found that PEEP increased R_{RS} in patients with ARDS and in normal controls (150). In patients with ARDS, Mols and colleagues observed that the pattern of τ_{E1-5} and R_{RS1-5} was highly variable, with patients demonstrating steady increases, steady declines or no discernible pattern during passive expiration (136). Similarly, other authors have demonstrated that increases in PEEP and V_T increase R_{RS} in subjects with lung injury or ARDS(11, 146, 190).

There are several possible explanations for the finding that increases in PEEP or V_T may increase R_{RS}. First, injured lung is characterized by inhomogeneity of distension, and high levels of PEEP could further over-distend some units, thereby increasing time constant inhomogeneity. Second, increased R_{RS} at higher PEEP or V_T values may in part be due to stress adaptation phenomena and specifically increases in viscoeleastic resistance at higher PEEP values and lung volumes (146, 150). Third, it has been suggested that the longitudinal stretching of airways at

high PEEP and V_T levels may narrow their cross-sectional area and thus increase resistance to gas flow (49). Given these data, observation of the pattern of τ_E during expiration may facilitate the choice of less injurious strategies of mechanical ventilation during the care of patients with ARDS or lung injury.

Limitations

The current experiment reveals novel findings regarding the relationships between lung injury, the parameters of mechanical ventilation, and the pattern of $\dot{V}_E$. However, several limitations must be considered. First, we did not measure P_{TR} directly in this experiment. Instead, like Guttmann, we estimated P_{TR} from P_{AW} using a previously validated method (81, 82, 213). Guttmann and colleagues measured P_{AW} at the ventilator wye and observed that the calculated τ_E for sequential volume segments in mechanically ventilated ARDS patients were almost identical throughout expiration (81). The similar τ_E was due to the significant flow-dependant resistance of the endotracheal tube and ventilator (R_{AW})(82, 208). Given that flow is greatest at the onset of passive expiration, the relative contribution of R_{AW} on τ_E is higher during early expiration and lower in late expiration, which masks the influence of R_L (82, 208). When they eliminated the effect of the endotracheal tube by estimating P_{TR} and used these values to calculate segmental values for τ_E, Guttman and colleagues found a pattern of steadily increasing τ_E throughout expiration. Similarly, our data demonstrates that τ_E increases steadily throughout expiration when a segmented model that excludes the resistance of the endotracheal tube was used (Figure 5.2).

Conclusions

Our study provides several novel insights into the details of expiratory gas flow in animals before and after experimental lung injury. It has previously been observed that τ_E values are smaller

in subjects with injured lungs when compared to controls. However, we are the first to demonstrate this change within subjects and that τ_E increased throughout expiration both before and after injury when examined with a multiple compartment model. Finally, we have demonstrated that increases in PEEP or V_T increased τ_E throughout expiration, but did not appear to have effects that differed between the uninjured and injured state. Whether incorporating the pattern of $\tau_{E,}$ will improve strategies of mechanical ventilation in lung injury and ARDS needs to be assessed in future studies.

Figures

A **B**

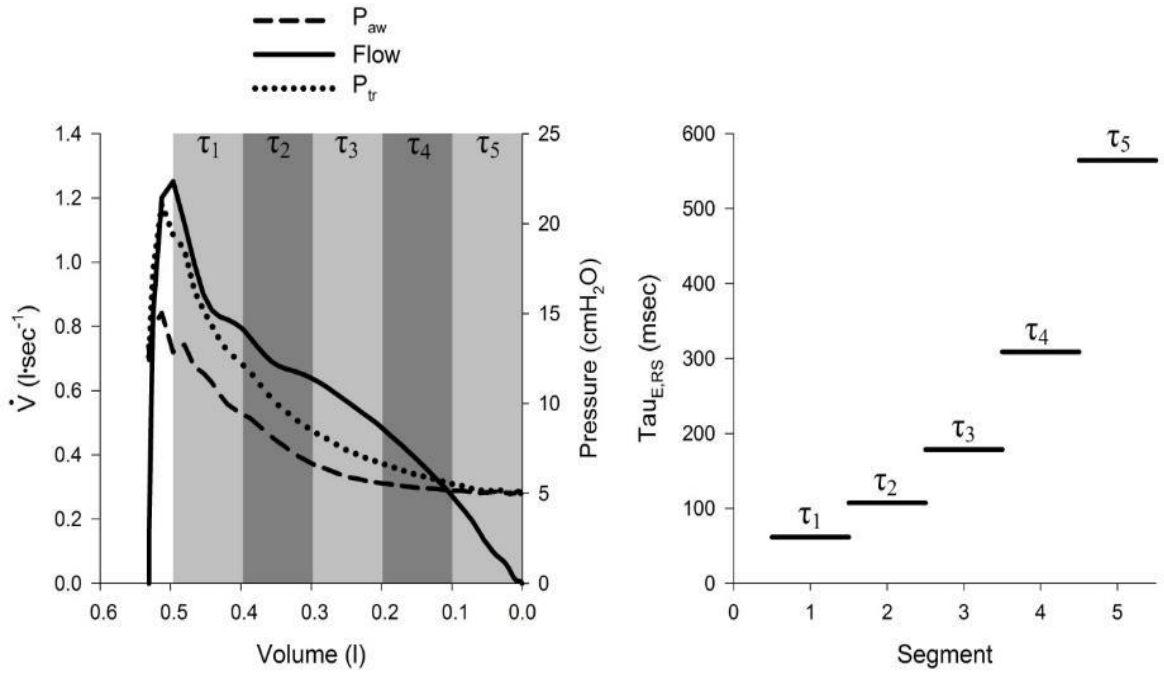

Figure 5.1 Graphical representation of the method used to derive segmental expiratory time constants (τ_E) values

A: flow-volume ($\dot{V}V$) curve (black line), a pressure-volume (PV) curve using pressures measured at the ventilator wye and including the effects of the endotracheal tube and ventilator apparatus (dashed line), and a PV curve using tracheal pressures excluding the effects of the endotracheal tube and ventilator apparatus (dotted line) were created for each animal. Each ensemble from maximum expiratory flow to end expiration was divided into 5 equivolumetric segments. B: For each segment the expiratory $\dot{V}V$ curve was replaced by a least-squares fitted straight line. The slope of each segment provides the τ_E for that segment. In this figure only the expiratory time constant of the respiratory system ($\tau_{E,RS}$) is displayed.

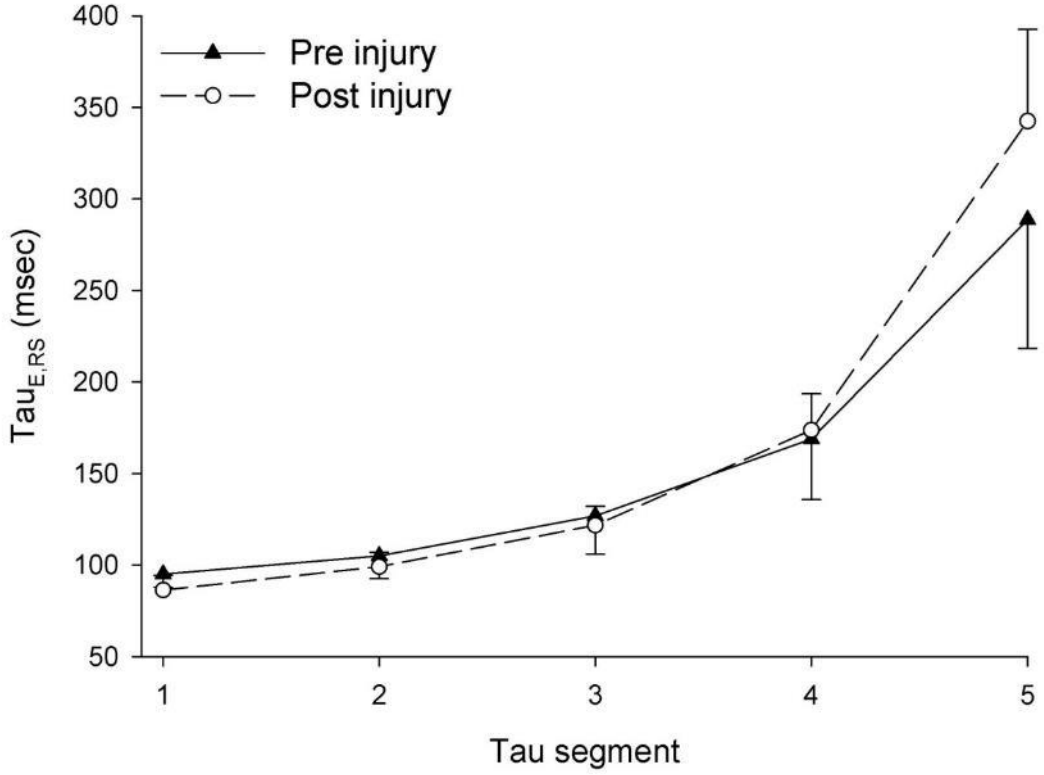

Figure 5.2 Values for $\tau_{E,RS1}$ to $\tau_{E,RS5}$ before and after injury are displayed as mean values ± 95% confidence interval.

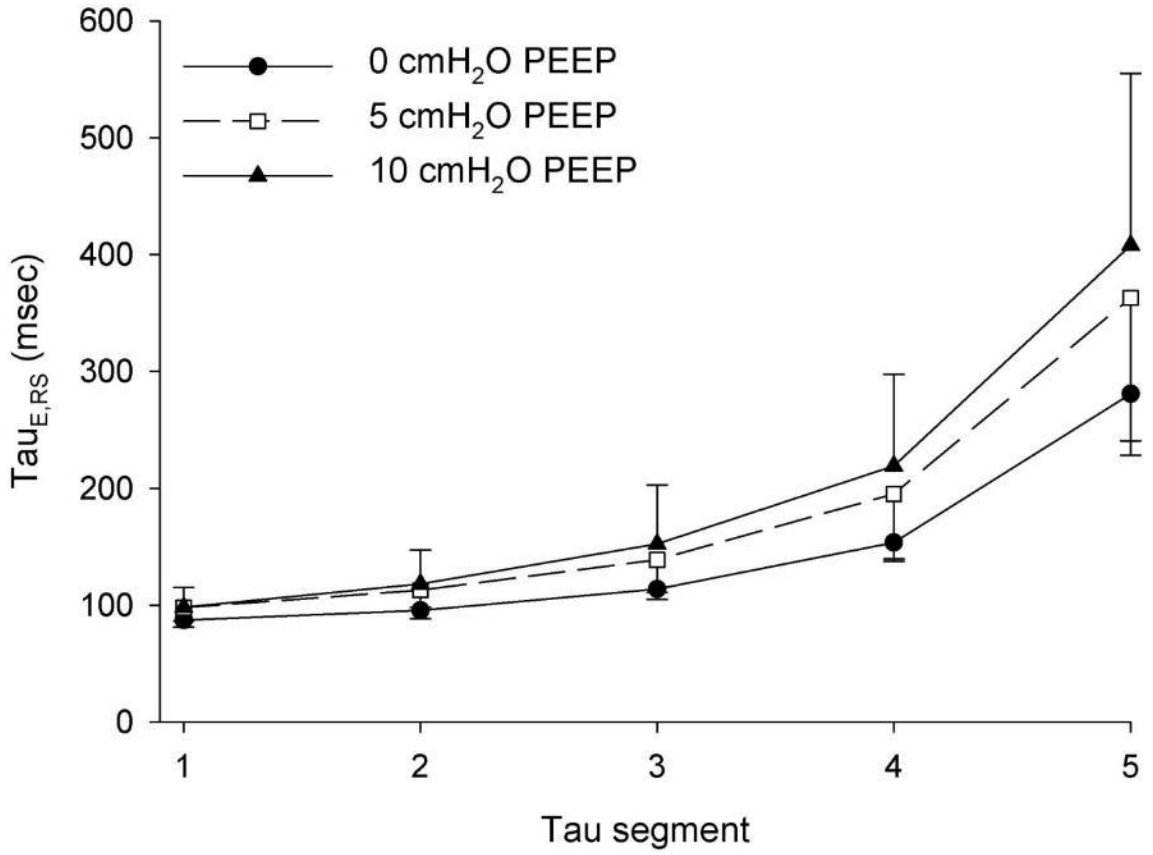

Figure 5.3 Values for $\tau_{E,RS1}$ to $\tau_{E,RS5}$ at each positive end expiratory pressure (PEEP) setting are displayed as mean values ± 95% confidence interval.

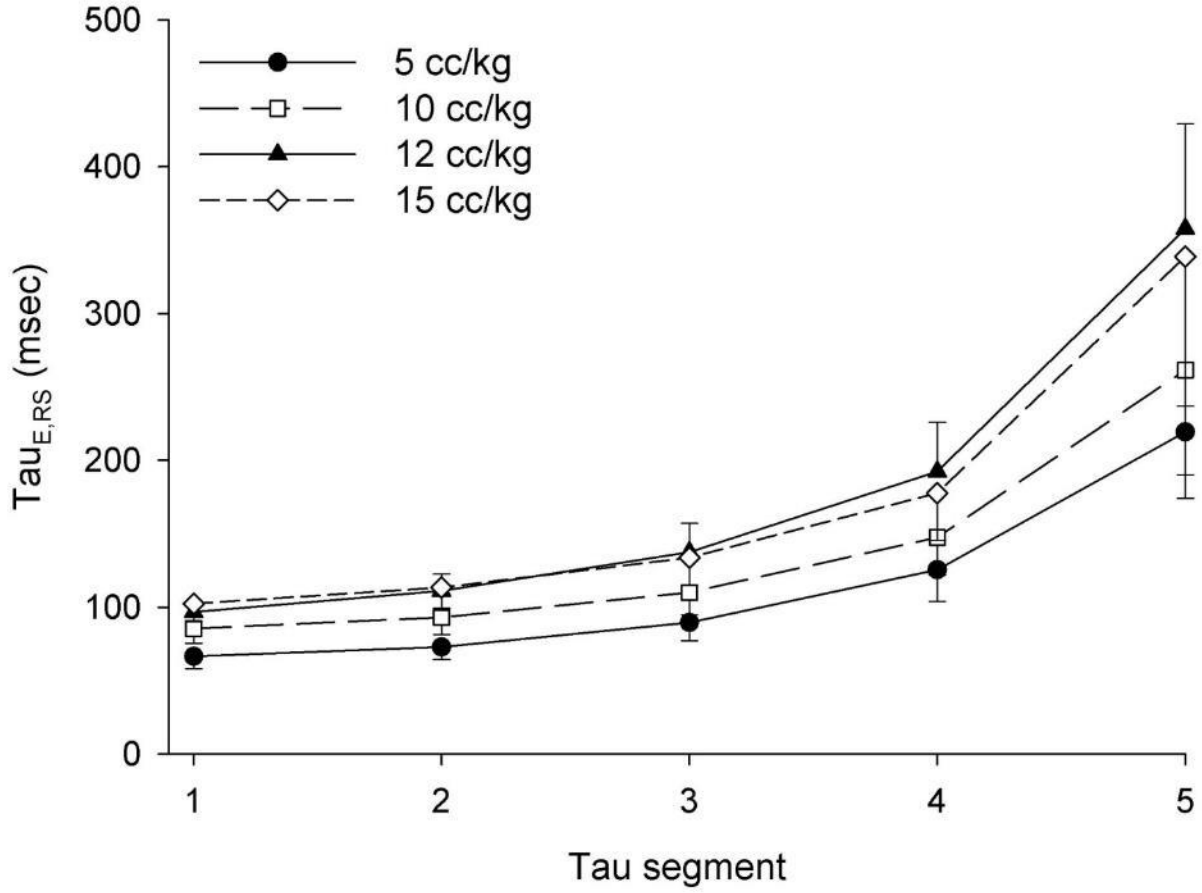

Figure 5.4 Values for $\tau_{E,RS1}$ to $\tau_{E,RS5\ RS5}$ at each tidal volume (V_T) setting are displayed as mean values ± 95% confidence interval.

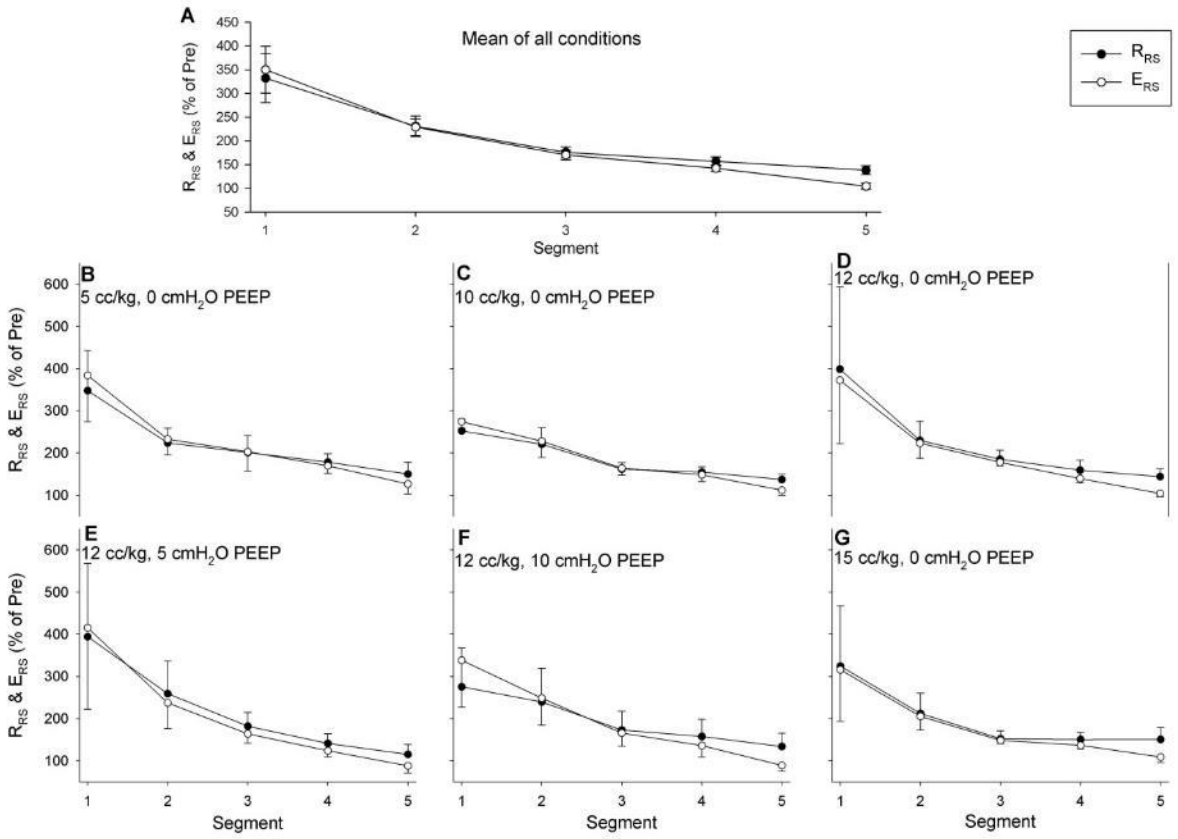

Figure 5.5 Relative values (comparing post injury to pre injury state) for R_{RS} and E_{RS} for each equivolemic segment

Values are displayed as the mean of all positive end expiratory pressure (PEEP) and tidal volume (V_T) values (Panel A), and for individual combinations of PEEP and V_T (Panels B through G).

Tables

Table 5.1 Pulmonary mechanical data before and after experimental lung injury

	E_{RS} (cmH_20/L)	R_{RS} ($cmH_20/L/sec$)	E_L (cmH_20/L)	R_L ($cmH_20/L/sec$)	E_{CW} (cmH_20/L)	R_{CW} ($cmH_20/L/sec$)
Before Injury	37.6±11.9	7.1±1.6	25.5±10.0	6.1±1.6	12.1±4.7	1.0± 0.3
After Injury	65.6±27.6	18.2±5.7	55.4±27.8	16.9±5.4	10.2±3.3	1.3±1.0
P-value	0.010	0.0026	0.011	0.0024	0.16	0.29

E_{RS}, elastance of the respiratory system; E_L, elastance of the lung; E_{CW}, elastance of the chest wall; R_{RS}, resistance of the respiratory system; R_L, resistance of the lung; R_{CW}, resistance of the chest wall. Elastance data for this table were collected during end-inspiratory plateau conditions. All data presented as mean and 95% confidence intervals. P-value compares before and after injury values.

Table 5.2 Effect of Injury by Expired Volume Segment on τ_E

	$\tau_{E,RS1}$ (msec)	$\tau_{E,RS2}$ (msec)	$\tau_{E,RS3}$ (msec)	$\tau_{E,RS4}$ (msec)	$\tau_{E,RS5}$ (msec)
Before Injury	95.1 (46.6, 143.7)	105.1 (56.5, 153.7)	126.9 (78.3, 175.4)	168.9 (120.4, 217.5)	288.6 (240.1, 337.2)
After Injury	86.4 (37.9, 135.0)	99.1 (50.6, 147.7)	121.8 (73.2, 170.3)	173.7 (125.2, 222.3)	342.4 (298.9, 391.0)
Difference	-8.7 (-67.8, 50.4)	-6.0 (-65.1, 53.1)	-5.1 (-64.2, 53.9)	4.8 (-54.2, 63.9)	53.8 (-5.3, 112.9)

$\tau_{E,RS1-5}$, expiratory time constant for expired volume slice 1 through 5; msec, milliseconds. All data presented as mean and 95% confidence intervals.

Table 5.3 Effect of Injury by Expired Volume Segment on R_{RS}

	R_{RS1} ($cmH_20/L/sec$)	R_{RS2} ($cmH_20/L/sec$)	R_{RS3} ($cmH_20/L/sec$)	R_{RS4} ($cmH_20/L/sec$)	R_{RS5} ($cmH_20/L/sec$)
Before Injury	5.3 (3.6, 7.0)	4.6 (2.9, 6.4)	4.4 (2.7, 6.1)	4.8 (3.0, 6.5)	7.4 (5.7, 9.1)
After Injury	14.3 (12.6, 16.1)	9.4 (7.7, 11.2)	7.0 (5.3, 8.7)	6.9 (5.1, 8.6)	8.5 (6.7, 10.2)
Difference	9.1 (5.9, 12.2)	4.8 (1.7, 7.9)	2.6 (-0.5, 5.7)	2.1 (-1.0, 5.2)	1.1 (-2.0, 4.2)

R_{RS1-5}, respiratory system resistance for expired volume slice 1 through 5. All data presented as mean and 95% confidence intervals.

Table 5.4 Effect of Injury by Expired Volume Segment on E_{RS}

	E_{RS1} (cmH_20/L)	E_{RS2} (cmH_20/L)	E_{RS3} (cmH_20/L)	E_{RS4} (cmH_20/L)	E_{RS5} (cmH_20/L)
Before Injury	54.1 (39.6, 68.5)	45.1 (30.6, 59.5)	36.5 (22.0, 50.9)	30.5 (16.0, 44.9)	27.6 (13.1, 42.0)
After Injury	159.8 (145.4, 174.3)	96.1 (81.7, 110.6)	60.6 (46.1, 75.0)	42.8 (28.4, 57.3)	27.5 (13.0, 41.9)
Difference	105.8 (82.3, 129.2)	51.0 (27.6, 74.5)	24.1 (0.6, 47.5)	12.3 (-11.1, 35.8)	0.1 (-23.4, 23.5)

E_{RS1-5}, elastance for expired volume slice 1 through 5. All data presented as mean and 95% confidence intervals.

Table 5.5 Raw values for selected pulmonary mechanical variables by Expired Volume Segment

V_T	PEEP (cmH_2O)	Volume Segment	PRE R_{RS} (cmH_2O/L/sec)	PRE E_{RS} (cmH_2O/L)	PRE τ_E (msec)	POST R_{RS} (cmH_2O/L/sec)	POST E_{RS} (cmH_2O/L)	POST τ_E (msec)
5ml/kg	0	1	2.80±0.78	41.02±12.76	70.39±12.51	9.25±4.48	143.01±60.48	62.76±11.61
		2	2.93±0.67	39.58±8.56	75.49±13.32	6.28±2.20	90.55±33.48	70.29±11.82
		3	3.45±1.01	38.42±8.20	91.35±19.74	6.35±2.34	74.13±27.15	87.62±16.56
		4	4.01±0.86	34.15±8.08	124.90±38.10	7.00±1.92	58.07±18.76	126.16±24.62
		5	5.47±1.78	28.79±9.36	203.46±75.87	7.37±2.09	33.58±11.70	235.24±53.06
10ml/kg	0	1	3.97±1.14	43.59±9.64	90.02±14.92	9.65±2.68	116.61±16.97	80.98±13.73
		2	3.65±0.87	39.42±9.94	94.65±17.13	7.51±1.78	85.30±23.93	91.18±16.95
		3	3.99±0.73	36.90±5.81	110.96±23.21	6.24±0.89	60.46±13.97	108.93±21.88
		4	4.34±0.89	31.50±6.15	144.29±39.92	6.47±0.81	45.90±10.33	150.71±35.35
		5	6.31±2.13	28.98±5.92	238.36±107.91	8.16±1.82	31.82±7.39	284.91±100.36
12ml/kg	0	1	4.79±1.52	49.16±14.25	96.79±14.43	14.14±7.69	149.95±71.98	91.99±13.97
		2	4.33±1.30	43.62±15.65	103.16±18.40	9.21±3.12	91.07±27.21	101.98±16.63
		3	3.89±0.66	33.10±6.27	121.45±25.22	6.95±1.09	59.02±12.42	121.86±18.84
		4	4.60±1.20	30.53±6.70	156.62±44.02	6.81±1.05	41.89±8.06	169.40±32.67
		5	7.02±3.12	28.20±6.36	266.85±127.02	9.21±2.85	28.92±5.94	338.55±114.55
	5	1	5.89±2.06	57.53±19.26	101.23±13.41	17.02±8.87	176.77±78.07	94.50±19.94
		2	4.99±1.39	45.84±14.11	113.16±27.05	10.85±3.48	98.40±31.72	112.23±13.84
		3	4.45±1.39	34.34±8.30	138.47±53.03	7.33±1.70	54.73±14.47	138.95±25.55
		4	5.24±2.29	29.66±6.76	195.02±106.88	6.53±1.39	35.94±9.40	194.97±55.95
		5	10.97±8.69	30.06±9.71	359.14±252.48	7.75±2.66	22.59±5.16	366.49±126.25
	10	1	8.05±2.39	75.98±21.50	106.19±22.35	18.52±10.52	211.11±84.45	89.93±26.05
		2	6.87±2.26	56.84±15.54	129.55±57.07	12.95±4.26	122.80±36.86	106.62±16.74
		3	6.08±2.43	41.77±11.06	165.48±102.51	8.71±2.10	64.25±17.74	139.31±20.17
		4	5.81±3.13	29.11±6.42	221.92±150.90	7.75±3.05	36.93±11.97	216.26±64.67
		5	7.31±4.39	22.53±4.86	375.12±271.56	8.39±3.98	19.05±5.50	440.72±139.74
15ml/kg	0	1	6.17±2.01	57.13±14.99	106.23±15.33	17.41±13.24	162.55±100.61	98.47±19.98
		2	5.06±1.59	45.10±14.08	114.58±20.68	9.80±3.24	88.55±26.18	112.34±21.17
		3	4.42±0.77	34.44±6.90	133.52±27.92	6.50±1.07	50.90±10.48	133.88±28.33
		4	4.57±0.84	27.95±4.40	170.75±46.66	6.64±1.03	38.17±7.34	184.88±48.11
		5	7.24±2.80	26.82±5.27	288.82±134.81	9.95±3.11	29.07±7.90	388.69±153.55

V_T, tidal volume; ml/kg; milliliters per kilogram of body weight; R_{RS}, resistance of the respiratory system; E_{RS}, elastance of the respiratory system; $\tau_{E,}$ time constant of expiration; PRE, before injury; POST, after injury. All data presented as mean and 95% confidence intervals.

Chapter 6: Conclusions

Overall Summary

Acute respiratory distress syndrome (ARDS) is a lung injury characterized by hypoxia and impaired pulmonary mechanics. The associated histologic changes, such as alveolar flooding and collapse, airway edema, and altered surfactant function, are heterogeneous in distribution within the lungs (43).

The awareness of anatomical heterogeneity in ARDS has led to meaningful improvements in patient care. The use of small tidal volumes, PEEP, assessment of FRC and the calculation of stress and strain have gained adoption in the clinical management of ARDS. Unfortunately, all of these measures are "whole lung" measurements, and none account for the local heterogeneity of mechanical characteristics found in injured lung. Because of this heterogeneity, some lung units have abnormal values of R and/or E, while others have values that are similar to those found in healthy lung (7, 13, 20, 29). It is therefore possible that susceptible lung units are subject to critically injurious forces even when global measures of volume, pressure, stress and strain appear acceptable (133).

Recent physiological and clinical trials have demonstrated that careful attention to the mechanical ventilation pressures and volumes can improve outcomes in patients with ARDS (8, 78, 187). In this thesis, I have provided evidence that whole lung measures of τ_E and ε do not reliably reflect regional measures, and that regional values may substantially exceed the average values described by conventional measures. This raises the concerning possibility that clinicians may be continuing to place patients at risk of VALI when using global measures of ε and τ_E to guide ventilation management. Regional variation in ε may be assessed using anatomic imaging (as in Study 1, Chapter 2), or by using surrogate techniques such as FRC measurement or

EIT(40, 198, 205). Similarly, regional τ_E may be assessed using the application of computational fluid dynamics to imaging data (Study 1, Chapter 2), or may be inferred from the dissection of the flow-volume curve during passive expiration (Studies 3 and 4, Chapters 4 and 5). The data provided in this thesis provide support for the idea that, at least in some lung regions, regional τ_E and ε are correlated (Study 1, Chapter 2). This raises the possibility that the continuous bedside measurement of τ_E using a multi-compartment model could alert clinicians to episodes of abnormal regional ε.

This thesis provides evidence that whole lung measures of ε and τ_E poorly reflect regional values, and that regional values may be affected by manipulating ventilatory variables such as V_T, PEEP and inspired gas density. However, it is not obvious how clinicians could modify regional values independent of other regions to mitigate the impact of abnormal τ_E and ε. Furthermore, while it is tempting to believe that regional abnormalities would lead to VALI, this hypothesis has not been well explored or demonstrated. The work contained in this thesis was undertaken in an attempt to lay the groundwork for future research into this question.

Strengths and Limitations

The program of research outlined in this thesis has several strengths. First the use of novel assessment techniques, such as the computational fluid dynamics to develop a model of FRI allowed the detailed assessment of pressure, flow and volume characteristics within lung regions. This led to novel insights into the relationships between regional ε, regional τ_E and PEEP.

Second, the studies described in this thesis undertook careful physiological measurements that provided data that is often not measured in similar studies. Specifically, it is necessary to account for the flow-dependent resistance of the endotracheal tube in any evaluation of

expiratory mechanics in ventilated patients. While several similar past studies have failed to do this, the studies in this thesis either directly measured tracheal pressure, or calculated it from previously validated research (82).

There are some limitations to the studies presented in this thesis, and the data presented should therefore be interpreted cautiously. First, it must be recognized that cadaveric models, particularly isolated lung models, do not reflect all of the pulmonary mechanical forces found in live, whole animals. Specifically, the lack of a chest wall may substantially alter the forces that lung tissue is subject to during mechanical ventilation. Second, while pig lungs are similar to human lungs, differences in the lung architecture means that the findings generated from live animal models may only partially reflect the events that might occur in human lungs before and after injury (77). Finally, the experimental model of lung injury used in this thesis largely creates an epithelial injury (87). ARDS in humans often has a significant endothelial injury component (129). To the extent that ARDS in humans differs from this model in animal subjects, the results demonstrated in this thesis should be interpreted with caution.

Future Research

There are several unanswered questions related to this thesis that merit investigation in the future. For example, even if regional variation in lung ε and τ_E can be reliably assessed, does altering these improve clinical outcomes? It is by no means clear that high local ε or τ_E causes VALI, or that, even if they do, that these manipulations can alter the process of new injury. This thesis has focuses on τ_E and normal ε. Future investigations into shear stress and shear strain may provide novel insights into dynamic tissue injury during mechanical ventilation. At this time the evaluation of shear forces within whole animals or humans is difficult, but recent advances in

minimally invasive techniques and advanced imaging modalities may allow these forces to be more thoroughly evaluated.

Moreover, while ARDS is the focus of this thesis, and continues to be a highly lethal form of lung injury, there are other pulmonary disorders that could benefit from investigation in a manner similar to the studies presented in this manuscript. For example, it is not known what regional forces are at play in patients with pulmonary fibrosis or cystic fibrosis. While chronic obstructive pulmonary disease (COPD) and asthma are well studied, to date little research into regional forces within the lungs of patients with COPD or asthma has occurred.

Overall Conclusion

The purpose of this thesis was to evaluate the regional heterogeneity of pulmonary mechanical values within models of lung injury. We observed that regional variation of ε and τ_E occur, and that PEEP can decrease these values in a cadaveric model. We further observed that in a live porcine model of ARDS, that manipulations of PEEP, V_T and PEEP were able to alter the pattern of passive expiration and decrease the post-injury abnormalities in τ_E in the same model.

References

1. **Aerts JG**, **van den Berg B**, **Lourens MS**, **Bogaard JM**. Expiratory flow-volume curves in mechanically ventilated patients with chronic obstructive pulmonary disease. *Acta Anaesthesiol Scand* 43: 322–7, 1999.
2. **Agostoni A**, **Hyatt R**. Static behavior of the respiratory system. In: *The Respiratory System*, edited by Fishman A, Mead J, Geiger S. Baltimore, MD: Williams & Wilkins, 1986, p. 113–130.
3. **Albaiceta GM**, **Taboada F**, **Parra D**, **Blanco A**, **Escudero D**, **Otero J**. Differences in the deflation limb of the pressure-volume curves in acute respiratory distress syndrome from pulmonary and extrapulmonary origin. *Intensive Care Med* 29: 1943–9, 2003.
4. **Al-Rawas N**, **Banner MJ**, **Euliano NR**, **Tams CG**, **Brown J**, **Martin a D**, **Gabrielli A**. Expiratory time constant for determinations of plateau pressure, respiratory system compliance, and total resistance. *Crit Care* 17: R23, 2013.
5. **Amato MB**, **Barbas CS**, **Medeiros DM**, **Magaldi RB**, **Schettino GP**, **Lorenzi-Filho G**, **Kairalla RA**, **Deheinzelin D**, **Munoz C**, **Oliveira R**, **Takagaki TY**, **Carvalho CR**. Effect of a protective-ventilation strategy on mortality in the acute respiratory distress syndrome. *N Engl J Med* 338: 347–354, 1998.
6. **Amelon R**, **Cao K**, **Ding K**, **Christensen GE**, **Reinhardt JM**, **Raghavan ML**. Three-dimensional characterization of regional lung deformation. *J Biomech* 44: 2489–95, 2011.
7. **Andreassen S**, **Steimle KL**, **Mogensen ML**, **Bernardino de la Serna J**, **Rees S**, **Karbing DS**. The effect of tissue elastic properties and surfactant on alveolar stability. *J Appl Physiol* 109: 1369–77, 2010.
8. **ARDSNetwork**. Ventilation with lower tidal volumes as compared with traditional tidal volumes for acute lung injury and the acute respiratory distress syndrome. The Acute Respiratory Distress Syndrome Network. *N Engl J Med* 342: 1301–8, 2000.

10. **Ashbaugh DG**, **Bigelow DB**, **Petty TL**, **Levine BE**. Ashbaugh DG, Bigelow DB, Petty TL, Levine BE. Acute respiratory distress in adults. The Lancet, Saturday 12 August 1967. *Crit Care Resusc* 7: 60–1, 2005.
11. **Auler JO**, **Saldiva PH**, **Martins MA**, **Carvalho CR**, **Negri EM**, **Hoelz C**, **Zin WA**. Flow and volume dependence of respiratory system mechanics during constant flow ventilation in normal subjects and in adult respiratory distress syndrome. *Crit Care Med* 18: 1080–6, 1990.
12. **Bachofen M**, **Weibel ER**. Alterations of the gas exchange apparatus in adult respiratory insufficiency associated with septicemia. *Am Rev Respir Dis* 116: 589–615, 1977.
13. **De Backer JW**, **Vos WG**, **Gorlé CD**, **Germonpré P**, **Partoens B**, **Wuyts FL**, **Parizel PM**, **De Backer W**. Flow analyses in the lower airways: patient-specific model and boundary conditions. *Med Eng Phys* 30: 872–9, 2008.
14. **De Backer JW**, **Vos WG**, **Vinchurkar SC**, **Claes R**, **Drollmann A**, **Wulfrank D**, **Parizel PM**, **Germonpré P**, **De Backer W**. Validation of computational fluid dynamics

in CT-based airway models with SPECT/CT. *Radiology* 257: 854–62, 2010.

15. **De Backer LA**, **Vos W**, **De Backer J**, **Van Holsbeke C**, **Vinchurkar S**, **De Backer W**. The acute effect of budesonide/formoterol in COPD: a multi-slice computed tomography and lung function study. *Eur Respir J* 40: 298–305, 2012.
16. **De Backer W**, **Vos W**, **Van Holsbeke C**, **Vinchurkar S**, **Claes R**, **Hufkens A**, **Parizel PM**, **Bedert L**, **De Backer J**. The effect of roflumilast in addition to LABA/LAMA/ICS treatment in COPD patients. *Eur Respir J* 44: 527–9, 2014.
17. **Barber RE**, **Hamilton WK**. Oxygen toxicity in man. A A/Barber RE, Lee J, Hamilton WK: Oxygen toxicity in man. A prospective study in patients with irreversible brain damage. *N Engl J Med* 283: 1478–84, 1970.
18. **Barberis L**, **Manno E**, **Guérin C**. Effect of end-inspiratory pause duration on plateau pressure in mechanically ventilated patients. *Intensive Care Med* 29: 130–4, 2003.
19. **Bates JHT**. Lung Mechanics. Cambridge: Cambridge University Press, 2009.
20. **Bates JHT**. The linear single-compartment model. In: *Lung Mechanics*. Cambridge, UK: Cambridge University Press, 2009, p. 37–61.
21. **Baydur A**, **Behrakis PK**, **Zin WA**, **Jaeger M**, **Milic-Emili J**. A simple method for assessing the validity of the esophageal balloon technique. *Am Rev Respir Dis* 126: 788–91, 1982.
22. **Bernard GR**, **Artigas A**, **Brigham KL**, **Cat-let J**, **Falke K**, **Hudson L**, **Lamy M**, **Legall JR**, **Morris A**, **Spragg R**, **Committee C**. Report of the American-European Consensus Conference on the Acute Respiratory Distress Syndrome. *J Crit Care* 9: 72–81, 1994.
23. **Bevilacqua MP**, **Pober JS**, **Wheeler ME**, **Cotran RS**, **Gimbrone MA**. Interleukin 1 acts on cultured human vascular endothelium to increase the adhesion of polymorphonuclear leukocytes, monocytes, and related leukocyte cell lines. *J Clin Invest* 76: 2003–11, 1985.
24. **Bikker IG**, **van Bommel J**, **Reis Miranda D**, **Bakker J**, **Gommers D**. End-expiratory lung volume during mechanical ventilation: a comparison with reference values and the effect of positive end-expiratory pressure in intensive care unit patients with different lung conditions. *Crit Care* 12: R145, 2008.
25. **Bilek AM**, **Dee KC**, **Gaver DP**. Mechanisms of surface-tension-induced epithelial cell damage in a model of pulmonary airway reopening. *J Appl Physiol* 94: 770–83, 2003.
26. **Blank R**, **Napolitano LM**. Epidemiology of ARDS and ALI. *Crit Care Clin* 27: 439–58, 2011.
27. **Blankman P**, **Gommers D**. Lung monitoring at the bedside in mechanically ventilated patients. *Curr Opin Crit Care* 18: 261–6, 2012.
28. **Blankman P**, **Hasan D**, **Bikker IG**, **Gommers D**. Lung stress and strain calculations in mechanically ventilated patients in the intensive care unit. *Acta Anaesthesiol Scand* 60: 69–78, 2016.
29. **Boehme S**, **Bentley AH**, **Hartmann EK**, **Chang S**, **Erdoes G**, **Prinzing A**, **Hagmann M**, **Baumgardner JE**, **Ullrich R**, **Markstaller K**, **David M**. Influence of Inspiration to Expiration Ratio on Cyclic Recruitment and Derecruitment of Atelectasis in a Saline Lavage Model of Acute Respiratory Distress Syndrome. *Crit. Care Med.* (2014).

30. **Boiselle PM**. Imaging of the large airways. *Clin Chest Med* 29: 181–93, vii, 2008.

31. **Brochard L**, **Roudot-Thoraval F**, **Roupie E**, **Delclaux C**, **Chastre J**, **Fernandez-Mondéjar E**, **Clémenti E**, **Mancebo J**, **Factor P**, **Matamis D**, **Ranieri M**, **Blanch L**, **Rodi G**, **Mentec H**, **Dreyfuss D**, **Ferrer M**, **Brun-Buisson C**, **Tobin M**, **Lemaire F**. Tidal volume reduction for prevention of ventilator-induced lung injury in acute respiratory distress syndrome. The Multicenter Trail Group on Tidal Volume reduction in ARDS. *Am J Respir Crit Care Med* 158: 1831–8, 1998.

32. **Broseghini C**, **Brandolese R**, **Poggi R**, **Bernasconi M**, **Manzin E**, **Rossi A**. Respiratory resistance and intrinsic positive end-expiratory pressure (PEEPi) in patients with the adult respiratory distress syndrome (ARDS). *Eur Respir J Off J Eur Soc Clin Respir Physiol* 1: 726–31, 1988.

33. **Brower RG**, **Shanholtz CB**, **Fessler HE**, **Shade DM**, **White P**, **Wiener CM**, **Teeter JG**, **Dodd-o JM**, **Almog Y**, **Piantadosi S**. Prospective, randomized, controlled clinical trial comparing traditional versus reduced tidal volume ventilation in acute respiratory distress syndrome patients. *Crit Care Med* 27: 1492–8, 1999.

34. **Brower RGRRG**, **Lanken PPNPN**, **MacIntyre N**, **Matthay MAMA**, **Morris A**, **Ancukiewicz M**, **Schoenfeld D**, **Thompson BTT**, **others**. Higher versus lower positive end-expiratory pressures in patients with the acute respiratory distress syndrome. *N Engl J Med* 351: 327, 2004.

35. **Bruhn A**, **Bugedo D**, **Riquelme F**, **Varas J**, **Retamal J**, **Besa C**, **Cabrera C**, **Bugedo G**. Tidal volume is a major determinant of cyclic recruitment-derecruitment in acute respiratory distress syndrome. *Minerva Anestesiol* 77: 418–26, 2011.

36. **Brunner JX**, **Laubscher TP**, **Banner MJ**, **Iotti G**, **Braschi a**. Simple method to measure total expiratory time constant based on the passive expiratory flow-volume curve. *Crit Care Med* 23: 1117–22, 1995.

37. **Cai J**, **Sheng K**, **Benedict SH**, **Read PW**, **Larner JM**, **Mugler JP**, **de Lange EE**, **Cates GD**, **Miller GW**. Dynamic MRI of grid-tagged hyperpolarized helium-3 for the assessment of lung motion during breathing. *Int J Radiat Oncol Biol Phys* 75: 276–84, 2009.

38. **Chelucci GL**, **Brunet F**, **Dall'Ava-Santucci J**, **Dhainaut JF**, **Paccaly D**, **Armaganidis A**, **Milic-Emili J**, **Lockhart A**. A single-compartment model cannot describe passive expiration in intubated, paralysed humans. *Eur Respir J* 4: 458–64, 1991.

39. **Chiumello D**, **Carlesso E**, **Cadringher P**. Lung stress and strain during mechanical ventilation of the acute respiratory distress syndrome. *J Respir* 178: 346–55, 2008.

40. **Choi S**, **Hoffman E a**, **Wenzel SE**, **Tawhai MH**, **Yin Y**, **Castro M**, **Lin C-L**. Registration-based assessment of regional lung function via volumetric CT images of normal subjects vs. severe asthmatics. *J Appl Physiol* 115: 730–42, 2013.

41. **Crapo JD**, **Barry BE**, **Foscue HA**, **Shelburne J**. Structural and biochemical changes in rat lungs occurring during exposures to lethal and adaptive doses of oxygen. *Am Rev Respir Dis* 122: 123–43, 1980.

42. **Cressoni M**, **Cadringher P**, **Chiurazzi C**, **Amini M**, **Gallazzi E**, **Marino A**, **Brioni M**, **Carlesso E**, **Chiumello D**, **Quintel M**, **Bugedo G**, **Gattinoni L**. Lung inhomogeneity in

patients with acute respiratory distress syndrome. *Am J Respir Crit Care Med* 189: 149–58, 2014.

43. **Dakin J**, **Jones A**, **Hansell D**. Changes in lung composition and regional perfusion and tissue distribution in patients with ARDS. *Respirology* 2011: 1265–1272, 2011.

44. **Dengler V**, **Downey GP**, **Tuder RM**, **Eltzschig HK**, **Schmidt EP**. Neutrophil Intercellular Communication in Acute Lung Injury: Emerging Roles of Microparticles and Gap Junctions. *Am. J. Respir. Cell Mol. Biol.* (March 14, 2013).

45. **Determann RM**, **Royakkers A**, **Wolthuis EK**, **Vlaar AP**, **Choi G**, **Paulus F**, **Hofstra J-J**, **de Graaff MJ**, **Korevaar JC**, **Schultz MJ**. Ventilation with lower tidal volumes as compared with conventional tidal volumes for patients without acute lung injury: a preventive randomized controlled trial. *Crit Care* 14: R1, 2010.

46. **Dreyfuss D**, **Saumon G**. Ventilator-induced lung injury: lessons from experimental studies. *Am J Respir Crit Care Med* 157: 294–323, 1998.

47. **Dreyfuss D**, **Soler P**, **Basset G**, **Saumon G**. High inflation pressure pulmonary edema. Respective effects of high airway pressure, high tidal volume, and positive end-expiratory pressure. *Am Rev Respir Dis* 137: 1159–64, 1988.

48. **Dreyfuss D**, **Soler P**, **Saumon G**. Mechanical ventilation-induced pulmonary edema. Interaction with previous lung alterations. *Am J Respir Crit Care Med* 151: 1568–75, 1995.

49. **Eissa NT**, **Ranieri VM**, **Corbeil C**, **Chasse M**, **Braidy J**, **Milic Emili J**. Effects of positive end-expiratory pressure, lung volume, and inspiratory flow on interrupter resistance in patients with adult respiratory distress syndrome. *Am Rev Respir Dis* 144: 538–543, 1991.

50. **Eissa NT**, **Ranieri VM**, **Corbeil C**, **Chassé M**, **Robatto FM**, **Braidy J**, **Milic-Emili J**. Analysis of behavior of the respiratory system in ARDS patients: effects of flow, volume, and time. *J Appl Physiol* 70: 2719–29, 1991.

51. **Eissa NT**, **Ranieri VM**, **Corbeil C**, **Chassé M**, **Robatto FM**, **Braidy J**, **Milic-Emili J**. Analysis of behavior of the respiratory system in ARDS patients: effects of flow, volume, and time. *J Appl Physiol* 70: 2719–29, 1991.

52. **Enhorning G**, **Holm BA**. Disruption of pulmonary surfactant's ability to maintain openness of a narrow tube. *J Appl Physiol* 74: 2922–7, 1993.

53. **Erickson SE**, **Martin GS**, **Davis JL**, **Matthay M a**, **Eisner MD**. Recent trends in acute lung injury mortality: 1996-2005. *Crit Care Med* 37: 1574–9, 2009.

54. **Fan L**, **Zeng M**, **Zhou S**, **Lu L**, **Huang Y**. Preliminary study of the relationship between water absorbency and zeta potentials of crosslinked poly(acrylic acid). *J Control Release* 152 Suppl : e260–2, 2011.

55. **Flick MR**, **Perel A**, **Staub NC**. Leukocytes are required for increased lung microvascular permeability after microembolization in sheep. *Circ Res* 48: 344–51, 1981.

56. **Folkesson HG**, **Matthay MA**, **Hébert CA**, **Broaddus VC**. Acid aspiration-induced lung injury in rabbits is mediated by interleukin-8-dependent mechanisms. *J Clin Invest* 96: 107–16, 1995.

57. **Gajic O**, **Lee J**, **Doerr CH**, **Berrios JC**, **Myers JL**, **Hubmayr RD**. Ventilator-induced cell wounding and repair in the intact lung. *Am J Respir Crit Care Med* 167: 1057–63, 2003.

58. **Ganter M**, **Hensel A**. Cellular variables in bronchoalveolar lavage fluids (BALF) in selected healthy pigs. *Res Vet Sci* 63: 215–7.

59. **Ganzert S**, **Möller K**, **Steinmann D**, **Schumann S**, **Guttmann J**. Pressure-dependent stress relaxation in acute respiratory distress syndrome and healthy lungs: an investigation based on a viscoelastic model. *Crit Care* 13: R199, 2009.

60. **Gattinoni L**, **Caironi P**, **Pelosi P**, **Goodman LR**. What has computed tomography taught us about the acute respiratory distress syndrome? *Am J Respir Crit Care Med* 164: 1701–11, 2001.

61. **Gattinoni L**, **Caironi P**. Refining ventilatory treatment for acute lung injury and acute respiratory distress syndrome. *JAMA* 299: 691–3, 2008.

62. **Gattinoni L**, **Carlesso E**, **Cadringher P**, **Valenza F**, **Vagginelli F**, **Chiumello D**. Physical and biological triggers of ventilator-induced lung injury and its prevention. *Eur Respir J* 22: 15s–25s, 2003.

63. **Gattinoni L**, **Carlesso E**, **Caironi P**. Stress and strain within the lung. *Curr Opin Crit Care* 18: 42–7, 2012.

64. **Gattinoni L**, **Chiumello D**, **Carlesso E**, **Valenza F**. Bench-to-bedside review: chest wall elastance in acute lung injury/acute respiratory distress syndrome patients. *Crit Care* 8: 350–5, 2004.

65. **Gattinoni L**, **Pelosi P**, **Suter P**. Acute respiratory distress syndrome caused by pulmonary and extrapulmonary disease. Different syndromes? *J Respir* 158: 3–11, 1998.

66. **Gattinoni L**, **Pesenti A**, **Avalli L**, **Rossi F**, **Bombino M**. Pressure-volume curve of total respiratory system in acute respiratory failure. Computed tomographic scan study. *Am Rev Respir Dis* 136: 730–6, 1987.

67. **Gehrke I**, **Pabst R**. Cell composition and lymphocyte subsets in the bronchoalveolar lavage of normal pigs of different ages in comparison with germfree and pneumonic pigs. *Lung* 168: 79–92, 1990.

68. **Goddon S**, **Fujino Y**, **Hromi JM**, **Kacmarek RM**. Optimal mean airway pressure during high-frequency oscillation: predicted by the pressure-volume curve. *Anesthesiology* 94: 862–9, 2001.

69. **Goebel U**, **Haberstroh J**, **Foerster K**, **Dassow C**, **Priebe H-J**, **Guttmann J**, **Schumann S**. Flow-controlled expiration: a novel ventilation mode to attenuate experimental porcine lung injury. *Br J Anaesth* 113: 474–83, 2014.

70. **Goligher EC**, **Kavanagh BP**, **Rubenfeld GD**, **Adhikari NKJ**, **Pinto R**, **Fan E**, **Brochard LJ**, **Granton JT**, **Mercat A**, **Marie Richard J-C**, **Chretien J-M**, **Jones GL**, **Cook DJ**, **Stewart TE**, **Slutsky AS**, **Meade MO**, **Ferguson ND**. Oxygenation response to positive end-expiratory pressure predicts mortality in acute respiratory distress syndrome. A secondary analysis of the LOVS and ExPress trials. *Am J Respir Crit Care Med* 190: 70–6, 2014.

71. **González-López A**, **García-Prieto E**, **Batalla-Solís E**, **Amado-Rodríguez L**, **Avello N**, **Blanch L**, **Albaiceta GM**. Lung strain and biological response in mechanically ventilated patients. *Intensive Care Med* 38: 240–7, 2012.

72. **Goodman LR**, **Fumagalli R**, **Tagliabue P**, **Tagliabue M**, **Ferrario M**, **Gattinoni L**, **Pesenti A**. Adult respiratory distress syndrome due to pulmonary and extrapulmonary causes: CT, clinical, and functional correlations. *Radiology* 213: 545–52, 1999.

73. **Gottfried SB**, **Higgs BD**, **Rossi A**, **Carli F**, **Mengeot PM**, **Calverly PM**, **Zocchi L**, **Milic-Emili J**. Interrupter technique for measurement of respiratory mechanics in anesthetized humans. *J Appl Physiol* 59: 647–52, 1985.

74. **Gottfried SB**, **Rossi A**, **Higgs BD**, **Calverley PM**, **Zocchi L**, **Bozic C**, **Milic-Emili J**. Noninvasive determination of respiratory system mechanics during mechanical ventilation for acute respiratory failure. *Am Rev Respir Dis* 131: 414–20, 1985.

75. **Griese M**. Pulmonary surfactant in health and human lung diseases: state of the art. *Eur Respir J Off J Eur Soc Clin Respir Physiol* 13: 1455–76, 1999.

76. **Gross D**, **Hauger W**, **Schröder J**, **Wall W**, **Bonet J**. Engineering Mechanics 2. Berlin, Heidelberg: Springer Berlin Heidelberg, 2011.

77. **Guérin C**, **Bayle F**, **Debord S**, **Poupelin J-C**, **Badet M**, **Lemasson S**, **Richard J-C**. Viscoelastic properties of lungs and thoracic wall of anesthetized mechanically ventilated piglets. *Vet Anaesth Analg* 34: 331–8, 2007.

78. **Guérin C**, **Reignier J**, **Richard J-C**, **Beuret P**, **Gacouin A**, **Boulain T**, **Mercier E**, **Badet M**, **Mercat A**, **Baudin O**, **Clavel M**, **Chatellier D**, **Jaber S**, **Rosselli S**, **Mancebo J**, **Sirodot M**, **Hilbert G**, **Bengler C**, **Richecoeur J**, **Gainnier M**, **Bayle F**, **Bourdin G**, **Leray V**, **Girard R**, **Baboi L**, **Ayzac L**. Prone Positioning in Severe Acute Respiratory Distress Syndrome. *N. Engl. J. Med.* (May 20, 2013).

79. **Guérin C**, **Reignier J**, **Richard J-C**, **Beuret P**, **Gacouin A**, **Boulain T**, **Mercier E**, **Badet M**, **Mercat A**, **Baudin O**, **Clavel M**, **Chatellier D**, **Jaber S**, **Rosselli S**, **Mancebo J**, **Sirodot M**, **Hilbert G**, **Bengler C**, **Richecoeur J**, **Gainnier M**, **Bayle F**, **Bourdin G**, **Leray V**, **Girard R**, **Baboi L**, **Ayzac L**. Prone positioning in severe acute respiratory distress syndrome. *N Engl J Med* 368: 2159–68, 2013.

80. **Günther A**, **Ruppert C**, **Schmidt R**, **Markart P**, **Grimminger F**, **Walmrath D**, **Seeger W**. Surfactant alteration and replacement in acute respiratory distress syndrome. *Respir Res* 2: 353–64, 2001.

81. **Guttmann J**, **Eberhard L**, **Fabry B**, **Bertschmann W**, **Zeravik J**, **Adolph M**, **Eckart J**, **Wolff G**. Time constant/volume relationship of passive expiration in mechanically ventilated ARDS patients. *Eur Respir J* 8: 114–120, 1995.

82. **Guttmann J**, **Eberhard L**, **Fabry B**. Continuous calculation of intratracheal pressure in tracheally intubated patients. *Anesthesiology* 79: 503–513, 1993.

83. **Hager DN**, **Krishnan J a**, **Hayden DL**, **Brower RG**. Tidal volume reduction in patients with acute lung injury when plateau pressures are not high. *Am J Respir Crit Care Med* 172: 1241–5, 2005.

84. **de Haro C**, **Martin-Loeches I**, **Torrents E**, **Artigas A**. Acute respiratory distress syndrome: prevention and early recognition. *Ann Intensive Care* 3: 11, 2013.

85. **Haskins S**. Cardiac Output Monitoring. In: *Advanced Monitoring and Procedures for Small Animal Emergency and Critical Care*, edited by Creedon J, Davis H. Chichester, UK: John Wiley & Sons, Ltd, 2012, p. 159–176.

86. **Heinze H**, **Eichler W**. Measurements of functional residual capacity during intensive care treatment: the technical aspects and its possible clinical applications. *Acta Anaesthesiol Scand* 53: 1121–30, 2009.

87. **Henderson WR**, **Barnbrook J**, **Dominelli PB**, **Griesdale DEG**, **Arndt T**, **Molgat-Seon Y**, **Foster G**, **Ackland GL**, **Xu J**, **Ayas NT**, **Sheel AW**. Administration of intrapulmonary sodium polyacrylate to induce lung injury for the development of a porcine model of early acute respiratory distress syndrome. *Intensive Care Med Exp* 2: 5, 2014.

88. **Henderson WR**, **Dominelli PB**, **Griesdale DEG**, **Talmor D**, **Sheel AW**. Airway pressure and transpulmonary pressure during high-frequency oscillation for acute respiratory distress syndrome. *Can Respir J* 21: 107–11, 2014.

89. **Henderson WR**, **Molgat-Seon Y**, **Dominelli PB**, **Brasher PMA**, **Griesdale DEG**, **Foster GE**, **Yacyshyn A**, **Ayas NT**, **Sheel AW**. Gas density alters expiratory time constants before and after experimental lung injury. *Exp Physiol* 100: 1217–28, 2015.

90. **Henderson WR**, **Sheel AW**. Pulmonary mechanics during mechanical ventilation. *Respir Physiol Neurobiol* 180: 162–72, 2012.

91. **Hernandez LA**, **Coker PJ**, **May S**, **Thompson AL**, **Parker JC**. Mechanical ventilation increases microvascular permeability in oleic acid-injured lungs. *J Appl Physiol* 69: 2057–61, 1990.

92. **Hickling KG**. Reinterpreting the pressure-volume curve in patients with acute respiratory distress syndrome. *Curr Opin Crit Care* 8: 32–8, 2002.

93. **Hicks R**, **Satti AK**, **Leach GD**, **Naylor IL**. Characterization of toxicity involving haemorrhage and cardiovascular failure, caused by parenteral administration of a soluble polyacrylate in the rat. *J Appl Toxicol* 9: 191–8, 1989.

94. **Hoppin F**, **Hildebrandt J**. Mechanical properties of the lung. In: *Vol. 3. Lung Biology in Health and Disease. Bioengineering Aspects of the Lung*, edited by West JB E. New York: Dekker, 1977, p. 83–162.

95. **Hotchkiss JR**, **Simonson DA**, **Marek DJ**, **Marini JJ**, **Dries DJ**. Pulmonary microvascular fracture in a patient with acute respiratory distress syndrome. *Crit Care Med* 30: 2368–70, 2002.

96. **Hudson LD**, **Milberg JA**, **Anardi D**, **Maunder RJ**. Clinical risks for development of the acute respiratory distress syndrome. *Am J Respir Crit Care Med* 151: 293–301, 1995.

97. **Jardin F**, **Genevray B**, **Brun-Ney D**, **Bourdarias JP**. Influence of lung and chest wall compliances on transmission of airway pressure to the pleural space in critically ill patients. *Chest* 88: 653–8, 1985.

98. **Kaczka DW**, **Cao K**, **Christensen GE**, **Bates JHT**, **Simon B a**. Analysis of regional mechanics in canine lung injury using forced oscillations and 3D image registration. *Ann Biomed Eng* 39: 1112–24, 2011.

99. **Kaczka DW**, **Hager DN**, **Hawley ML**, **Simon B a.** Quantifying Mechanical Heterogeneity in Canine Acute Lung Injury. *Anesthesiology* 103: 306–312, 2005.

100. **Kaczka DW**, **Lutchen KR**, **Hantos Z**. Emergent behavior of regional heterogeneity in the lung and its effects on respiratory impedance. *J Appl Physiol* 110: 1473–81, 2011.

101. **Kao S**, **Wang D**, **Yeh D**, **Hsu K**. Static Inflation Attenuates Ischemia/Reperfusion Injury in an Isolated Rat Lung In Situ*. *Chest* 126: 552–558, 2004.

102. **Katz JA**, **Zinn SE**, **Ozanne GM**, **Fairley HB**. Pulmonary, chest wall, and lung-thorax elastances in acute respiratory failure. *Chest* 80: 304–11, 1981.

103. **Katzenstein AL**, **Bloor CM**, **Leibow AA**. Diffuse alveolar damage--the role of oxygen, shock, and related factors. A review. *Am J Pathol* 85: 209–28, 1976.

104. **Knight PR**, **Druskovich G**, **Tait AR**, **Johnson KJ**. The role of neutrophils, oxidants, and proteases in the pathogenesis of acid pulmonary injury. *Anesthesiology* 77: 772–8, 1992.

105. **Kondili E**, **Alexopoulou C**, **Prinianakis G**, **Xirouchaki N**, **Georgopoulos D**. Pattern of lung emptying and expiratory resistance in mechanically ventilated patients with chronic obstructive pulmonary disease. *Intensive Care Med* 30: 1311–8, 2004.

106. **Kondili E**, **Prinianakis G**, **Athanasakis H**, **Georgopoulos D**. Lung emptying in patients with acute respiratory distress syndrome: effects of positive end-expiratory pressure. *Eur Respir J* 19: 811–819, 2002.

107. **Kumar A**, **Pontoppidan H**, **Falke KJ**, **Wilson RS**, **Laver MB**. Pulmonary barotrauma during mechanical ventilation. *Crit Care Med* 1: 181–6.

108. **Lai-Fook SJ**, **Hyatt RE**, **Rodarte JR**. Effect of parenchymal shear modulus and lung volume on bronchial pressure-diameter behavior. *J Appl Physiol* 44: 859–68, 1978.

109. **Lim C-M**, **Kim EK**, **Lee JS**, **Shim TS**, **Lee S Do**, **Koh Y**, **Kim WS**, **Kim DS**, **Kim WD**. Comparison of the response to the prone position between pulmonary and extrapulmonary acute respiratory distress syndrome. *Intensive Care Med* 27: 477–485, 2001.

110. **Lin C-L**, **Tawhai MH**, **McLennan G**, **Hoffman EA**. Computational fluid dynamics. *IEEE Eng Med Biol Mag* 28: 25–33.

111. **Liu MY**, **Wang LM**, **Li E**, **Enhorning G**. Pulmonary surfactant will secure free airflow through a narrow tube. *J Appl Physiol* 71: 742–8, 1991.

112. **Liu Y**, **Merlin D**, **Burst SL**, **Pochet M**, **Madara JL**, **Parkos CA**. The role of CD47 in neutrophil transmigration. Increased rate of migration correlates with increased cell surface expression of CD47. *J Biol Chem* 276: 40156–66, 2001.

113. **Loring SH**, **O'Donnell CR**, **Behazin N**, **Malhotra A**, **Sarge T**, **Ritz R**, **Novack V**, **Talmor D**. Esophageal pressures in acute lung injury: do they represent artifact or useful information about transpulmonary pressure, chest wall mechanics, and lung stress? *J Appl Physiol* 108: 515–22, 2010.

114. **Lourens M**, **Van Den Berg B**, **Aerts J**, **Verbraak A**, **Hoogsteden H**, **Bogaard J**. Expiratory time constants in mechanically ventilated patients with and without COPD. *Intensive Care Med* 26: 1612–1618, 2000.

115. **Lourens MS**, **van den Berg B**, **Aerts JG**, **Verbraak AF**, **Hoogsteden HC**, **Bogaard JM**. Expiratory time constants in mechanically ventilated patients with and without

COPD. *Intensive Care Med* 26: 1612–8, 2000.

116. **Lucangelo U**, **Bernabé F**, **Blanch L**. Respiratory mechanics derived from signals in the ventilator circuit. *Respir Care* 50: 55–65; discussion 65–7, 2005.

117. **Lucangelo U**, **Bernabè F**, **Blanch L**. Lung mechanics at the bedside: make it simple. *Curr Opin Crit Care* 13: 64–72, 2007.

118. **M. L**, **Berg B Van Den**, **J. A**, **a. V**, **H. H**, **J. B**. Expiratory time constants in mechanically ventilated patients with and without COPD. *Intensive Care Med* 26: 1612–1618, 2000.

119. **Di Marco F**, **Rota Sperti L**, **Milan B**, **Stucchi R**, **Centanni S**, **Brochard L**, **Fumagalli R**. Measurement of functional residual capacity by helium dilution during partial support ventilation: in vitro accuracy and in vivo precision of the method. *Intensive Care Med* 33: 2109–15, 2007.

120. **Mariappan YK**, **Kolipaka A**, **Manduca A**, **Hubmayr RD**, **Ehman RL**, **Araoz P**, **McGee KP**. Magnetic resonance elastography of the lung parenchyma in an in situ porcine model with a noninvasive mechanical driver: correlation of shear stiffness with trans-respiratory system pressures. *Magn Reson Med* 67: 210–7, 2012.

121. **Martin AR**, **Katz IM**, **Terzibachi K**, **Gouinaud L**, **Caillibotte G**, **Texereau J**. Bench and mathematical modeling of the effects of breathing a helium/oxygen mixture on expiratory time constants in the presence of heterogeneous airway obstructions. *Biomed Eng Online* 11: 27, 2012.

122. **Martin TR**, **Hagimoto N**, **Nakamura M**, **Matute-Bello G**. Apoptosis and epithelial injury in the lungs. *Proc Am Thorac Soc* 2: 214–20, 2005.

123. **Matamis D**, **Lemaire F**, **Harf A**, **Brun-Buisson C**, **Ansquer JC**, **Atlan G**. Total respiratory pressure-volume curves in the adult respiratory distress syndrome. *Chest* 86: 58–66, 1984.

124. **Matthay MA**, **Ware LB**, **Zimmerman GA**. Review series The acute respiratory distress syndrome. 122: 2731–2740, 2012.

125. **Matthay MA**, **Wiener-Kronish JP**. Intact epithelial barrier function is critical for the resolution of alveolar edema in humans. *Am Rev Respir Dis* 142: 1250–7, 1990.

126. **Matthay MMAM**, **Zemans RRLR**. The acute respiratory distress syndrome: pathogenesis and treatment. *Annu Rev Pathol* 6: 147–163, 2011.

127. **Mattingley JS**, **Holets SR**, **Oeckler R a**, **Stroetz RW**, **Buck CF**, **Hubmayr RD**. Sizing the lung of mechanically ventilated patients. *Crit Care* 15: R60, 2011.

128. **Matute-Bello G**, **Downey G**, **Moore BB**, **Groshong SD**, **Matthay M a**, **Slutsky AS**, **Kuebler WM**. An official American Thoracic Society workshop report: features and measurements of experimental acute lung injury in animals. *Am J Respir Cell Mol Biol* 44: 725–38, 2011.

129. **Matute-Bello G**, **Frevert CW**, **Martin TR**. Animal models of acute lung injury. *Am J Physiol Lung Cell Mol Physiol* 295: L379–99, 2008.

130. **Maybauer MO**, **Maybauer DM**, **Herndon DN**. Incidence and outcomes of acute lung injury. *N Engl J Med* 354: 416–7; author reply 416–7, 2006.

131. **McGrath JJ**, **Purkiss LQ**, **Eberle M**, **McGrath WR**. Long-term effects of a cross-linked

polyacrylate superabsorbent in the hamster. *J Appl Toxicol* 15: 69–73, 1995.

132. **Mcilroy MB**, **Tierney DF**, **Nadel JA**. A new method for measurement of compliance and resistance of lungs and thorax. *J Appl Physiol* 18: 424–427, 1963.

133. **Mead J**, **Takishima T**, **Leith D**. Stress distribution pulmonary in lungs : a model of elasticity. *J Appl Physiol* 28: 596–608, 1970.

134. **Menezes SLS**, **Bozza PT**, **Neto HCCF**, **Laranjeira AP**, **Negri EM**, **Capelozzi VL**, **Zin W a**, **Rocco PRM**. Pulmonary and extrapulmonary acute lung injury: inflammatory and ultrastructural analyses. *J Appl Physiol* 98: 1777–83, 2005.

135. **Mertens M**, **Tabuchi A**, **Meissner S**, **Krueger A**, **Schirrmann K**, **Kertzscher U**, **Pries AR**, **Slutsky AS**, **Koch E**, **Kuebler WM**. Alveolar dynamics in acute lung injury: heterogeneous distension rather than cyclic opening and collapse. *Crit Care Med* 37: 2604–11, 2009.

136. **Mols G**, **Kessler V**, **Benzing A**, **Lichtwarck-Aschoff M**, **Geiger K**, **Guttmann J**. Is pulmonary resistance constant, within the range of tidal volume ventilation, in patients with ARDS? *Br J Anaesth* 86: 176, 2001.

137. **Nakagawa S**, **Schielzeth H**. A general and simple method for obtaining R2 from generalized linear mixed-effects models. *Methods Ecol Evol* : 133–142, 2013.

138. **Negri EM**, **Hoelz C**, **Barbas CS V**, **Montes GS**, **Saldiva PHN**, **Capelozzi VL**. Acute remodeling of parenchyma in pulmonary and extrapulmonary ARDS. An autopsy study of collagen-elastic system fibers. *Pathol Res Pract* 198: 355–61, 2002.

139. **Nelson R**, **Couto C**. Diagnostic tests for the lower respiratory tract. In: *Small Animal Internal Medicine, 3rd Ed.* 2003, p. 252–268.

140. **Notter R**. *Lung surfactant: basic science and clinical applications.* New York: Marcel Dekker, 2000.

141. **Okazawa M**, **D'Yachkova Y**, **Paré PD**. Mechanical properties of lung parenchyma during bronchoconstriction. *J Appl Physiol* 86: 496–502, 1999.

142. **Opitz B**, **van Laak V**, **Eitel J**, **Suttorp N**. Innate immune recognition in infectious and noninfectious diseases of the lung. *Am J Respir Crit Care Med* 181: 1294–309, 2010.

143. **Otto CM**, **Markstaller K**, **Kajikawa O**, **Karmrodt J**, **Syring RS**, **Pfeiffer B**, **Good VP**, **Frevert CW**, **Baumgardner JE**. Spatial and temporal heterogeneity of ventilator-associated lung injury after surfactant depletion. *J Appl Physiol* 104: 1485–94, 2008.

144. **Parmigiani S**, **Solari E**. The era of pulmonary surfactant from Laplace to nowadays. *Acta Biomed* 74: 69–75, 2003.

145. **Patroniti N**, **Bellani G**, **Manfio A**, **Maggioni E**, **Giuffrida A**, **Foti G**, **Pesenti A**. Lung volume in mechanically ventilated patients: measurement by simplified helium dilution compared to quantitative CT scan. *Intensive Care Med* 30: 282–9, 2004.

146. **Pelosi P**, **Cereda M**, **Foti G**, **Giacomini M**, **Pesenti A**. Alterations of lung and chest wall mechanics in patients with acute lung injury: effects of positive end-expiratory pressure. *Am J Respir Crit Care Med* 152: 531–7, 1995.

147. **Pelosi P**, **Gattinoni L**. Acute respiratory distress syndrome of pulmonary and extra-pulmonary origin: fancy or reality? *Intensive Care Med* 27: 457–460, 2001.

148. **Pelosi P**, **Goldner M**, **Mckibben A**, **Adams A**, **Eccher G**, **Caironi P**, **Losappio S**, **Gattinoni L**, **Marini JJ**. Recruitment and Derecruitment During Acute An Experimental Study. *Crit Care Med* 164: 122–130, 2001.

149. **Perchiazzi G**, **Rylander C**, **Vena A**, **Derosa S**, **Polieri D**, **Fiore T**, **Giuliani R**, **Hedenstierna G**. Lung regional stress and strain as a function of posture and ventilatory mode. *J Appl Physiol* 110: 1374–83, 2011.

150. **Pesenti a**, **Pelosi P**, **Rossi N**, **Virtuani A**, **Brazzi L**, **Rossi A**. The effects of positive end-expiratory pressure on respiratory resistance in patients with the adult respiratory distress syndrome and in normal anesthetized subjects. *Am Rev Respir Dis* 144: 101–7, 1991.

151. **Pesenti A**, **Pelosi P**, **Rossi N**, **Aprigliano M**, **Brazzi L**, **Fumagalli R**. Respiratory mechanics and bronchodilator responsiveness in patients with the adult respiratory distress syndrome. *Crit Care Med* 21: 78–83, 1993.

152. **Petty TL**, **Newman JH**. Adult respiratory distress syndrome. *West J Med* 128: 399–407, 1978.

153. **Phua J**, **Badia JR**, **Adhikari NKJ**, **Friedrich JO**, **Fowler R a**, **Singh JM**, **Scales DC**, **Stather DR**, **Li A**, **Jones A**, **Gattas DJ**, **Hallett D**, **Tomlinson G**, **Stewart TE**, **Ferguson ND**. Has mortality from acute respiratory distress syndrome decreased over time?: A systematic review. *Am J Respir Crit Care Med* 179: 220–7, 2009.

154. **Piantadosi CA**, **Schwartz DA**. The Acute Respiratory Distress Syndrome. *Ann Intern Med* 141: 460–470, 2004.

155. **Polese G**, **Rossi A**, **Appendini L**, **Brandi G**, **Bates JH**, **Brandolese R**. Partitioning of respiratory mechanics in mechanically ventilated patients. *J Appl Physiol* 71: 2425–33, 1991.

156. **Pontoppidan H**, **Geffin B**, **Lowenstein E**. Acute respiratory failure in the adult. 3. *N Engl J Med* 287: 799–806, 1972.

157. **Prange HD**. LAPLACE'S LAW AND THE ALVEOLUS: A MISCONCEPTION OF ANATOMY AND A MISAPPLICATION OF PHYSICS. *AJP Adv Physiol Educ* 27: 34–40, 2003.

158. **Protti A**, **Cressoni M**, **Santini A**, **Langer T**, **Mietto C**, **Febres D**, **Chierichetti M**, **Coppola S**, **Conte G**, **Gatti S**, **Leopardi O**, **Masson S**, **Lombardi L**, **Lazzerini M**, **Rampoldi E**, **Cadringher P**, **Gattinoni L**. Lung stress and strain during mechanical ventilation: any safe threshold? *Am J Respir Crit Care Med* 183: 1354–62, 2011.

159. **Pulletz S**, **Kott M**, **Elke G**, **Schädler D**, **Vogt B**, **Weiler N**, **Frerichs I**. Dynamics of regional lung aeration determined by electrical impedance tomography in patients with acute respiratory distress syndrome. (2012).

160. **Raghavendran K**, **Nemzek J**, **Napolitano LM**, **Knight PR**. Aspiration-induced lung injury. *Crit Care Med* 39: 818–26, 2011.

161. **Ranieri VM**, **Giuliani R**, **Mascia L**, **Grasso S**, **Petruzzelli V**, **Bruno F**, **Fiore T**, **Brienza a.** Chest wall and lung contribution to the elastic properties of the respiratory system in patients with chronic obstructive pulmonary disease. *Eur Respir J* 9: 1232–1239, 1996.

162. **Ranieri VM**, **Rubenfeld GD**, **Thompson BT**, **Ferguson ND**, **Caldwell E**, **Fan E**, **Camporota L**, **Slutsky AS**. Acute respiratory distress syndrome: the Berlin Definition. *JAMA* 307: 2526–33, 2012.

163. **Rausch SMK**, **Haberthür D**, **Stampanoni M**, **Schittny JC**, **Wall WA**. Local strain distribution in real three-dimensional alveolar geometries. *Ann Biomed Eng* 39: 2835–43, 2011.

164. **Retamal J**, **Libuy J**, **Jiménez M**, **Delgado M**, **Besa C**, **Bugedo G**, **Bruhn A**. Preliminary study of ventilation with 4 ml/kg tidal volume in acute respiratory distress syndrome: feasibility and effects on cyclic recruitment - derecruitment and hyperinflation. *Crit Care* 17: R16, 2013.

165. **Ricard JD**, **Dreyfuss D**, **Saumon G**. Production of inflammatory cytokines in ventilator-induced lung injury: a reappraisal. *Am J Respir Crit Care Med* 163: 1176–1180, 2001.

166. **Riva DR**, **Oliveira MBG**, **Rzezinski AF**, **Rangel G**, **Capelozzi VL**, **Zin WA**, **Morales MM**, **Pelosi P**, **Rocco PRM**. Recruitment maneuver in pulmonary and extrapulmonary experimental acute lung injury. *Crit Care Med* 36: 1900–8, 2008.

167. **De Robertis E**, **Liu JM**, **Blomquist S**, **Dahm PL**, **Thörne J**, **Jonson B**. Elastic properties of the lung and the chest wall in young and adult healthy pigs. *Eur Respir J Off J Eur Soc Clin Respir Physiol* 17: 703–11, 2001.

168. **Rotta AT**, **Gunnarsson B**, **Fuhrman BP**, **Hernan LJ**, **Steinhorn DM**. Comparison of lung protective ventilation strategies in a rabbit model of acute lung injury. *Crit Care Med* 29: 2176–84, 2001.

169. **Rubin JM**, **Horowitz JC**, **Sisson TH**, **Kim K**, **Ortiz LA**, **Hamilton JD**. Ultrasound Strain Measurements for Evaluating Local Pulmonary Ventilation. *IEEE Int Ultrason Symp [proceedings] IEEE Int Ultrason Symp* 2015, 2015.

170. **Russell JA**, **Walley KR**, **Singer J**, **Gordon AC**, **Hébert PC**, **Cooper DJ**, **Holmes CL**, **Mehta S**, **Granton JT**, **Storms MM**, **others**. Vasopressin versus norepinephrine infusion in patients with septic shock. *N Engl J Med* 358: 877–887, 2008.

171. **Rylander C**, **Hogman M**, **Perchiazzi G**, **Magnusson A**, **Hedenstierna G**. Functional Residual Capacity and Respiratory Mechanics as Indicators of Aeration and Collapse in Experimental Lung Injury. *Anesth. Analg.* (March 2004).

172. **Salerno FG**, **Ludwig MS**. Elastic moduli of excised constricted rat lungs. *J Appl Physiol* 86: 66–70, 1999.

173. **Santana MCE**, **Garcia CSNB**, **Xisto DG**, **Nagato LKS**, **Lassance RM**, **Prota LFM**, **Ornellas FM**, **Capelozzi VL**, **Morales MM**, **Zin WA**, **Pelosi P**, **Rocco PRM**. Prone position prevents regional alveolar hyperinflation and mechanical stress and strain in mild experimental acute lung injury. *Respir Physiol Neurobiol* 167: 181–188, 2009.

174. **Santos FB**, **Nagato LKS**, **Boechem NM**, **Negri EM**, **Guimarães A**, **Capelozzi VL**, **Faffe DS**, **Zin W a**, **Rocco PRM**. Time course of lung parenchyma remodeling in pulmonary and extrapulmonary acute lung injury. *J Appl Physiol* 100: 98–106, 2006.

175. **Scarpelli EM**. The alveolar surface network: a new anatomy and its physiological significance. *Anat Rec* 251: 491–527, 1998.

176. **Scheiermann C**, **Kunisaki Y**, **Jang J-E**, **Frenette PS**. Neutrophil microdomains: linking heterocellular interactions with vascular injury. *Curr Opin Hematol* 17: 25–30, 2010.

177. **Schiller HJ**, **McCann UG**, **Carney DE**, **Gatto LA**, **Steinberg JM**, **Nieman GF**. Altered alveolar mechanics in the acutely injured lung. *Crit Care Med* 29: 1049–55, 2001.

178. **Schwenninger D**, **Runck H**, **Schumann S**, **Haberstroh J**, **Guttmann J**. Locally measured shear moduli of pulmonary tissue and global lung mechanics in mechanically ventilated rats. *J Appl Physiol* 113: 273–80, 2012.

179. **Silversides JA**, **Ferguson ND**. Clinical review: Acute respiratory distress syndrome - clinical ventilator management and adjunct therapy. *Crit Care* 17: 225, 2013.

180. **Simon BA**, **Christensen GE**, **Low DA**, **Reinhardt JM**. Computed tomography studies of lung mechanics. *Proc Am Thorac Soc* 2: 517–21, 506–7, 2005.

181. **Spieth PM**, **Bluth T**, **Gama De Abreu M**, **Bacelis A**, **Goetz AE**, **Kiefmann R**. Mechanotransduction in the lungs. *Minerva Anestesiol* 80: 933–41, 2014.

182. **Spragg RG**, **Bernard GR**, **Checkley W**, **Curtis JR**, **Gajic O**, **Guyatt G**, **Hall J**, **Israel E**, **Jain M**, **Needham DM**, **Randolph AG**, **Rubenfeld GD**, **Schoenfeld D**, **Thompson BT**, **Ware LB**, **Young D**, **Harabin AL**. Beyond mortality: future clinical research in acute lung injury. *Am J Respir Crit Care Med* 181: 1121–7, 2010.

183. **Stamenovic D**, **Yager D**. Elastic properties of air- and liquid-filled lung parenchyma. *J Appl Physiol* 65: 2565–70, 1988.

184. **Stewart TE**, **Meade MO**, **Cook DJ**, **Granton JT**, **Hodder R V**, **Lapinsky SE**, **Mazer CD**, **McLean RF**, **Rogovein TS**, **Schouten BD**, **Todd TR**, **Slutsky AS**. Evaluation of a ventilation strategy to prevent barotrauma in patients at high risk for acute respiratory distress syndrome. Pressure- and Volume-Limited Ventilation Strategy Group. *N Engl J Med* 338: 355–61, 1998.

185. **Su X**, **Johansen M**, **Looney MR**, **Brown EJ**, **Matthay MA**. CD47 deficiency protects mice from lipopolysaccharide-induced acute lung injury and Escherichia coli pneumonia. *J Immunol* 180: 6947–53, 2008.

186. **Suter PM**, **Fairley HB**, **Isenberg MD**. Effect of tidal volume and positive end-expiratory pressure on compliance during mechanical ventilation. *Chest* 73: 158–62, 1978.

187. **Talmor D**, **Sarge T**, **Malhotra A**, **O'Donnell CR**, **Ritz R**, **Lisbon A**, **Novack V**, **Loring SH**. Mechanical ventilation guided by esophageal pressure in acute lung injury. *N Engl J Med* 359: 2095–2104, 2008.

188. **Talmor D**, **Sarge T**, **O'Donnell CR**, **Ritz R**, **Lisbon A**, **Loring SH**. Esophageal and transpulmonary pressures in acute respiratory failure. *Crit Care* 34: 1389–1394, 2008.

189. **Tantucci C**, **Corbeil C**, **Chasse M**, **Robatto FM**, **Nava S**, **Braidy J**, **Matar N**, **Milic-Emili J**. Flow and volume dependence of respiratory system flow resistance in patients with adult respiratory distress syndrome. *Am J Respir Crit Care Med* 145: 355, 1992.

190. **Tantucci C**, **Corbeil C**, **Chasse M**, **Robatto FM**, **Nava S**, **Braidy J**, **Matar N**, **Milic-Emili J**. Flow and volume dependence of respiratory system flow resistance in patients with adult respiratory distress syndrome. *Am J Respir Crit Care Med* 145: 355–60, 1992.

191. **Terragni PP**, **Rosboch G**, **Tealdi A**, **Corno E**, **Menaldo E**, **Davini O**, **Gandini G**,

Herrmann P, **Mascia L**, **Quintel M**, **Slutsky AS**, **Gattinoni L**, **Ranieri VM**. Tidal hyperinflation during low tidal volume ventilation in acute respiratory distress syndrome. *Am J Respir Crit Care Med* 175: 160–6, 2007.

192. **Terragni PP**, **Del Sorbo L**, **Mascia L**, **Urbino R**, **Martin EL**, **Birocco A**, **Faggiano C**, **Quintel M**, **Gattinoni L**, **Ranieri VM**. Tidal volume lower than 6 ml/kg enhances lung protection: role of extracorporeal carbon dioxide removal. *Anesthesiology* 111: 826–35, 2009.

193. **Träuble H**, **Eibl H**, **Sawada H**. Respiration--a critical phenomenon? Lipid phase transitions in the lung alveolar surfactant. *Naturwissenschaften* 61: 344–54, 1974.

194. **Uchiyama A**, **Chang C**, **Suzuki S**, **Mashimo T**, **Fujino Y**. An expiratory assist during spontaneous breathing can compensate for endotracheal tube resistance. *Anesth Analg* 109: 434–40, 2009.

195. **Uttman L**, **Bitzén U**, **De Robertis E**, **Enoksson J**, **Johansson L**, **Jonson B**. Protective ventilation in experimental acute respiratory distress syndrome after ventilator-induced lung injury: a randomized controlled trial. *Br J Anaesth* 109: 584–94, 2012.

196. **Verbrugge SJC**, **Lachmann B**, **Kesecioglu J**. Lung protective ventilatory strategies in acute lung injury and acute respiratory distress syndrome: from experimental findings to clinical application. *Clin Physiol Funct Imaging* 27: 67–90, 2007.

197. **Villar J**, **Slutsky AS**. Is acute respiratory distress syndrome an iatrogenic disease? *Crit Care* 14: 120, 2010.

198. **Vogt B**, **Pulletz S**, **Elke G**, **Zhao Z**, **Zabel P**, **Weiler N**, **Frerichs I**. Spatial and temporal heterogeneity of regional lung ventilation determined by electrical impedance tomography during pulmonary function testing. *J Appl Physiol* 113: 1154–61, 2012.

199. **Vos W**, **De Backer J**, **Poli G**, **De Volder A**, **Ghys L**, **Van Holsbeke C**, **Vinchurkar S**, **De Backer L**, **De Backer W**. Novel functional imaging of changes in small airways of patients treated with extrafine beclomethasone/formoterol. *Respiration* 86: 393–401, 2013.

200. **Ware LB**, **Matthay MA**. Alveolar fluid clearance is impaired in the majority of patients with acute lung injury and the acute respiratory distress syndrome. *Am J Respir Crit Care Med* 163: 1376–83, 2001.

201. **Weiser MR**, **Pechet TT**, **Williams JP**, **Ma M**, **Frenette PS**, **Moore FD**, **Kobzik L**, **Hines RO**, **Wagner DD**, **Carroll MC**, **Hechtman HB**. Experimental murine acid aspiration injury is mediated by neutrophils and the alternative complement pathway. *J Appl Physiol* 83: 1090–5, 1997.

202. **Wellman T**, **Winkler T**. Effect of regional lung inflation on ventilation heterogeneity at different length scales during mechanical ventilation of normal sheep lungs. *J Appl …* 113: 947–957, 2012.

203. **Wiener-Kronish JP**, **Albertine KH**, **Matthay MA**. Differential responses of the endothelial and epithelial barriers of the lung in sheep to Escherichia coli endotoxin. *J Clin Invest* 88: 864–75, 1991.

204. **Williams MR**, **Azcutia V**, **Newton G**, **Alcaide P**, **Luscinskas FW**. Emerging mechanisms of neutrophil recruitment across endothelium. *Trends Immunol* 32: 461–9,

2011.

205. **Wolf GK**, **Arnold JH**. Noninvasive assessment of lung volume: respiratory inductance plethysmography and electrical impedance tomography. *Crit Care Med* 33: S163–9, 2005.

206. **Wolf GK**, **Gómez-Laberge C**, **Rettig JS**, **Vargas SO**, **Smallwood CD**, **Prabhu SP**, **Vitali SH**, **Zurakowski D**, **Arnold JH**. Mechanical ventilation guided by electrical impedance tomography in experimental acute lung injury. *Crit Care Med* 41: 1296–304, 2013.

207. **Wright P**, **Carmichael L**. Effect of bronchodilators on lung mechanics in the acute respiratory distress syndrome (ARDS). *Chest* 106: 1517–1523, 1994.

208. **Wright PE**, **Bernard GR**. The role of airflow resistance in patients with the adult respiratory distress syndrome. *Am J Respir Crit Care Med* 139: 1169, 1989.

209. **Xie Y**, **Chao M**, **Xing L**. Tissue feature-based and segmented deformable image registration for improved modeling of shear movement of lungs. *Int J Radiat Oncol Biol Phys* 74: 1256–65, 2009.

210. **Yilmaz C**, **Tustison NJ**, **Dane DM**, **Ravikumar P**, **Takahashi M**, **Gee JC**, **Hsia CCW**. Progressive adaptation in regional parenchyma mechanics following extensive lung resection assessed by functional computed tomography. *J Appl Physiol* 111: 1150–8, 2011.

211. **Zemans RL**, **Colgan SP**, **Downey GP**. Transepithelial migration of neutrophils: mechanisms and implications for acute lung injury. *Am J Respir Cell Mol Biol* 40: 519–35, 2009.

212. **Zhang B**, **Yu D**, **Liu H**, **Hu Y**. Osmotic coefficients of polyelectrolyte solutions, measurements and correlation. *Polymer (Guildf)* 43: 2975–2980, 2002.

213. **Zhao Z**, **Steinmann D**, **Frerichs I**, **Guttmann J**, **Möller K**. Ventilation inhomogeneity is one criterion among many in multidimensional PEEP titration. *Crit Care* 14: 424, 2010.

214. **Zhou X**, **Dai Q**, **Huang X**. Neutrophils in acute lung injury. *Front Biosci* 17: 2278–83, 2012.

215. **Zimmerman GA**, **Albertine KH**, **Carveth HJ**, **Gill EA**, **Grissom CK**, **Hoidal JR**, **Imaizumi T**, **Maloney CG**, **McIntyre TM**, **Michael JR**, **Orme JF**, **Prescott SM**, **Topham MS**. Endothelial activation in ARDS. *Chest* 116: 18S–24S, 1999.

216. **Zin WA**, **Böddener A**, **Silva PR**, **Pinto TM**, **Milic-Emili J**. Active and passive respiratory mechanics in anesthetized dogs. *J Appl Physiol* 61: 1647–55, 1986.

217. **Zin WA**, **Pengelly LD**, **Milic-Emili J**. Single-breath method for measurement of respiratory mechanics in anesthetized animals. *J Appl Physiol* 52: 1266–71, 1982.

Appendices

Appendix A Candidate's List of Publications During the Doctoral Program (2009-2016)

(From a total of 68 publications)

Journal

1. Henderson WR, Dominelli PB, Molgat-Seon Y, Lipson R, Griesdale DEG, Sekhon M, Ayas N, Sheel AW. Effect of Tidal Volume and Positive End Expiratory Pressure on Expiratory Time Constants in Experimental Lung Injury. Physiol Reports. 2016 Mar;4(5). pii: e12737.

2. Henderson WR, Molgat-Seon Y, Dominelli PB, Brasher PM, Griesdale DE, Foster GE, Yacyshyn A, Ayas NT, Sheel AW Gas density alters expiratory time constants before and after experimental lung injury. Exp Physiol. 2015 Oct 1;100(10):1217-28.

3. Dominelli PB, Molgat-Seon Y, Foster GE, Dominelli GS, Haverkamp HC, Henderson WR, Sheel AW. Quantifying the shape of maximal expiratory flow-volume curves in healthy humans and asthmatic patients. Respir Physiol Neurobiol. 2015 Sep 18;220:46-53.

4. Dominelli PB, Foster GE, Guenette JA, Haverkamp HC, Eves ND, Dominelli GS, Henderson WR, O'Donnell DE, Sheel AW. Quantifying the shape of the maximal expiratory flow-volume curve in mild COPD. Respir Physiol Neurobiol. 2015 Aug 12;219:30-35.

5. Mowat I, Tang R, Vaghadia H, Krebs C, Henderson WR, Sawka A. Comparison of the distribution of dye in the epidural space administered via an epidural catheter: Bolus versus infusion, a porcine model. Brit J Anes. Accepted Aug 2015 as BJA-2015-00696.

6. The NICE-SUGAR Study Investigators. Intensive versus Conventional Glucose Control in Critically Ill Patients with Traumatic Brain Injury: Long term follow up of a subgroup of patients from the NICE SUGAR Study. Intens Care Med. 2015 Jun;41(6):1037-47.

7. Griesdale DE, Sekhon MS, Menon DK, Lavinio A, Donnelly J, Robba C, Sekhon IS, Taylor A, Henderson WR, Turgeon AF, Gupta AK. Hemoglobin Area and Time Index Above 90 g/L are Associated with Improved 6-Month Functional Outcomes in Patients with Severe Traumatic Brain Injury. Neurocrit Care. 2014 Dec 16.

8. Joshua C Tremblay, Andrew T Lovering, Philip N Ainslie,Mike Stembridge, Keith R Burgess, Akke Bakker, Joseph Donnelly, Samuel J.E. Lucas, Nia C.S Lewis, Paolo B Dominelli, William R Henderson, Giulio Dominelli, A William Sheel, Glen E Foster. Hypoxia, not pulmonary vascular pressure induces blood flow through intrapulmonary arteriovenous anastomoses. J Physiol, *593(3):723-37, 2015 Feb 1*.

9. Henderson WR, Griesdale DEG, Dominelli P, Ronco JJ. Does prone positioning improve oxygenation and reduce mortality in patients with ARDS? Can Respir J. 2014 Jul-Aug;21(4):213-5.

10. Griesdale DE, Ortenwall V, Norena M, Wong H, Sekhon MS, Kolmodin L, Henderson WR, Dodek P. Adherence to guidelines for management of cerebral perfusion pressure and outcome in patients who have severe traumatic brain injury. J Crit Care. 2014 Jul 31. pii: S0883-9441(14)00315-3.

11. Sekhon MS, McBeth P, Zou J, Qiao L, Kolmodin L, Henderson WR, Reynolds S, Griesdale DE. Association between optic nerve sheath diameter and mortality in patients with severe traumatic brain injury. Neurocrit Care. 2014 Jun 27.

12. Henderson WR, Barnbrook J, Dominelli PB, Griesdale DEG, Arndt T, Molgat-Seon Y, Foster GE, Ackland GL, Xu J, Ayas NT and Sheel AW. Administration of intrapulmonary sodium polyacrylate to induce lung injury for the development of a porcine model of early acute respiratory distress syndrome. Intensive Care Medicine Experimental. 2014 2:5.

13. Dominelli PB, Foster GE, Dominelli GS, Henderson WR, Koehle MS, McKenzie DC, Sheel AW. Exercise-induced arterial hypoxemia is unaffected by intense physical training: a case report. Applied Physiology, Nutrition, and Metabolism, 2014, 39:(2), 266–269.

14. Kolmodin L, Sekhon MS, Henderson WR, Turgeon AF, Griesdale DE. Hypernatremia in patients with severe traumatic brain injury: a systematic review. Ann Intensive Care. 2013 Nov 6;3(1):35.

15. Henderson WR, Dominelli PB, Griesdale DE, Talmor D, Sheel AW. Airway pressure and transpulmonary pressure during high-frequency oscillation for acute respiratory distress syndrome. Can Respir J. 2013 Oct 17.

16. Dominelli PB, Foster GE, Dominelli GS, Henderson WR, Koehle MS, McKenzie DC, Sheel AW. Exercise-induced arterial hypoxaemia and the mechanics of breathing in healthy young women. J Physiol. 2013 Jun 15;591(Pt 12):3017-34.

17. Querido JS, Ainslie PN, Foster GE, Henderson WR, Halliwill JR, Ayas NT, Sheel AW. Dynamic cerebral autoregulation during and following acute hypoxia: role of carbon dioxide. J Appl Physiol. 2013 May;114(9):1183-90.

18. Griesdale DE, Sekhon MS, Henderson WR. Hypernatremia and intracranial pressure: more questions than answers. Crit Care. 2013 Jan 7;17(1):401.

19. The NICE-SUGAR Study Investigators. Hypoglycemia and Risk of Death in Critically Ill Patients. N Engl J Med 2012; 367:1108-18.

20. Mendelson AA, Gillis C, Henderson WR, Ronco JJ, Dhingra V, Griesdale DEG. Intracranial Pressure Monitors in Traumatic Brain Injury: A Systematic Review. Can J Neurol Sci. 2012; 39: 571-576.
21. Sekhon MS, McLean N, Henderson WR, Chittock DR, Griesdale DEG. Association of hemoglobin concentration and mortality in critically ill patients with severe traumatic brain injury. Critical Care 2012, 16:R128
22. Dominelli PB, Foster GE, Dominelli GS, Querido JS, Henderson WR, Koehle MS, Sheel AW. Repeated exercise-induced arterial hypoxemia in a healthy untrained woman. Respir Physiol Neurobiol. 183 (2012) 201– 205.

23. Henderson WR, Guenette JA, Dominelli PB, Griesdale DE, Querido JS, Boushel R, Sheel AW. Limitations of respiratory muscle and vastus lateralis blood flow during continuous exercise. Respir Physiol Neurobiol. 2012 May 31;181(3):302-7.

24. Kennedy JM, Koehle MS, Potts JE, Sandor GG, Potts MT, Houghton K, Henderson WR, Sheel AW. Exercise-induced intrapulmonary arteriovenous shunt in healthy women. Respir Physiol Neurobiol. 2012. Apr 15;181(1):8-13.

25. Henderson WR, Sheel AW. Pulmonary mechanics during mechanical ventilation. Respir Physiol Neurobiol. 2012.180:162– 172.

26. Querido JS, Wehrwein EA, Hart EC, Charkoudian N, Henderson WR, Sheel AW. Baroreflex control of muscle sympathetic nerve activity as a mechanism for persistent sympathoexcitation following acute hypoxia in humans. Am J Physiol Regul Integr Comp Physiol. 2011 Dec;301(6):R1779-85.

27. Guenette JA, Henderson WR, Dominelli PB, Querido JS, Brasher PM, Griesdale DE, Boushel R, Sheel AW. Blood flow index using near-infrared spectroscopy and indocyanine green as a minimally invasive tool to assess respiratory muscle blood flow in humans. Am J Physiol Regul Integr Comp Physiol. 2011 Apr;300(4):R984-92.

28. Griesdale DE, Henderson WR, Green RS. Airway management in critically ill patients. Lung. 2011 Jun;189(3):181-92.

29. Sekhon MS, Dhingra VK, Sekhon IS, Henderson WR, McLean N, Griesdale DE. The safety of synthetic colloid in critically ill patients with severe traumatic brain injuries. J Crit Care. 2011 Aug;26(4):357-62.

30. Negash DT, Dhingra VK, Copland M, Griesdale D, Henderson W. Intensity of continuous renal replacement therapy in acute kidney injury in the intensive care unit: a systematic review and meta-analysis. Vasc Endovascular Surg. 2011 Aug;45(6):504-10.

31. Henderson WR, Griesdale DE, Walley KR, Sheel AW. Clinical review: Guyton - the role of mean circulatory filling pressure and right atrial pressure in controlling cardiac output. Crit Care. 2010 Dec 1;14(6):243.

32. Henderson WR, Finfer S. Differences in outcome between the NICE-SUGAR and Leuven trials: possible methodological explanations. Crit Care Resusc. 2009 Sep;11(3):175-7.

33. Henderson WR, Dhingra V, Chittock D, Foster D, Hebert P, Cook D, Heyland D, Dodek P, Griesdale D, Schulzer M, Ronco JJ; Canadian Critical Trials Group. The efficacy and safety of glucose control algorithms in intensive care: a pilot study of the Survival Using Glucose Algorithm Regulation (SUGAR) trial. Pol Arch Med Wewn. 2009 Jul-Aug;119(7-8):439-46.
34. The NICE-SUGAR Study Investigators. Intensive versus conventional glucose control in critically ill patients. N Engl J Med 2009;360:1283-97.

35. Griesdale DEG, de Souza RJ, van Dam RM, Heyland DK, Cook DJ, Malhotra A, Dhaliwal R, Henderson WR, Chittock DR, Finfer S, Talmor D. Intensive insulin therapy and mortality among critically ill patients: a meta-analysis including NICE-SUGAR study data. CMAJ. 2009. 180:821 - 827

Letters

1. Henderson WR, Griesdale DEG. Guyton: More Fire than Smoke. J Physiol. December 11, 2013 (published online).

2. Griesdale DEG, Sekhon MS, Henderson WR. Hypernatremia and intracranial pressure: more questions than answers. Critical Care 2013, 17:4010.

Abstracts

1. Paolo B. Dominelli, Yannick Molgat-Seon, Giulio S. Dominelli, William R. Henderson, Carli M. Peters, Jean-Sébastien Blouin, Lee M. Romer, Michael S. Koehle, Glen E. Foster and A. William Sheel. Reducing respiratory muscle work and hypoxemia similarly attenuates exercise-induced locomotor fatigue in men and women. ATS 2016.

2. Lamarche D, Rossi L, Shah M, Zytaruk N, Clarke F, Hand L, Lee J, Lee Y, Smith O, Jakab M, Shah S, Breton SJ, Langlois H, Porteous R, Watpool I, Acres S, Foster F, Meade M, Marshall JC, Lauzier F, Mehta S, McIntyre LL, Pagliarello G, Henderson W, Johnstone J, Heyland D, Thebane L, Bowdish D, Cook DJ, Surette M for the PROSPECT Investigators and the Canadian Critical Care Trials Group. Quality Control In the Conduct of a Probiotic Randomized Trial. Can Crit Care Forum 2014 (submitted).

3. Dominelli PB, Foster GE, Dominelli GS, Henderson WR, Koehle MS, McKenzie DC, Sheel AW. Exercise-induced arterial hypoxemia in healthy young women, the effect of altering breathing mechanics with heliox inspiration. Canadian Society of Exercise Physiology Annual Meeting 2012. Applied Physiology, Nutrition and Metabolism. 37:S11, 2012

4. Dominelli, P.D., Foster, G.E., Dominelli, G.S., Henderson, W.R., Koehle, M.S., McKenzie D.C. and Sheel A.W. 2012. Exercise-induced arterial hypoxemia and respiratory mechanics in young healthy women. Medicine & Science in Sports & Exercise. 44:5 S9 Abstract
5. Guenette JA, Henderson WR, Dominelli PB, Querido JS, Greisdale DE, Sheel AW. Blood flow index using near infrared spectroscopy and indocyanine green dye as a minimally invasive method for assessing respiratory muscle blood flow in humans. Chest. 138:917A, 2010. Oral Presentation. American College of Chest Physicians Annual Meeting, Vancouver, BC, Canada.

Book Chapters

1. Henderson WR, Sekhon M: Central nervous system toxicology. In: Sekhon M, Griesdale D (eds): Neurocritical care essentials : a practical guide. 1st ed. New York: Cambridge University Press; 2015.

2. Henderson WR, Sekhon M: Severe traumatic brain injury. In: Sekhon M, Griesdale D (eds): Neurocritical care essentials : a practical guide. 1st ed. New York: Cambridge University Press; 2015.

3. Henderson WR, Pare PA, Ayas NT: Respiratory system mechanics and energetics. In Broaddus VC, Mason RJ, Murray JF, Nadel JA, King TE Jr, Ernst J, Lazarus SC, Slutsky AS (eds): Murray & Nadel's Textbook of Respiratory Medicine, 6/e. Philadelphia: Elsevier, 2014.